# A Modelling Study of Thunderstorm Electrification and Lightning Flash Rate

by

Robert Solomon

A dissertation submitted in partial fulfillment
of the requirements for the degree of

Doctor of Philosophy

University of Washington

1997

Approved by M B Baker

Chairperson of Supervisory Committee

Program Authorized
to Offer Degree Department of Atmospheric Sciences

Date February 10, 1997

UMI Number: 9730077



UMI
300 North Zeeb Road
Ann Arbor, MI 48103

University of Washington

Abstract

# A Modelling Study of Thunderstorm Electrification and Lightning Flash Rate

by

**Robert Solomon**

Chairperson of the Supervisory Committee:
Professor Marcia Baker, Department of Atmospheric Sciences

Observing the range of spatial scales important in thunderstorm electrification and subsequent lightning development is huge and would be an impossible task. The charge transfer processes within clouds takes place during collisions of particles with diameters on the order of 10-1000 μm, whereas the distance between the centers of accumulated charge and the length of lightning channels are on the order of kilometers.

Numerical models have proved to be an effective means of gaining insight into the processes leading to thunderstorm electrification and lightning production. A one-and-a-half-dimensional cloud model is developed that retains those processes thought to be most important in the small and large scale generation and separation of charge. This model is combined with a lightning parameterization that treats the lightning channel as a conductor whose final length is determined by a crude charge criterion. Charge induced on the channel surface modifies the surrounding electric field and is redistributed onto hydrometeors prior to the next lightning flash.

Observations and results from the numerical thunderstorm model are used together to examine thunderstorm development and lightning flash rates in a variety of environments. The dependence of lightning occurrence, flash rate and type (cloud-to-ground and intracloud) on variations in cloud condensation nucleus concentrations, primary and secondary glaciation mechanisms, liquid water flux and updraft velocities is studied.

Observations and model results suggest that in order for a cloud to become electrified, threshold values of both liquid water flux and updraft velocity near -5°C must be exceeded.

Once electrified, ice crystal concentrations at temperatures between -10 and -20°C greatly influence the lightning flash rate.

Initially, lightning channels initiated within the simulated thunderclouds are intracloud. With further development of the cloud, long, intracloud channels deposit positive charge below the main, lower region of negative charge which leads to the initiation of cloud-to-ground channels. In general, lightning channels initiated between the two main bodies of positive and negative charge result in intracloud lightning, whereas channels initiated below the maximum negative charge region result in cloud-to-ground lightning. Lightning continues until the separation of charge is insufficient to maintain the electric fields needed to initiate lightning.

## Table of Contents

# List of Figures

## Introduction



## The Thunderstorm Model

## Case Studies: Observations and Model Simulations

## Thunderstorm Electrification and Lightning Flash Rate

## Appendix B: Instrumentation

# List of Tables

# Acknowledgments

I am eternally grateful to far too many people to attempt to list them and their contributions in the last six years. Foremost, my deepest appreciation goes to Marcia Baker, who at more than one time patiently put up with my idiosyncracies while always providing insight to the issues at hand. I would not be at this point without her generosity. Hugh Christian (NASA/MSFC) has gone out of his way to insure that I continued to be fed through the years. I also had the privilege of working with him during the CAPE field project. Likewise, I and am grateful for being allowed to work with Jim Dye at the CAPE field project. Useful input and discussions with John Latham always proved extremely helpful and interesting. The hospitality of Pierre Laroche and Claire Mary at the Office National d'Études et de Recherches Aérospatiales (ONERA) was an immense pleasure and I look forward to future collaborations with them. There were many useful suggestions given by my office mates (past and present) and my committee: Robert Holzworth, Robert Houze, Peter Hobbs, Robert Winglee and Greg Dash. I owe no small part of my sanity to all friends, the ubiquitous college inn pub crowd, and many others for giving me an outlet for other creative urges outside of work. And, many thanks for the continued support of my parents and grandparents during these many years of education. I'm sure we all learned from the process.

I obtained data sets and support from David Raymond, William Winn (Socorro, New Mexico), Steve Williams (CAPE) and The National Center for Atmospheric Research (CAPE and TOGA-COARE).

Funding for this work came from the Air Force Office of Scientific Research (AFOSR) grant # AFOSR 91-0012, National Aeronautics and Space Administration/Marshall Space Flight Center (NASA/MSFC) Graduate Fellowship grant # NGT 51047 and from the University Space Research Association/Institute for Global Change Research and Education (USRA/IGCRE) grant/co-op agrmt # sub 95-193.

...and I love those tropical storms:
huge, dark clouds rolling in over the country side
and the sound of the rain outside my window.

and I think of the thunder as the voice of my father,
which does not frighten me,
it's the only way he knows how to speak.
he'd speak softly, if he could.

Joe Frank - Works in Progress

Plut au ciel que le lecteur, enhardi et devenu momentanément féroce comme ce qu'il lit, trouve, sans se désorienter, son chemin abrupt et sauvage, à travers les marécages désolés de ces pages sombres et pleines de poison; car, à moins qu'il n'apporte dans sa lecture une logique rigoureuse et une tension d'esprit égale au moins a sa défiance, les émanations mortelles de ce livre imbiberont son âme comme l'eau le sucre. Il n'est pas bon que tout le monde lise les pages qui vont suivre; quelques-uns seuls savoureront ce fruit amer sans danger.

May it please heaven that the reader, emboldened and having for the time being become as fierce as what he is reading, should, without being led astray, find his rugged and treacherous way across the desolate swamps of these sombre and poison-filled pages; for, unless he brings to his reading a rigorous logic and a tautness of mind equal at least to his wariness, the deadly emanations of this book will dissolve his soul as water does sugar. It is not right that everyone should read the pages which follow; only a few will be able to savour this bitter fruit with impunity.

Comte de Lautréamont - Les Chants de Maldoror

# I. Introduction

## 1.1 Thunderstorms and the Global Circuit

It has been known for centuries that the earth is almost permanently electrified with the surface of the earth bearing net negative charge and positive charge distributed throughout the atmosphere (Roble and Tzur, 1986). The typical "fair-weather" electric field associated with this charge is approximately 100 V/m at the surface of the Earth. The atmospheric conductivity increases with altitude due mostly to ions produced by cosmic-rays. Without some source of current, the Earth would discharge in 5 to 40 minutes. Thunderstorms are believed to be the dominant source of upward current in the "global circuit" though there may be other sources (eg, Williams and Heckman, 1993). Thunderstorms typically deposit negative charge to ground via cloud-to-ground lightning and negative charge flows to cloud top from the environment. (Alternatively one can see this as a source of positive charge for the upper atmosphere.) This in turn drives a downward current in regions that do not contain thunderstorms (see Figure 1.1). Using this model of the global circuit, rough estimates suggest

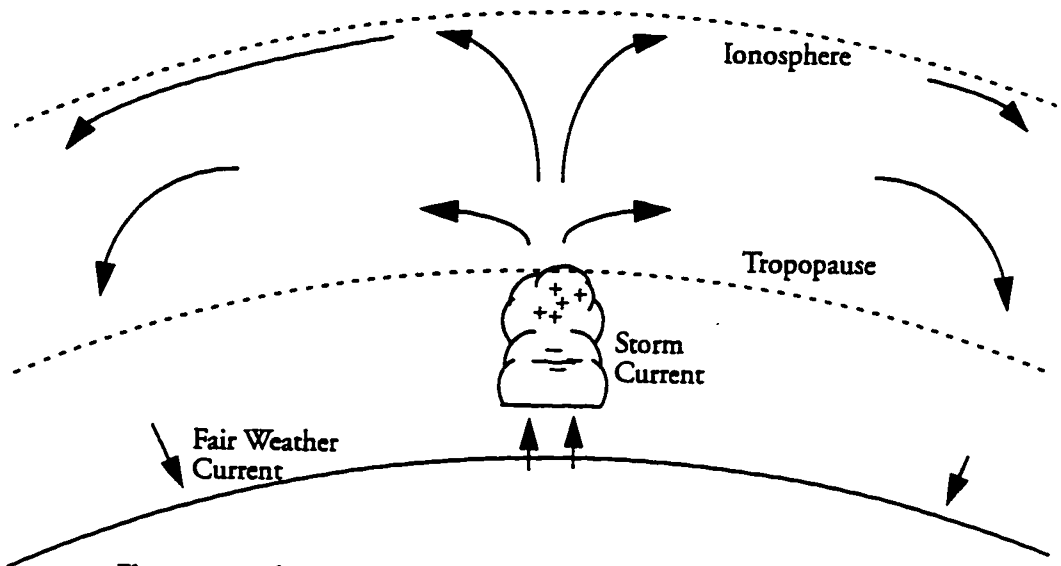


**Figure 1.1. Schematic of the "Global Circuit" with storm driven currents. By convention, the current designates the current of positive charge.**

that there are between 1000-2000 active thunderstorms at any given time (Raymond and Tzur, 1986).

### 1.1.1 Thunderstorm characteristics

In most convective storms that produce lightning, initial electrification (growth of the electric field before the first occurrence of lightning) can be observed in as little as 5-10 minutes after cloud growth begins (Krehbiel, 1986). Typically, the charge distribution in the early stages of development of isolated convective thunderstorms is that of an electric dipole.

Figure 1.2 (Krehbiel, 1986) is a qualitative illustration of observations showing that the main body of negative charge is typically confined to the region between approximately -5 to -25°C for a large range of geographical locations and seasons. There is a more diffuse positive charge

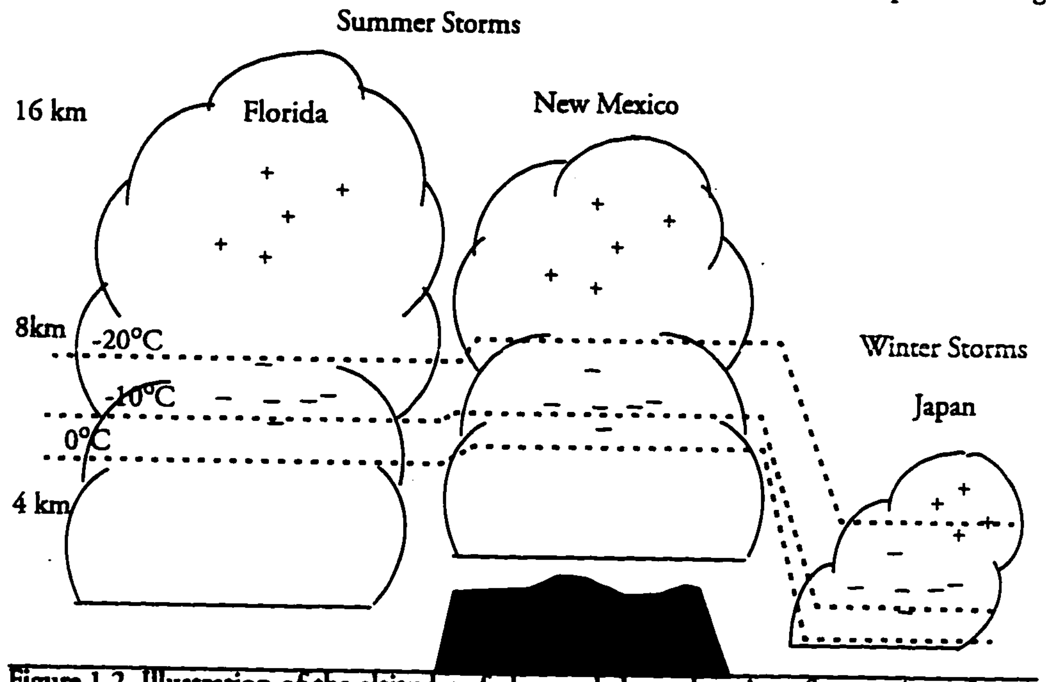


**Figure 1.2. Illustration of the altitudes of observed charge locations for a variety of storms (from Krehbiel *et al,* 1980).**

zone above the lower negative and sometimes a smaller positively charged region at lower altitudes (eg, Latham, 1981; Williams, 1989). The electric field of the in-cloud charges drives screening currents that cause charge to accumulate at the cloud boundary due to the relatively low conductivity of cloudy air. More recent electric field observations taken with instrumented balloons and rockets (Marshall *et al,* 1995b) suggest that active thunderstorms may have six or more alternating charge layers.

Electric field observations made outside of clouds have been used to identify the altitudes and magnitudes of the main bodies of charge. In South Africa, Malan (1963) calculated that about

+10 C of charge was located at an altitude of 2 km, -40 C at 5 km and +40 C at 10 km. In Japan, Huzita and Ogawa (1976) calculated that +24 C of charge was located at 3 km, -120 C at 6 km and +120 C at 8.5 km. In-cloud observations of the electric field and charge densities give magnitudes of charge that are similar to the out-of-cloud observations (Uman, 1987).

In recent literature (eg Marshall *et al*, 1995a,b) the maximum observed electric field within thunderclouds rarely exceeds 150 kV/m and all reported electric fields are far below the electric field needed for electrical breakdown, $E_{breakdown}$, of dry air at sea level, 2600 kV/m. Only at altitudes greater than ~20 km, greater than typical maximum cloud top heights, are the largest of the reported electric fields near the magnitude of the electric field needed for electrical breakdown.

### 1.1.2 Thunderstorm charging mechanisms

There are two classes of mechanisms proposed for electrification of thunderstorms: convective and precipitation based. In the former, convective air motions are responsible for separating charge generated outside the cloud via corona discharges at the surface and ionization from cosmic rays and radiation. In precipitation based mechanisms, hydrometeors are responsible for separating charge.

Vonnegut (1951), the author of the convective theory, suggests that initially positive space charge near the surface of the earth is "caught" by aerosols and carried upward in the cloud. In turn, negative charge is attracted to cloud top and is carried downward by downdrafts along the side of the cloud. Though this hypotheses can explain the generally observed dipole structure, it does not explain the observation that the negative charge region is consistently found in the same temperature range for storms forming in vastly differing regions, or the absence of lightning in warm rain clouds (those without any ice present) (Krehbiel, 1986).

Many different precipitation based charge separation mechanisms have been suggested. All are based on the idea that charge is transferred, or separated, during collisions between hydrometeors and that the charged particles are separated because of differing fall velocities. Inductive charge transfer by colliding ice and graupel was proposed by Muhler-Hillebrand (1954) in which the amount of charge transferred depends on the magnitude of the in-cloud electric field. According to this hypothesis, particles residing in an electric field have a polarization charge on their surface. Small rebounding particles carry some of the charge away when they strike the surface. Latham and Mason (1962) conducted experiments in which ice crystals bounced off ice targets and found that the induced charge transferred was negligible because the contact time was too short to allow for electrical relaxation. The inductive mechanism also does not account for observations of highly charged particles found in the early stages of thunderstorm development and cannot, by itself, explain the magnitude of charge observed on particles (Saunders, 1993).

Recent laboratory observations (Takahashi, 1978; Jayaratne *et al*, 1983; Baker *et al*, 1987; Saunders *et al*, 1991) have shown that non-inductive ice-hail collisions are capable of separating large amounts of charge that are independent of the magnitude of the in-cloud electric field. Generally these laboratory observations show that over a given range of temperatures and liquid water contents, consistent with those observed within the mixed phased region of clouds, a riming hail particle charges negatively (see Figure 1.3) after

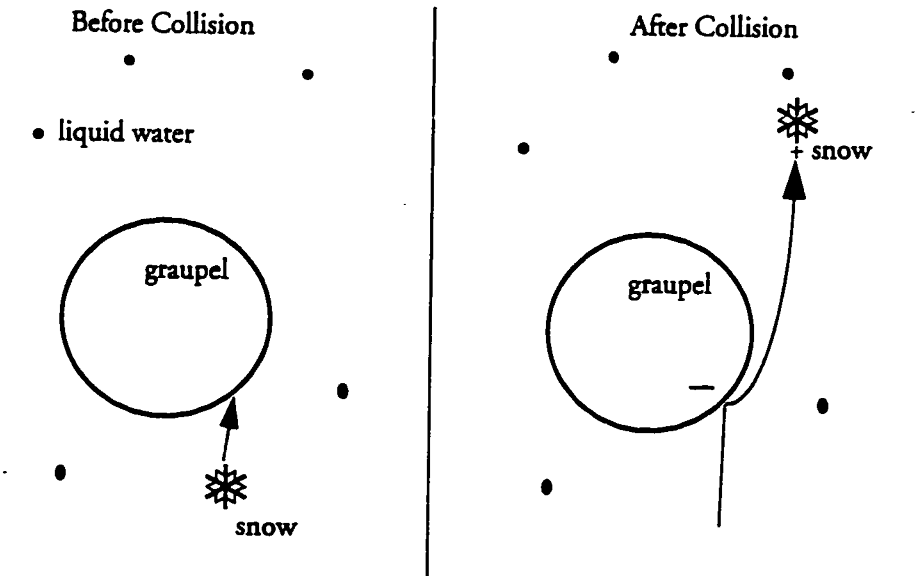


**Figure 1.3. Illustration of the non-inductive ice-ice charge separation mechanism resulting in negatively charged graupel and a positively charged snow crystal.**

collision with an ice particle. Takahashi (1978) and Saunders *et al* (1991) have shown that the magnitude and sign of the charge transferred to each particle in these collisions are strong functions of the liquid water content and temperature. For high liquid water contents at any temperature graupel charges positively; for intermediate values of liquid water the sign of charge received by graupel changes from positive to negative at some temperature, $T_{rev}$, though the two sets of experiments give slightly different values of the temperature and liquid water content at which the sign of charge is observed to switch. At low liquid water contents graupel is observed to charge positively, though again, the two experiments give somewhat conflicting results as to the values of temperature and liquid water content where the graupel charges positively (see Figure 1.4).

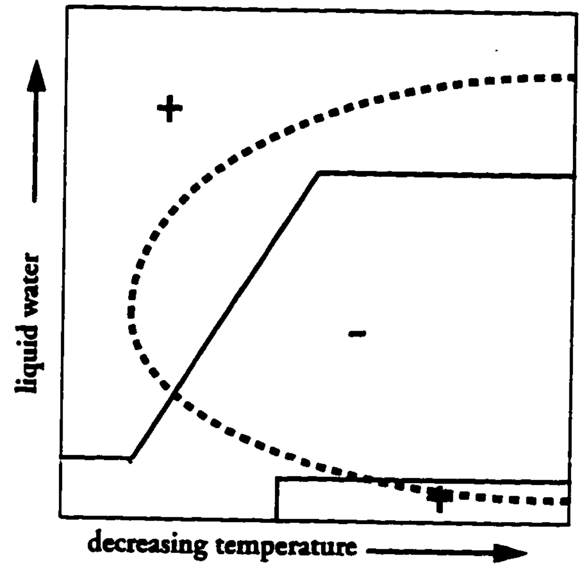


**Figure 1.4. Schematic of the sign of charge received by graupel during non-inductive ice-graupel collisions. Regions demarcated by the solid lines are the charging regions observed by Saunders *et al* (1991). The region enclosed by the dotted line is the negative charge region observed by Takahashi (1978).**

The physical processes responsible for non-inductive charge transfer are not well understood (Saunders, 1993). Baker *et al* (1987) explain the sign of charge in ice-graupel collisions as a function of temperature in terms of the growth rates of the two colliding particles. Baker and Dash (1989) suggested that the charge transfer is due to an excess of negative ions in the melt layer on the surface of the ice particles. According to the hypothesis, charge transfer is accompanied by some amount of mass transfer.

Saunders (1994) compares the predictions of various theories of charging with laboratory observations of charge generated by ice-graupel collisions (shown in Figure 1.4). Only the charging mechanism suggested by Baker and Dash (1989) explains the variation of the sign of charge separated with variations in temperature and liquid water content found in laboratory observations.

Non-inductive charge transfer between ice and graupel requires the coexistence of ice, graupel and supercooled liquid water. The charging zone is defined as that region where ice, graupel and supercooled liquid water coexist. After ice and graupel collide, the negatively charged graupel, whose fall velocity is comparable to the updraft velocity in the charging zone, is suspended within the charging zone or sediments downward and the positively charged ice crystals are carried upward in the cloud. Numerical model results support the idea that the ice-ice collision mechanism can generate and separate enough charge to achieve the electric fields observed within lightning producing clouds (Norville *et al*, 1991; Ziegler *et al*, 1991; Helsdon *et al*, 1987; Solomon and Baker, 1994). Field studies support the idea that the dominant charge carriers are graupel and snow for negative and positive charge respectively (eg, Gardiner *et al*, 1985; Dye *et al*, 1986). Once a sufficient amount of charge has been separated to raise the electric field at some point in-cloud to the value necessary for local breakdown, lightning is initiated.

## 1.2 Lightning

Cloud-to-ground lightning, that which is most often observed directly, is a large electric discharge, usually over distances of several kilometers, between the lower regions of the thunderclouds and the ground. There are around 40 million cloud-to-ground lightning flashes within the United States each year (Orville, 1986). However, the most common form of lightning is intracloud lightning, a discharge which develops between regions of opposite charge within thunderclouds.

### 1.2.1 Lightning initiation

Little is known about lightning initiation which appears to occur when the magnitude of the electric field is $\sim \frac{1}{10}E_{breakdown}$. After a period of "preliminary breakdown" within the cloud, lasting tens of milliseconds (Uman, 1987), a branched discharge propagates bi-directionally away from the initiation point (Mazur, 1989; Mazur and Ruhnke, 1993).

One theory (Latham, 1981) reconciling the low values of in-cloud breakdown electric fields suggests that the electric field is accentuated near the ends of ice crystals or near the filaments created from glancing collisions between rain drops. Electrons in this locally enhanced electric field collide with molecules, generating an electron avalanche. However, the spatial extent of the high fields needed to initiate lightning seems to be much greater than that of the hydrometeor enhanced electric field.

Another theory suggests that breakdown is the result of electron avalanches created by high energy cosmic rays (Gurevich *et al*, 1992). Comic rays with sufficiently high energy (approximately 1.8 MeV), can accelerate in the relatively low electric fields present within thunderstorms and produce an avalanche of high energy ("runaway") electrons. The "debris" of electrons and ions left in the wake of the high energy cosmic ray is thought to constitute the lightning channel.

**1.2.2 Cloud-to-ground lightning**

In a cloud-to-ground lightning flash there is a downward propagating streamer (generally negative) called the stepped-leader. The stepped-leader typically propagates in steps of tens of meters with a propagation time of 1 μsec and a pause of 50 μsec after each step. The average leader travels at approximately $2x10^5$ m/s and has a current around 100-1000 A. The potential at the tip of the descending stepped leader is in excess of $10^7$ V. As the stepped-leader approaches the ground, large electric fields are generated at the surface near sharp points and irregularities on the surface of the earth, causing breakdown of the air. One or more upward propagating discharges are initiated at the ground, traveling from the ground toward the downward propagating stepped-leader. When the two make contact, the stepped leader is brought to ground potential as a ground potential wave, and the return stroke travels upward. The return stroke is the brightest phase of the lightning stroke with peak currents around 40,000 amps, a channel temperature of 30,000 K and energies around $10^9$ to $10^{10}$ Joules. The return stroke propagation velocity is around $10^8$ m $s^{-1}$. After 40 to 80 milliseconds, most cloud-to-ground flashes produce a new leader, called a dart leader, which propagates down the previously established channel and initiates another return stroke. This may continue two or more times and in rare cases over 20 times. Charges transferred during cloud-to-ground flashes average between 20-30 C but vary from around 1 to more that 200 C (Uman, 1987)

Kasemir (1960) and Mazur and Ruhnke (1993) present a conceptual model of the lightning discharge as a propagating plasma consisting of a positive and negative streamer moving away from each other. Concurrent with the development of the stepped-leader, a highly branched positive leader propagates away from the stepped-leader, The growing branches act like current producers and current production continues only as long as the branches continue to propagate. When the branches cease propagation, all lightning process come to an end.

Observations (e.g., Krehbiel, 1981; Goodman *et al*, 1988; MacGorman and Nielsen, 1991; Laroche and Mary personal communications) suggest that initially storms produce only intracloud lightning channels. As the storm ages, cloud-to-ground channels are initiated. Data obtained via the Systeme de Surveillance et d'Alerte Foudre par Interferometrie Radioelectrique (SAFIR) also suggests that the initiation points for cloud-to-ground lightning channels are lower than those for intracloud channels. Murphy *et al* (1996) give observations of cloud-to-ground lightning that suggest the lower positive charge often observed below the main body of negative charge in thunderstorms is important in the initiation of cloud-to-ground flashes. The mechanisms by which this lower positive charge forms have not been established. Suggested sources for this lower positive charge are positive corona from the ground, the descent of positively charged precipitation (Krehbiel, 1986), breakup charging of droplets (McTaggart-Cowan and List, 1975), the recirculation of positively charged snow and charge redistribution due to lightning.

In addition to the more common, negative cloud-to-ground lightning, some cloud-to-ground flashes are observed to lower positive charge to ground (see, for example, Brook et al, 1989 and Rutledge *et al*, 1990). These positive cloud-to-ground flashes may be initiated in storms growing in environments with a large amount of shear. The tilted dipole of the cloud may be sufficient to allow for the upper positive charge region to initiate a cloud-to-ground channel. Lightning channels may be initiated at the ground and travel upward to the cloud; these are typically initiated from the peaks of mountains or other large structures (Uman, 1987) and will not be dealt with here.

### 1.2.3 Intracloud lightning

Intracloud lightning has been studied much less than cloud-to-ground lightning due to the difficulties in obtaining direct measurements and the interest in the damage caused by cloud-to-ground lightning. Observations show that the total duration of an intracloud flash is about the same as that of a cloud-to-ground flash. Charges transferred during intracloud flashes range between 1 C and 60 C with a mean of 20 C (Uman, 1987). Intracloud lightning flashes are thought to be vertically oriented during early stages of cloud evolution but as the storm matures, other channel orientations may be observed as charge moved by previous lightning flashes and precipitation create strong horizontal fields (Liu and Krehbiel, 1985).

### 1.2.4 Intracloud/cloud-to-ground lightning ratio

The ratio of the number of intracloud, $N_{IC}$, to number of cloud-to-ground, $N_{CTG}$, lightning flashes is defined as

$$R \equiv \frac{N_{IC}}{N_{CTG}} \qquad \text{(EQ 1.1)}$$

The factors determining R and its variation with storm life, location and duration are unknown. Prentice and Mackerras (1977) found the largest value of R in the tropics with R decreasing with increasing latitude.

Several hypotheses have been advanced to explain the observed variation of R with cloud and/or environmental parameters. Pierce (1970) suggested that the higher freezing levels associated with clouds in lower latitudes lead to a lower probability for cloud-to-ground flashes in the tropics. Price and Rind (1993) attribute the higher ratio at the equator to an increase in the depth of the cold sector of the cloud (the depth of the cloud above the freezing level) in tropical convective clouds. The larger cold sector favors more intracloud lightning, thereby raising the ratio at low latitudes.

As the storm ages the total charging rate decreases as the updrafts subside and less graupel can be supported by the cloud. This will be observed as a decrease in the cloud reflectivity and an increase in the precipitation measured at the ground. As the charge centers lower, the ratio of intracloud and cloud-to-ground lightning flashes change (in favor of increased cloud-to-ground flashes). Goodman *et al* (1988) gives an example of a storm where cloud-to-ground lightning begins only after the center of mass of the storm has reached a maximum in altitude and begins to descend. This period is also marked by a decrease in the total lightning flash rate. The precipitation characteristics change as well, with an increase in precipitation rate as large particles fall then decreasing as smaller particles fall.

## 1.3 Lightning Climatology

With the recent advent of satellite observation platforms, we have global data on the variations in lightning with season, time of day and latitude. Orville and Henderson (1986) published satellite observations of the number and density of lightning flashes observed at midnight local time from the DMSP satellite. The observations showed that lightning appears predominantly over land. More recent satellite platforms, such as the Optical Transient Detector (OTD), have been able to observe lightning at all times of the day. Figure 1.5 shows

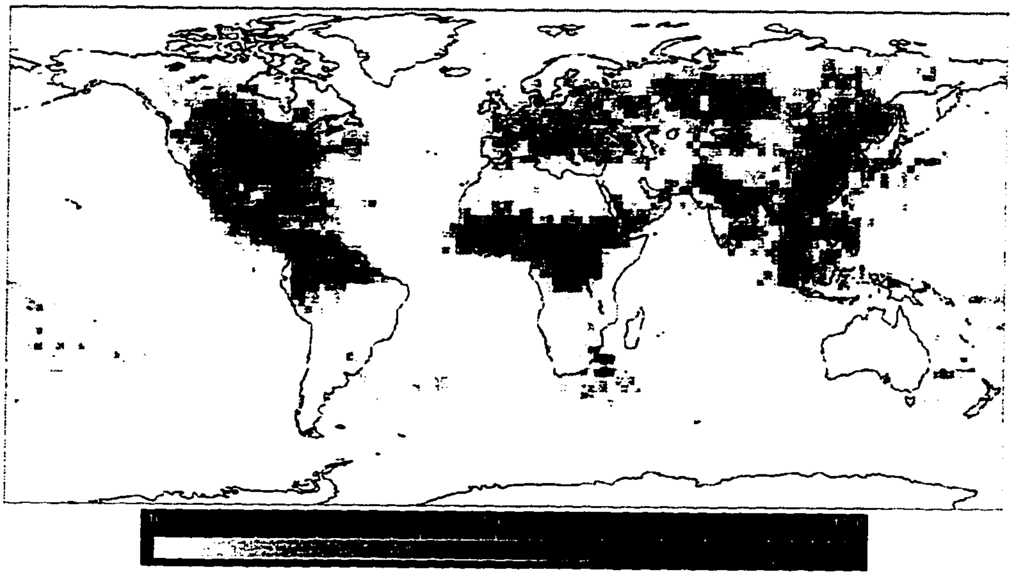

**Figure 1.5. Average hourly lightning flash rate per 2.5° x 2.5° latitude-longitude grid for June, July and August of 1995 as measured by the Optical Transient Detector (taken from Christian *et al*, 1996).**

the average hourly lightning flash rate per 2.5°x2.5° latitude longitude grid for June, July and August of 1995 as measured by the OTD (Christian *et al*, 1996). Again, there is a very strong tendency for continental storms to produce more lightning than maritime storms, although (not easily seen in this figure) warm currents on the Gulf Stream seem to be associated with relatively high lightning flash rates (Biswas and Hobbs, 1990).

Observations taken during the Down Under Doppler and Electricity Experiment (DUNDEE) have shown lightning flash rates up to 60 $min^{-1}$ in storms forming from continental air masses but lightning flash rates rarely higher than 10 $min^{-1}$ and more often no electrification in maritime environments, despite heavy precipitation in both (Rutledge *et al*, 1992). There are several possible reasons for these differences. The soundings in which clouds grow are noticeably different in the two regimes. Tropical maritime environments typically have low amounts of convectively available potential energy (CAPE) (between 0 and 1000 J $kg^{-1}$) and potential wet bulb temperatures at the surface, $\theta_w$(surface), (less than approximately 25°C) but high boundary layer moisture values, while tropical continental environments tend to be drier and have higher CAPE and $\theta_w$ (both CAPE and $\theta_w$ will be defined below). Radar images suggest that maritime clouds rarely have high reflectivity regions extending above the freezing level (Rutledge *et al*, 1992). Without snow, graupel and liquid water present at these colder temperatures, the onset of electrification is unlikely.

Observations (eg, Twomey and Wojciechowski, 1969) show the number concentration of cloud condensation nuclei (CCN) over oceans is much lower than over continental regions. Low numbers of CCN can result in broader droplet spectra (Squires, 1958). A broader droplet spectrum allows for faster removal of water from the cloud as precipitation than in continental storms with a narrow droplet spectrum. As liquid water is removed by precipitation, a smaller amount of liquid is injected into the charging zone, decreasing the potential for large amounts of charge separation. The formation of large riming graupel particles would also be hindered, decreasing the likelihood of storm electrification.

Precipitation is an extremely important variable in the climate system and one that is very difficult to measure over large regions of the globe. Since the microphysical processes leading to lightning appear to be collisions involving precipitation particles, and since lightning frequency is now easily monitored from space on global scales, it is tempting to consider the use of lightning flash rate, as observed from space, as a surrogate for precipitation. Buechler *et al* (1990) give observations of 21 storms taken on 6 days over the Tennessee Valley region showing an increase in the peak convective rain flux with increasing peak flash rate. Analysis of individual storms from the same project (Goodman and Buechler, 1990) give a good correlation between increasing flash rate and increasing rain flux. However, Williams *et al* (1992) show a comparison between precipitation and cloud-to-ground lightning for continental and monsoon storms. In this comparison, continental and monsoon storms had similar total precipitation yields though the total number of cloud-to-ground lightning flashes differed by an order of magnitude. Thus the correlation between precipitation rate and cloud-to-ground lightning flash rate depends on the type of cloud system.

## 1.4 Prediction of Storm Electrification and Lightning Flash Rate

There have been a number of suggestions linking thunderstorm electrification to measurable environmental parameters (eg, Goodman, 1990; Williams *et al*, 1992; Williams and Renno, 1991; Price and Rind, 1992), which will be referred to as "lightning predictors."

Williams *et al* (1992) shows that the total number of cloud-to-ground lightning events for tropical convective storms is closely related to the CAPE of a parcel raised from cloudbase, $Z_{cb}$, to cloudtop, $Z_{ct}$.

$$\mathrm{CAPE} \equiv \int_{Z_{cb}}^{Z_{ct}} g \frac{(T_{v,\,ad} - T_{v,\,env})}{T_{v,\,ad}} dz \qquad \text{(EQ 1.2)}$$

where $T_{v,env}$ and $T_{v,ad}$ are the virtual temperatures in the environment computed from soundings along a reversible moist adiabat through cloudbase at $Z_{cb}$. Environments with low levels of CAPE, eg, the Monsoon season, had relatively few cloud-to-ground lightning flashes. High CAPE environments produced much more cloud-to-ground lightning. Within the tropics, Williams and Renno (1991) show that CAPE is closely related to the potential wet bulb temperature at the surface, $\theta_w(z=0)$, which is the temperature at which the pseudoadiabat through the isentropic condensation point of air at the surface intercepts the isobar $p = 1000$ mb (Rogers and Yau, 1989). This suggests that the surface conditions dictate the future electrical state of storms forming in tropical environments. Solomon and Baker (1994) show that CAPE is a reasonable predictor for the future electrical state of storms forming in New Mexico; however, CAPE and $\theta_w(z=0)$ are not related for midlatitude continental storms forming in New Mexico.

Simple parcel theory predicts that updraft velocities are low in storms forming in low CAPE environments. This results in a small liquid water flux into the charging zone and an inability to suspend the large riming particles necessary for charge separation in the charging zone. Randell *et al* (1994) modelled several tropical storms forming in a variety of environments having low, high and no CAPE. These different environments represent monsoon, continental and stratiform conditions. They find that CAPE is related to the altitude at which the sign of charge received by graupel particles during non-inductive ice-graupel collisions changes sign, $Z_{rev}$, and the height at which the updraft velocity matches the fall velocity of hail/graupel, $Z_{bal}$. For low CAPE environments, the difference between $Z_{bal}$ and $Z_{rev}$, $\delta Z_{cz}$, is small and little charge is generated. For high CAPE environments $\delta Z_{cz}$ is large and there is a much larger depth of cloud that can efficiently separate charge. The zero CAPE case, generates an inverted dipole structure which may account for the large number of positive cloud-to-ground flashes observed from electrified stratiform clouds.

However, since tropical continental and tropical maritime storms may have similar maximum cloud top heights but drastically different electrical characteristics (Rutledge *et al*, 1992), the maximum cloud top height, $Z_{ct,max}$, is not a very reliable predictor in that environment. The physical mechanism linking $Z_{ct,max}$ and lightning flash rate in some circumstance but not others has not been established.

Cherna and Stansbury (1986) have shown that the lightning flash rate is related to the cloud area, though cloud top height is the dominant parameter determining lightning flash rate for isolated thunderstorms near Montreal, Canada. Price and Rind (1992) found that the global lightning flash rate fit an empirical relationship between the maximum total flash rate, F, and cloud top height,

$$F = 3.44 \times 10^{-5} Z_{ct,\,max}^{4.9} \qquad \text{(EQ 1.3)}$$

where $Z_{ct,max}$ is the maximum cloud top height suggesting that the vertical cloud volume (especially that above the freezing level) is very important in determining the electrification/charging rate.

Goodman (1990) shows that the lifted index, $L_i$, defined as the difference at 500 mb between the temperatures of the environment and of a parcel of air raised adiabatically to 500 mb from the lowest 100 mb of the sounding, correlates well with total cloud-to-ground lightning. Goodman also shows that $L_i$ is better correlated to the total number of cloud-to-ground lightning than CAPE for storms observed in the Southeast United States.

Thus, CAPE, $\theta_w(z=0)$, $Z_{ct,max}$ and $L_i$ have all been linked to lightning flash rate climatologically. These relationships are largely empirical; they have been proposed on the basis of observed climatological correlations. The predictors we shall consider are:

1. Convectively Available Potential Energy (Williams *et al*, 1992),
2. Potential Wet Bulb Temperature, $\theta_w(z=0)$ (Williams and Renno, 1991),

3. Maximum Cloud Top Height, $Z_{ct,max}$ (Price and Rind, 1992),

4. Lifted Index, $L_i$ (Goodman, 1990).

These predictors are, in any case, only partially successful. Seemingly small variations in environmental quantities can have drastic effects on the nature of electrical development of storms. This is well illustrated in New Mexico during the summer, where storms form from an intrusion of moist air from the south which has similar properties on those days that it occurs (Blyth and Latham, 1993). Variation in horizontal winds are small and the magnitude of the vertical shear is typically less than $10^{-3}$ $s^{-1}$. With very light winds, storms remain attached to the mountain range or drift very slowly (Dye *et al*, 1989). Storms in this rather steady meteorological environment exhibit a broad range of electrical activity. Some storms develop quite rapidly, producing intense thunderstorms. Other storms in the same environment on the same days show moderate or weak growth rates; some become electrified, and others do not. (Dye *et al*, 1989; Solomon and Baker, 1994).

Since the first step in electrification is non-inductive charge transfer between colliding ice crystals and graupel, electrification requires that updrafts loft and maintain the supply of liquid water and graupel in the charging zone for the time necessary to build up electric fields to the threshold magnitude for the initiation of lightning. Solomon and Baker (1994) suggested that the cloud updraft velocity must exceed a threshold value for a minimum length of time for New Mexico summer storms to become electrified. Those storms that did not meet the criterion did not become electrified or were only weakly electrified, producing no lightning. The range of observed electrical activity in this region, unmarked by large deviations in soundings, demonstrates that the electrical activity is strongly influenced by parameters not reflected in the soundings alone. A similar conclusion follows examination of observations taken in Florida which show that during the summer, land heating produces deep convection in the afternoon. Interactions between the synoptic wind field and the sea-breeze circulation are very important in determining the timing and locations of convective activity, as well as its severity (eg, Neumann, 1971; Pielk, 1974). On the other hand, We have already alluded to the strong correlations of lightning occurrence with CAPE, surface temperature and cloudtop observed in climatological studies by Williams *et al* (1992), Price and Rind (1992), Zipser (1994), Zipser and Lutz (1994) and others.

The physical and particularly the microphysical processes linking these environmental predictors and the subsequent electrical development of storms are not well understood. In order to understand the relative success (or lack of success) of these predictors, we need a better understanding of the in-cloud processes responsible for determining the electrical state of clouds.

Since the dominant charging mechanism is dependent on the sizes and concentrations of graupel particles and ice crystals in the charging zone, it is reasonable to assume that CCN concentrations, primary and secondary glaciation rates are important in the determination of lightning flash rate. Another important consideration is variations in the altitude where significant amounts of ice are formed. If ice production is only significant at high altitudes (above the charging zone), charging will be inefficient.

We wish to understand the observed correlations between the cloud electrification and lightning flash rate with the predictors in terms of the in-cloud processes these predictors represent.

The previous discussion gives a general background on thunderstorms and lightning leading to a set of questions which form the basis of the research to be described in this dissertation. In particular these questions relate to semi-tropical/mid-latitude continental and tropical maritime storms.

1. Which factors are most important in determining whether tropical maritime, semi-tropical continental and mid-latitude continental storms become electrified?
2. Why is there typically more lightning (total and cloud-to-ground) over semi-tropical and mid-latitude continental land masses than over tropical marine environments?
3. What factors influence lightning flash rates in tropical marine/continental and mid-latitude thunderstorms?
4. What factors influence the intracloud/cloud-to-ground lightning ratio in tropical maritime, semi-tropical continental or mid-latitude continental storms?
5. What are the relationships between lightning flash rate and precipitation in isolated convective thunderstorms forming in tropical maritime, semi-tropical continental or mid-latitude continental environments?

## 1.5 Methodology and Organization

In order to answer the questions raised, we simulate isolated convective thunderstorms under a variety of environmental conditions using a numerical cloud model, and compare these results to observations taken from a wide variety of locations in which storms develop. The model will be used to generate a large number of sensitivity tests to various environmental parameters. We will focus on the trends predicted by the model to understand the processes that are important in determining the onset of storm electrification and lightning characteristics. Though quantitative details of some of the processes (the charging mechanism for example) are to some extent uncertain, we show our model reproduces observed trends and correlations of electrical behavior with environmental characteristics, and that it is a useful tool for understanding the in-cloud processes responsible for these trends.

We outline the thunderstorm model in Chapter II. In Chapter III, we summarize observations of non-electrified and electrified clouds forming in a variety of environments and compare modelled thunderstorms with observations. In Chapter IV, we examine how variations in environmental conditions influence initial electrification, lightning flash rate and the ratio of intracloud to cloud-to-ground lightning. Chapter V contains the conclusions and summary.

# II. The Thunderstorm Model

## 2.1 One and a Half Dimensional Cloud Model

Modelling of cumulus clouds, and especially thunderstorms, is challenging due to the wide range of important spatial and temporal scales. The usual approach to this task has been to explicitly model the processes of interest and to parameterize the others. Since charge transfer mechanisms are sensitive functions of particle size (Saunders *et al,* 1991), this goal can be met only by explicit representation of the size dependent microphysical processes. We employ a one-and-a-half dimensional dynamic model for dynamic simplicity and short execution time for simulations. The geometric simplicity also allows for the inclusion of a lightning parameterization (Solomon and Baker, 1996) whereas this task becomes increasingly difficult in higher dimensions and severely decreases the number of simulations for sensitivity tests due to computational times. The following chapter describes the cloud model (based on that of Taylor, 1989 and Norville *et al,* 1991), hereafter referred to as FILIGREE.

### 2.1.1 Dynamics

The dynamics in FILIGREE are based on those of Asai and Kasahara (1967) and Yau (1980). The model domain is axi-symmetric, consisting of three communicating coaxial cylinders: inner and outer cloudy regions and an unsaturated environment (see Figure 2.1). FILIGREE

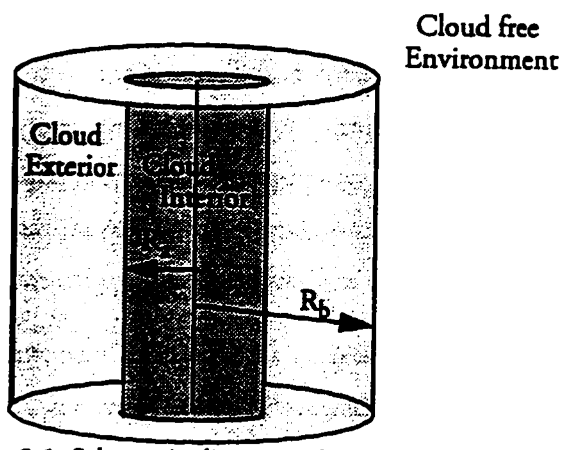


**Figure 2.1. Schematic diagram of the model geometry with two connecting cloudy cylinders with radii A and B.**

retains all the original dynamic equations of Taylor (1989).

**Cloud base forcing**

The air entering the base of a convective cloud does not necessarily have the same thermodynamic and for dynamic properties as the surrounding air. The differences between the temperature and/or velocity of the cloudbase air and those of the environment at the level of cloudbase are referred to as 'cloudbase forcing' parameters. FILIGREE employes two types of forcing:

1. 'kinetic,' or momentum forcing:

$$F_{kin} \equiv w_{cb} \qquad \text{(EQ 2.1)}$$

where $w_{cb}$ is the updraft velocity of air entering cloudbase, assumed to have the thermodynamic properties of the environmental air at that level, and

2. 'thermal' forcing:

$$F_{th} \equiv \delta T_v \qquad \text{(EQ 2.2)}$$

where $\delta T_v$ is a temperature perturbation in excess of the environmental temperature, $T_{v,env}$, at cloudbase altitude.

In the 'real' world, of course, cloud forcing is some combination of these effects and can arise from many different mechanisms. For example, convergence of air near the surface of the Earth will result in upward, "kinetic forcing" or solar heating of the land can create a source of "thermal forcing." The strength of forcing is not usually known from soundings. Using a range of forcings, the effects of both types of forcing on cloud development can be compared. If it appears that the two produce similar results (insofar as electrification is concerned) then for our purposes, it is not so important to know how Nature splits energy between them.

FILIGREE is initialized with a sustained velocity and/or a cloud base temperature perturbation. For the duration of the cloud-base forcing, the water vapor mixing ratio is set to the cloud base value for $Z < Z_{cb}$, and the sub-cloud temperature lapse rate is assumed to be adiabatic. At the end of the forcing period the water vapor and temperature profiles are set to environmental values. We discuss the artifacts produced by this procedure in later sections.

### 2.1.2 Microphysics

The evolution of the water and ice microphysical distributions are explicitly calculated. The microphysical processes included are growth by deposition, riming and collection, melting, drop breakup and primary glaciation and secondary ice production via the Hallet-Mossop process. The basic microphysical equations are taken from Norville *et al* (1991). However, the model of Norville *et al* utilized a kinematic framework where the model of Taylor (1989) was used to generate the temperature and velocity fields which were used to drive to the microphysics. We have replaced the parameterized microphysics of Taylor with the explicit microphysics used by Norville *et al* in addition to expanding the microphysical processes to include more warm rain processes.

**Mass grid**

Water and ice particle masses are defined on a common grid (as in Berry, 1967). The mass of particles in the *i*-th mass bin is

$$M_i = M_0 2^{((i-1)/2)} \qquad \text{(EQ 2.3)}$$

where $M_0$ is the mass of the lowest category, $M_0 \sim 5\times10^{-10}$ g. There are 80 mass categories for water and ice. Cloud condensation nuclei (CCN) and ice condensation nuclei are assumed to be spherical particles with a radius of 0.25 μm.

**Ice density**

Each ice category has an associated density and all particles are assumed to be spherical. This assumption may be reasonable for larger particles but small ice crystals have distinctly non-spherical shapes. To compensate for the error introduced by assuming spherical particles, the ice density for non-riming ice crystals is set to 0.1 g cm$^{-3}$. This value is the ice crystal density needed to give a sphere the same radius as a plate with the same mass (Norville *et al*, 1991). Ice crystals have diameters less than a critical riming diameter, $D_r$. For diameters greater than $D_r$, the value of the density of riming particles with mass $M_f$ is given by

$$\rho(M_f) = \rho(M_d) + \int_{M_d}^{M_f}\left(1 - \frac{\rho(M)}{\rho_a(M)}\right)\frac{dM}{\mathrm{Vol}(M)} \qquad \text{(EQ 2.4)}$$

$M_d$ is the mass of a particle with diameter D, Vol is the volume of the particle and $\rho_a$ is the density of the accreted rime,

$$\rho_a = \begin{cases} \rho_{light} = 0.11A^{0.76} \\ \rho_{medium} = 0.30A^{0.4} \end{cases} \tag{EQ 2.5}$$

where

$$A = -\frac{rV_{imp}}{T_{surf}} \tag{EQ 2.6}$$

and r is the radius of the cloud droplets impacting with velocity $V_{imp}$ on a target with surface temperature $T_{surf}$.

The light density case is based on the experiments of Macklin (1962) who studied the riming behavior of a cylinder to simulate hailstone growth. The medium density case was derived by Heymsfield and Pflaum (1985) for the riming behavior of free falling graupel.

**Fall velocities**

Fall velocities for drops and small ice particles are taken from Berry and Pranger (1974) while larger ice crystal and graupel fall velocities are taken from Heymsfield (1978). The Berry and Pranger fall velocity is a function of the Reynolds number and the drag coefficient which is only dependent on environmental temperature and pressure. Heymsfield uses empirical expressions derived from an observational analysis of summertime graupel.

**Vapor deposition**

Both water and ice particles grow via the deposition of vapor following the familiar explicit expression for spheres growing in a constant vapor field (Pruppacher and Klett, 1978). The depositional growth equation for n(M), the number concentration of particles with mass M, has the form of an advection equation where $\frac{\partial M}{\partial t}$ is analogous to the vertical velocity in a spatial domain. Therefore an advection scheme, similar to that of Smolarkiewicz (1984), is used to solve for n(M) (Norville *et al*, 1991).

**Collision and coalescence**

Collection of droplets by larger drops is calculated using the 'continuous collection' approach (Gillespie, 1975). Particles with diameters greater than a threshold size, $D_t$, collect smaller drops. The number of *collisions* in a time step, dt, is

$$N_{collisions} = n_{small} K_{cc}(d, D)\, dt \qquad \text{(EQ 2.7)}$$

where $n_{small}$ is the concentration of smaller particles and $K_{cc}$ is the geometric collision kernel,

$$K_{cc}(d, D) = \frac{\pi}{4}(D + d)^2 |\delta v| \qquad \text{(EQ 2.8)}$$

where D (d) is the diameter of the larger (smaller) particle and $\delta v$ is the difference in the fall velocities of the colliding drops. The number of particles *collected* per time step is $N_{collisions}$ times the sticking efficiency, $E_{si}$. Collision efficiencies are assumed to be 1.0 for drop-ice interactions, drop-drop sticking efficiencies are taken from Hall (1980) and ice-ice sticking efficiencies are set to a specified constant, 25%.

**Drop breakup**

Breakup of large unstable drops can be a significant factor governing the shape of the drop size distribution (Srivastava, 1971). Komabayasi *et al* (1964) suggested that the probability of breakup for a drop with diameter D [cm] is

$$P[\sec^{-1}] = 2.94 \times 10^{-7} e^{-17D} \qquad \text{(EQ 2.9)}$$

This gives a 100% probability for breakup for drops with D > 0.88 cm. The breakup of a drop gives rise to a size distribution of the fragments

$$N(d, D_0) = \frac{2ab}{D_0} \exp\left(-b\frac{d}{D_0}\right) \qquad \text{(EQ 2.10)}$$

where $N(d,D_0)$ is the number distribution of droplets with radius d resulting from the breakup of a drop with radius $D_0$, b is a constant determined from observations (b = 7) and a is computed to insure mass conservation (a = 63.4).

**Ice nucleation**

The prediction of primary ice-crystal concentrations in numerical cloud models is difficult since ice-nucleation is poorly understood. One popular method used to predict ice-crystal concentrations has been to use a temperature dependent function based on the compilation of ice-nuclei concentrations (e.g. Fletcher, 1962):

$$IN = \alpha e^{\beta(T_0 - T)} \qquad \text{(EQ 2.11)}$$

where IN [#/m$^3$] is the number of ice nuclei, T is the temperature, $T_0$ = 273.16 K, $\alpha$ and $\beta$ are parameters found from laboratory experiments with freezing drops ($\alpha$ = 0.01 m$^{-3}$ and $\beta$ = 0.6 K$^{-1}$).

This method typically underestimates ice-crystal concentrations at warm temperatures and greatly overestimates concentrations when extrapolated to temperatures below those for which it is valid (~ -25°C) (Meyers *et al*, 1992).

Based on a number of observations of ice concentration versus ice supersaturation, Meyers *et al* (1992) parameterize the number of pristine ice crystals predicted due to deposition-condensation freezing, $N_{id}$, as

$$N_{id}[l^{-1}] = e^{(j + k(S_i - 1))} \qquad \text{(EQ 2.12)}$$

where j and k are constants (j = -0.639 and k = 0.1296) and $S_i$ is the ice supersaturation. In a similar fashion, Meyers *et al* (1992) also quantify contact-freezing nuclei concentrations, $N_{ic}$, by fitting a function to a number of measurements,

$$N_{ic}[l^{-1}] = e^{(f + g(T_0 - T))} \qquad \text{(EQ 2.13)}$$

where f and g are constants (f = -2.80 and g = 0.262). At -40°C all drops are assumed to freeze.

Both the Fletcher and Meyers *et al* ice nucleation parameterizations have been included in FILIGREE. In later sections we will discuss the microphysical and cloud electrification sensitivities to both parameterizations.

**Secondary ice production**

Secondary ice production in cumulus clouds can have a dramatic effect on the number of ice particles, their spectrum within the cloud, evolution of clouds and possibly their electrification. Based on experiments by Hallet and Mossop (1974), Mossop and Wishart (1978) suggest that the mechanism responsible is the fracture of symmetrically freezing droplets. When droplets greater than 24 μm in diameter strike a portion of a rimed surface where small ($d < 13$ μm) droplets have accreted, these large droplets are in poor thermal contact with the graupel and tend to freeze from the outside inward. Subsequent freezing then causes shattering of the ice shell ejecting ice fragments. Mossop (1976) found that the secondary ice production rate is proportional to a linear function of the temperature for -8°C < T < -3°C and that one secondary ice particle was produced for each 250 droplets larger than 24 μm in diameter which accreted onto a riming rod at -5°C. Mossop (1978) also found that the production rate depended on the presence of small as well as large droplets.

The production of additional ice particles by the Hallet-Mossop process is simulated within FILIGREE by using the production rate parameterization given by Harris-Hobbs and Cooper (1987).

$$P_{sip}\left[m^{-3}\sec^{-1}\right] = 4Cf(T)\int_{r_0}\int_{R_0} gK_{cc}(r, R)\,N(R)\,n(r)\,dRdr \qquad \text{(EQ 2.14)}$$

where C is a constant determined from observations ($C = 0.16 \pm 0.05$), f(T) is a linear function of temperature ($f(T) = 1.0$ at -5°C and $f(T) = 0$ at -3°C and -8°C), $r_o$ ($R_o$) is the minimum radius for small droplets (graupel) that leads to secondary ice production and

$$g = \left(\int_0^{6.5\mu m} n(r)\,r^2 dr\right) \Bigg/ \left(\int_0^{all} n(r)\,r^2 dr\right) \qquad \text{(EQ 2.15)}$$

This function represents the approximate fraction of the graupel surface covered by droplets less than 13 μm in diameter.

**Melting**

When ice particles fall into environments with temperatures greater than $T_0$, some fraction of each ice particle melts. Following Cotton *et al* (1982), it is assumed that a melting ice particle is in thermodynamic equilibrium with a surface temperature $T_0$. The melting rate is then given by

$$\left.\frac{dM_g}{dt}\right|_{melt} = \frac{2\pi D}{L_{fi}}\left[Kf(Re)\,(T - T_f) + D_{vap}f(Re)\,(\rho_v - \rho_{vsfc})\right] \qquad \text{(EQ 2.16)}$$

where $dM_g/dt$ is the amount of melt mass for an ice particle, K is the thermal conductivity of the air, $D_{vap}$ is the diffusivity of water vapor, $L_{fi}$ the latent head of freezing, f(Re) is a ventilation factor that is a function of the Reynolds number, $\rho_v$ the vapor density and $\rho_{vsfc}$ the vapor density at the surface of the ice particle. The melt mass that accumulates during a time step, i.e. $(dM_g/dt)\Delta t$, is assumed to be "sloughed" off the ice particle and a droplet having this mass is created. If the resulting drop is smaller than the smallest size allowed, no material melts during the time step.

## 2.2 Model Electrification

### 2.2.1 Non-inductive ice-ice interactions

We assume, based on field and model results (Gardiner *et al*, 1985; Dye *et al*, 1986; Norville *et al*, 1991; Ziegler *et al*, 1991) that the dominant charge transfer mechanism is that involving collisions between ice crystals and graupel, or soft hail pellets (Takahashi, 1978; Jayaratne *et al*, 1983; Baker *et al*, 1987; Saunders *et al*, 1991). The instantaneous charge separation rate depends therefore on the liquid water content, the numbers and sizes of ice crystals and of hail particles.

The net amount of charge added to a graupel particle with diameter D, via collisions with $n_{small}(d)$ [$m^{-3}$] smaller ice crystals with diameter d is

$$\begin{aligned}\Delta Q(d,D) &= n_{small}(d)\,K_{cc}(d,D)\,(1.0 - E_{si})\,\delta Q_g(d,D)\\ &\quad + Q_{small}(d)\,nK_{cc}(d,D)\,E_{si}\end{aligned} \qquad \text{(EQ 2.17)}$$

where $Q_{small}(d)$ is the charge on small ice particles with diameter d, $\delta Q_g(d,D)$ is the amount of charge transferred per collision, $K_{cc}(d,D)$ is given by Equation 2.8 and $E_{si}$ is the ice-ice sticking efficiency.

Keith and Saunders (1989) show that the charge transferred per collision to the graupel target, $\delta Q_g$, depends on the ice crystal size, d, and the speed of the target, V,

$$\delta Q_g(d, D) = Bd^a V^b q(d, D) \qquad \text{(EQ 2.18)}$$

where B, a and b depend on the crystal size and the effective liquid water content. (See Figure 1.4 for a schematic illustration of the sign of charge received by graupel during collisions as a function of temperature and liquid water content.) We adopt the functional form for the magnitude and sign of charge transferred per collision, q(d,D), given by a parameterization of laboratory experiments supplied by Saunders *et al* (1991) (personal communications Saunders, 1992).

### 2.2.2 Screening charge layer

In addition to charge arising from the non-inductive ice-ice collisional mechanism, we include charge accumulation at the cloud boundary. A layer of charge forms at the boundary between the cloud and the environment because the conductivity of cloudy air is less than that of clear air. The atmospheric conductivity is an exponential function of altitude (Driscoll *et al*, 1992).

The rate of buildup of charge, $\rho_s$ at the boundary is given by the equation

$$\frac{\partial \rho_s}{\partial t} = -\nabla \bullet \mathbf{J} = -\nabla \bullet (\sigma_a \mathbf{E}) \qquad \text{(EQ 2.19)}$$

where $J \approx J_a - J_c$ where $J_a$ ($J_c$) [A/m$^2$] is the ambient (cloud) current, $\sigma_a$ [$\Omega^{-1}$ m$^{-1}$] is the atmospheric conductivity and **E** is the electric field. We assume the conductivity of cloudy air is much less than that of clear air so that Equation 2.19 is approximately

$$\frac{\partial \rho_s}{\partial t} + \frac{\sigma_a E}{l} \approx 0 \qquad \text{(EQ 2.20)}$$

where $l$ is the screening depth in the cloud and E is the electric field perpendicular to the cloud boundary.

$l$ is determined by the model geometry parameters. At cloud top $l$ is taken to be the vertical step size, $l = \Delta z$, and at the edges $l$ is the difference between the radii of the inner and outer cylinders, $l = R_b - R_a$.

## 2.3 The One-Dimensional Lightning Parameterization†

### 2.3.1 Lightning

In general, numerical models of thunderstorms have dealt only with early stages of electrification, before the first lightning flash (Ziegler *et al*, 1991; Norville *et al*, 1991; Helsdon *et al*, 1992; Solomon and Baker, 1994). Our ability to model the later stages of thundercloud development has been hampered by the lack of reasonable representations of lightning itself and of its modification of clouds. Some previous models attempted to remedy this defect without a physically based parameterization for the distribution of charge transferred by lightning. For example, in a simple lightning parameterization, Baker *et al* (1995) prescribed the endpoints of both intracloud and cloud-to-ground flashes as well as the amount of charge transferred per flash. In their model, Ziegler and MacGorman (1994), assume that each lightning flash removes a specified amount of charge only in regions where the charge density exceeds some prescribed threshold. With this sort of model it is clearly very difficult to utilize the wealth of information now available from ground based, *in situ* and remote sensing of lightning to improve our understanding of highly electrified clouds.

Lightning initiation and propagation are intensely dynamic phenomena. We shall make no attempt to simulate these processes, but will focus only on their final results; ie the charge redistribution and field change induced by a lightning flash. For this purpose we can solve a simple electrostatic problem, based on the ideas of Kasemir (1960) and Mazur and Ruhnke (1993). According to this conceptual model, the plasma filled, bi-directional leader channel can be thought of as a conductor placed in the cloud electric field. If the lightning channel does not touch the ground, there is no net charge on it but the surface of the 'conductor' carries a spatially nonuniform charge density representing the density of induced ionic and electronic charges. This induced charge moves some distance into the cloud after a discharge, thus modifying the in-cloud charge and field distributions.

---

†. Section 2.3 is reproduced largely from Solomon and Baker (1996).

This picture of the field and charge distribution following a lightning flash was used by Helsdon *et al* (1992) to derive a parameterization of intracloud flashes for use in their two dimensional cloud model. They represented the intracloud lightning channel by a prolate ellipsoidal conductor placed with its long axis along the in-cloud electric field and centered at the point where the in-cloud electric field reached a preset value $E_{threshold}$. The length of the conductor was fixed by the requirement that the ambient field at the ends of the lightning channel fell below 150 kV/m, a value suggested by the laboratory experiments of Griffiths and Phelps (1976). As Helsdon *et al* point out, this criterion does not take into account the field of the induced charges themselves, and it does not allow cloud-to-ground flashes to develop. The fact that the Helsdon *et al* cloud model was two-dimensional makes the calculated relationship between electric fields and charge distribution somewhat unrealistic, but the lightning parameterization gave good agreement with observations when used to simulate the evolution of an intracloud flash from a storm observed during the Cooperative Convective Precipitation Experiment (CCOPE).

Building on the ideas of Kasemir, Mazur and Ruhnke and Helsdon *et al*, we derived a lightning parameterization that can be used to study both intracloud and cloud-to-ground flashes. We have derived this model (hereafter referred to as OPAL) for use in FILIGREE, so that in the present form we assume all discharges propagate vertically.

### 2.3.2 The model

#### Lightning initiation

We assume that lightning is initiated wherever the vertical electric field exceeds a predetermined value, $E_{init}$. For the tests presented in this section, the value of $E_{init}$ is assumed to be constant with height. The value roughly approximates the maximum measured electric field within clouds.

#### The lightning channel

Following Helsdon *et al* (1992), it is convenient to analyze this problem in terms of prolate spheroidal coordinates $(\xi, \eta, \varphi)$ (Morse and Feshbach, 1953). The foci of the spheroids are at x=y=0 and $z = \pm a/2$. The distances to a point (x, y, z) on the surface of an ellipsoid from the two foci are

$$r_1 = \sqrt{\left(z+\frac{a}{2}\right)^2 + x^2 + y^2} \quad \text{and} \quad r_2 = \sqrt{\left(z-\frac{a}{2}\right)^2 + x^2 + y^2} \qquad \text{(EQS 2.21)}$$

The prolate spheroidal coordinate system is defined as

$$\begin{aligned} \xi &\equiv \frac{(r_1 + r_2)}{a} && 1 \le \xi < \infty \\ \eta &\equiv \frac{(r_1 - r_2)}{a} && -1 \le \eta \le 1 \\ \varphi &\equiv \tan^{-1}(y/x) && 0 \le \varphi \le 2\pi \end{aligned} \qquad \text{(EQS 2.22)}$$

The surface of the newly created ellipsoidal conductor is defined by

$$\xi = \xi_0 = \frac{2}{a}\sqrt{R_0^2 + \left(\frac{a}{2}\right)^2} = \frac{L}{a} \qquad \text{(EQ 2.23)}$$

where L is the length of the channel and $R_o$ is its maximum radius (see Figure 2.2). Upon initiation the channel has a prescribed radius at the midpoint which remains constant throughout the development of the channel and an initial length, $L_0$.

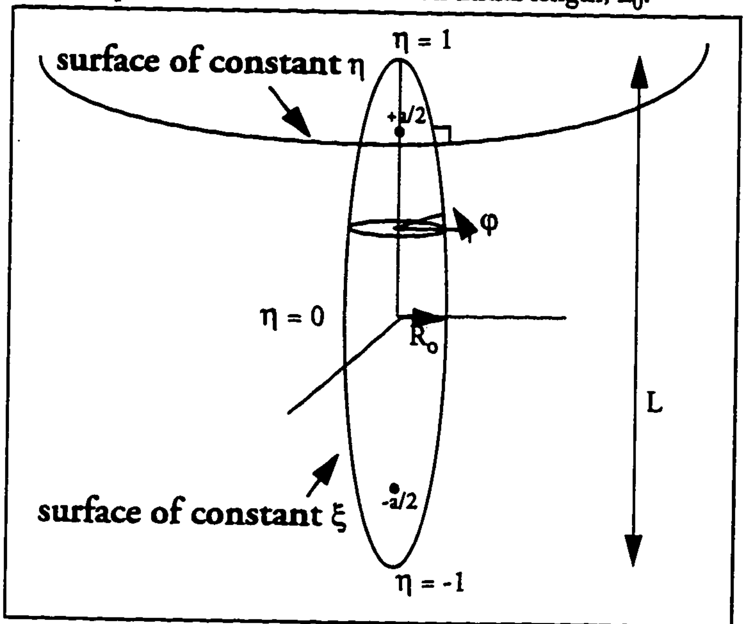


**Figure 2.2. The coordinate system used to represent the conducting channel (prolate spheroidal coordinates).**

The electrostatic potential on the surface of the conductor due to the charges on the hydrometeors is fitted to a function of the form

$$\psi_{ext}(\eta) = \sum_{n=0}^{N} V_n P_n(\eta) \qquad \text{(EQ 2.24)}$$

where $P_n(\eta)$ are Legendre polynomials of the first kind of order n and $V_n$ are constants. N is chosen to fit the potential to the desired accuracy: for the studies described here we chose $N = (L/\delta z) - 1$, where $\delta z$ is the vertical resolution of the lightning channel. The total potential on the surface of the conductor is then

$$\psi(\xi, \eta) = \psi_{ext}(\eta) + \psi_{conductor}(\xi, \eta) \qquad \text{(EQ 2.25)}$$

The electrostatic potential of the conductor is a solution to Laplace's equation which vanishes at infinity and yields zero net charge on the conductor. That is,

$$\psi_{conductor}(\xi, \eta) = -\sum_{n=1}^{N} \left[ V_n P_n(\eta) \frac{Q_n(\xi)}{Q_n(\xi_0)} \right] \qquad \text{(EQ 2.26)}$$

where $Q_n(\xi)$ are Legendre polynomials of the second kind of order n. (Note the different starting indexes for the summations).

The electric field is then

$$\mathbf{E} = -\nabla\psi \qquad \text{(EQ 2.27)}$$

where the gradient operator in prolate spheroidal coordinates is given by

$$\nabla = \frac{2}{a} \left\langle \sqrt{\frac{\xi^2 - 1}{\xi^2 - \eta^2}} \frac{\partial}{\partial \xi} \hat{e}_\xi ; \sqrt{\frac{1 - \eta^2}{\xi^2 - \eta^2}} \frac{\partial}{\partial \eta} \hat{e}_\eta ; \sqrt{(\xi^2 - 1)(1 - \eta^2)} \frac{\partial}{\partial \varphi} \hat{e}_\varphi \right\rangle \qquad \text{(EQ 2.28)}$$

and $\hat{e}_x$ is the unit vector in the $\xi$, $\eta$ or $\varphi$ direction. The surface charge density, $\sigma$ [C/m$^2$], is

$$\sigma = \varepsilon_0 (\mathbf{E} \cdot \mathbf{n}) \qquad \text{(EQ 2.29)}$$

where **n** is the unit vector normal to the surface and $\varepsilon_0$ is the dielectric permittivity of free space. Equations 2.25, 2.27 and 2.29 yield

$$\sigma_{ind}(\eta) = -\frac{2\varepsilon_0}{a}\sqrt{\frac{\xi_0^2-1}{\xi_0^2-\eta^2}}\left[\frac{\partial\psi_{ext}}{\partial\xi}+\frac{\partial\psi_{conductor}}{\partial\xi}\right]_{\xi=\xi_0} \quad \text{(EQ 2.30)}$$

The terms in brackets are normal components of the electric field due to the external charges and the electric field of the conductor, respectively. In the new coordinate system

$$z = \frac{a\xi\eta}{2} \quad \text{(EQ 2.31)}$$

and the external electric field normal to the surface of the conductor can now be given as

$$\frac{\partial\psi_{ext}}{\partial\xi} = \frac{E_{ext}(z)\,a\eta}{2} \quad \text{(EQ 2.32)}$$

It is easy to show that the charge, $q_{ind}$ [C], induced on the conductor between two points on the surface, $\eta_1$ and $\eta_2$, is

$$q_{ind}(\eta_1,\eta_2) = a\pi\varepsilon_0\sum_{n=1}^{N}\left[(n+1)V_n\left(\frac{Q_{n+1}(\xi_0)}{Q_n(\xi_0)}-\xi_0\right)\int_{\eta_0}^{\eta_1}P_n(\eta)\,d\eta\right] - \frac{E_{ext}\varepsilon_0 a^2\pi}{4}\left(\xi_0^2-1\right)\left(\eta_2^2-\eta_1^2\right) \quad \text{(EQ 2.33)}$$

where we have used the recursion relationships obeyed by $Q_n$ to evaluate their derivatives. Equation 2.33 includes contributions from the field of the conductor and from the ambient electric field.

**Channel length**

Since we use the lightning parameterization only to examine the lightning-induced vertical redistribution of charge within a cloud model, we are not concerned with the channel dynamics, but merely its final length, $L_{final}$. It is the specification of $L_{final}$, based on the physical processes involved in lightning propagation, which separates our parameterization from all its predecessors. We assume that the channel length grows, so long as the energy gained through the induction of charge on it by the ambient electric field is greater than the energy lost to dissipative processes, such as ionization of virgin air and channel heating. We have tested several ways to represent the energy lost through these dissipative processes. For the first set of tests described here, We assume this dissipated energy is the electrostatic energy of the induced charge in an electric field, whose magnitude, $E_{diss}$ [kV m$^{-1}$], remains constant throughout the development of the channel. We determine the final channel length by a series of tests, starting with a small conductor initially placed in the vertical electric field, to determine whether there is sufficient electrostatic energy in a given configuration for the channel to 'propagate.' Propagation in this context means that the original conductor is replaced by a larger one, changing the distance between foci to $a+\delta a$ and changing ellipsoid shape to $\xi_0+\delta\xi$. The criterion for propagation is

$$E_{tip}\,[\mathrm{kV/m}] > E_{diss} \qquad \text{(EQ 2.34)}$$

where $E_{tip}$ is the sum of the ambient electric field and that due to the conducting channel at a distance, $Z_t$, from the tip of the conductor. (This is equivalent to $\xi = \xi_0+\delta\xi$ where $\delta\xi = 2Z_t/a$.) The electric field due to the presence of the lightning channel at the tips ($\eta = \pm 1$) is given by

$$E_l(\xi) = \frac{2/a}{\left(\xi^2-1\right)}\sum_{n=1}(n+1)V_n P_n(\eta=\pm 1)\left(\frac{Q_{n+1}(\xi)-\xi Q_n(\xi)}{Q_n\left(\xi_0\right)}\right) \qquad \text{(EQ 2.35)}$$

We choose $Z_t = 25$ m for computational convenience.

The criterion is tested at both ends of the channel. If the criterion is met at either tip, the conductor is extended in that direction. The final channel length is that for which $E_{tip}$ falls below $E_{diss}$ at both ends.

OPAL differs from the parameterization of Helsdon *et al* (1992), who determined the length of the channel based on an arbitrary criterion, $E_{ext} > 150$ kV m$^{-1}$, which ignored the field of the conductor and was not based on physical principles. Since $E_{conductor}$ may be greater than $E_{diss}$ even in regions where $E_{ext} < E_{diss}$, the channels predicted by OPAL can penetrate further than in the Helsdon *et al* model. In particular, OPAL allows channels to propagate from cloud to ground, whereas Helsdon *et al* do not.

**Intracloud and cloud-to-ground flashes**

If the lower tip of the channel does not reach the ground, the channel always bears zero net charge. If, however, it does contact the ground when the surface of the channel is at potential $\psi_{cond}$, a net charge, $\delta q_{ctg}$ [C],

$$\delta q_{ctg} = \frac{2a\pi\varepsilon_0 \psi_{cond}}{Q_0(\xi_0)} \qquad \text{(EQ 2.36)}$$

flows from the ground to the channel and is evenly distributed along the channel. This brings the channel potential from $\psi_{cond}$ to zero (the potential at the ground). Downward 'propagation' is no longer possible though the top of the channel may continue upward.

### 2.3.3 Sensitivity of the lightning parameterization to variations in the charge profile

OPAL has been developed for use in FILIGREE. However, we wish to explore some general features of its predictions. To do so, we apply OPAL to a standard, idealized charge profile which can be altered in easily prescribed ways. The charge resides on a set of vertically stacked disks of radius $R_{cloud}$. The overall charge configuration is that of a vertical dipole, with a positively charged region above a negative one. The heights of the maximum positive and negative charge centers are specified, Z+ and Z- [m] with distance between them, D± [m]. The charge distribution in each charge center is defined by three parameters; the charge maximum, Q+max (Q-max) [C] and two lengths, $\Gamma +_{a(b)}$ and $\Gamma -_{a(b)}$ [m], the standard deviations of Gaussian distributions above (a) and below (b) the positions of maximum (+) and (-) charge. These widths effectively define the region of space occupied by the charge. The total amount of charge in each charge center is obtained by integrating over these Gaussian half-distributions, and is denoted Q+(total) (Q-(total)). The ambient electric field and potential are calculated from the resulting charge profile.

Figure 2.3 shows the charge profile and the resulting electric field for a case in which Q+(total) = -Q-(total) and all half widths are equal.

We use a standard, simple charge profile to test the sensitivity of the computed channel length, $L_{final}$, and induced charge, $q_{ind}$, to the following lightning parameters: (1) dissipation electric field, $E_{diss}$, and (2) the radius of the lightning channel, $R_0$, and to the following charge profile properties: (1) the distance between charge centers, D±, (2) the charge, Q+max

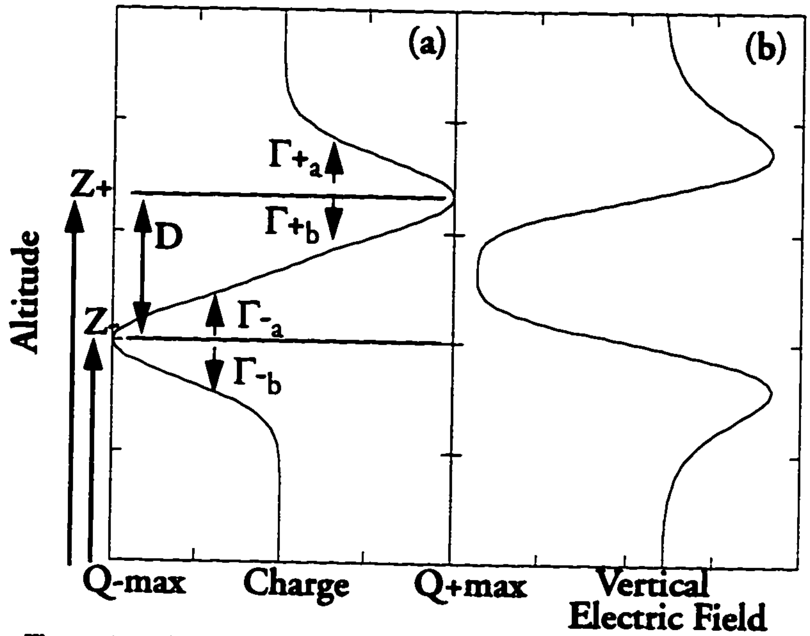

**Figure 2.3.** (a) A standard charge profile and (b) the resulting electric field as functions of height

and Q-max, and(3) the shape of the charge distribution, as determined by Z+, Z-, D±, Q+max, Q-max, $\Gamma +_{a(b)}$ and $\Gamma -_{a(b)}$, and ratios of these variables.

**Sensitivity to dissipation electric field**

We examine the sensitivity of the lightning channel development to the value chosen for the dissipation electric field, $E_{diss}$ [kV/m], by initiating a channel in the charge profile shown in Figure 2.3 (Q+(total) = -Q- (total)= 28 C, all $\Gamma$ = 750 m, Z+ = 9 km and Z- = 6 km). The final length of the channel was relatively constant for $150 < E_{diss} < 350$ and the induced charge varied between ±8 to ±7 C. For $E_{diss}$ < 100 kV/m, the final length of the channel is much greater and at $E_{diss}$ < 50 kV/m, the channel propagates outside the confines of the model. For $E_{diss}$ > 450 kV/m, the channel is unable to extend beyond its initial length.

Energy considerations show that extension of the channel toward a region with higher space charge density is favored over propagation away from this region so long as the dissipative effects remain constant. As the channel propagates toward the region of greater space charge density, more charge is induced on its surface, increasing the electric field at the tip. If the electric field is strong enough continued ionization occurs and the channel lengthens. As the channel tip continues past the region of high charge density, less charge is induced on its surface. This decreases the electric field near the tip where future growth would occur. At some point, this electric field is insufficient to overcome the energy loss due to the creation of new ions. This picture is crudely represented in OPAL as the variation in the predicted length of the channel versus the energy loss parameter, $E_{diss}$. For $E_{diss}$ very low, the lightning channel continues to propagate unhindered, and for $E_{diss}$ very high the channel length can not exceed the prescribed initial length $L_0$.

Figure 2.4 shows the electric field at 25 m from the tip of the channel, $E_{tip}$, versus channel length. As the channel lengthens $E_{tip}$ rises until the tip reaches the height of the maximum in charge density (Z+ or Z-) and it decreases as the tip extends past that point. Figure 2.4. shows

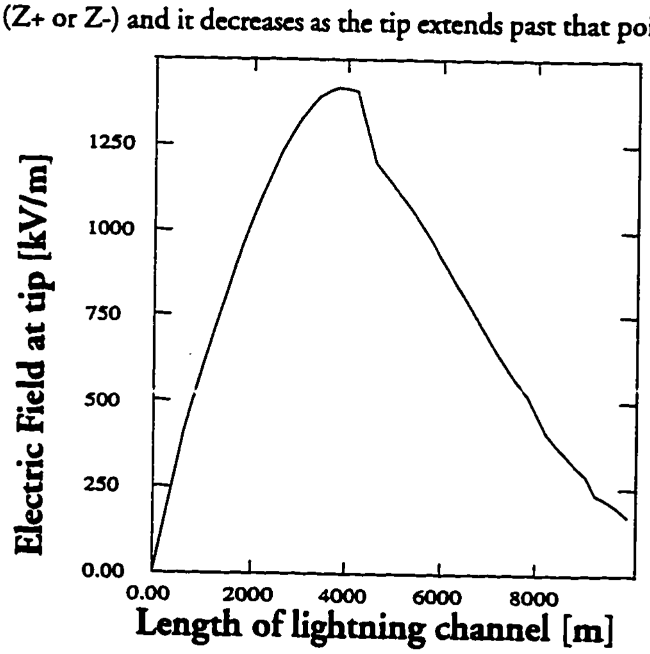


**Figure 2.4. Electric field at the tip of the channel as a function of channel length.**

that a channel with a larger initial length can propagate at higher values of $E_{diss}$ than can an initially shorter channel. However, the final length of the channel decreases relative to a short channel with the same value of $E_{diss}$. For subsequent model runs, we set the initial channel length $L_0 = 600$ m and $E_{diss} = 300$ kV m$^{-1}$.

**Sensitivity to channel radius, $R_0$**

We tested the sensitivity of $L_{final}$ and $q_{ind}$ to $R_0$ using the charge profile shown in Figure 2.3. The final length was relatively insensitive to changes in radius for 0.1 m < $R_0$ < 75 m the induced charged ranged from ±6 to ±9 C.

For subsequent runs, $R_0$ is set at 2.0 m. This is larger than the luminous radius of the return flash measured via photographs (eg., Uman, 1987) which are on the order of several centimeters; however, $R_0$ represents only the radius at the broadest point along the length of the channel; the radius toward the ends will be less than this and closer to the measured values of lightning channel radii. As stated above, the results are relatively insensitive to this parameter.

**Sensitivity to the ratio D± /Z-**

We examine the behavior of the lightning channel as the distance between the two charge regions is changed. The upper (positive) charge region remains centered at Z+ = 9 km while Z-, the position of the center of the lower charge region, is varied from 8 km to 2 km. Q+ and Q- were set to the same magnitude, and then were changed to keep the maximum electric field the same for each run while keeping the other charge profile variables constant.

Figure 2.5 shows the vertical extent of the final channel for each of these runs as well as the

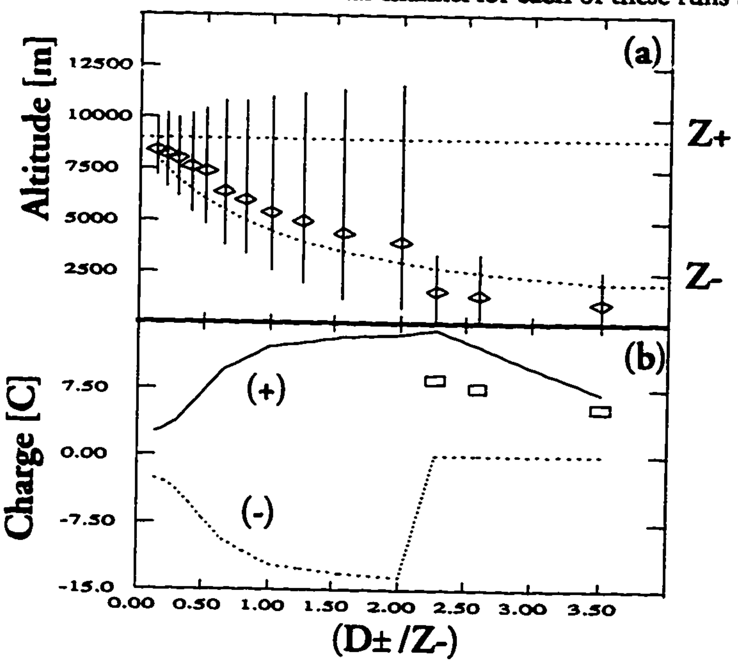


**Figure 2.5. Lightning channel characteristics as a function of the ratio (D± /Z-) (see Figure 2.3). (a) Lightning initiation point (<>) and final lightning channel extent (solid line) (Z+ and Z- are given by the dotted lines). (b) Positive (solid line) and negative charge (dashed)on the channel including transferred charge (▯) for cloud-to-ground channels.**

initiation point and charge induced on the channel. For cloud-to-ground channels, $q_{ctg}$ (Equation 2.36), is added to $q_{ind}$.

For (D± /Z-) < 2.0 the channel initiation point remains between the two charge regions, and the resulting channel is intracloud. As the lower charge region is placed closer to the ground, the image charge associated with it has a more important effect on the electric field profile. For (D± /Z-) > 2.0, the field between the lower charge and the ground is greater than that between the upper and lower charge regions; the initiation point is below the lower charge region and the resulting channel is cloud-to-ground.

**Sensitivity to in-cloud charge, Q+(total) and Q-(total)**

In all the previous tests, we assumed that the cloud was electrically neutral. This may not always be true; for example, a series of cloud-to-ground flashes can deplete the lower charge reservoir, or positive charge may be blown away from the top of the cloud. In the following tests we test for type of flash (intracloud or cloud-to-ground) as we vary the ratio Q+(total)/Q-(total). The results are shown in Figure 2.6.

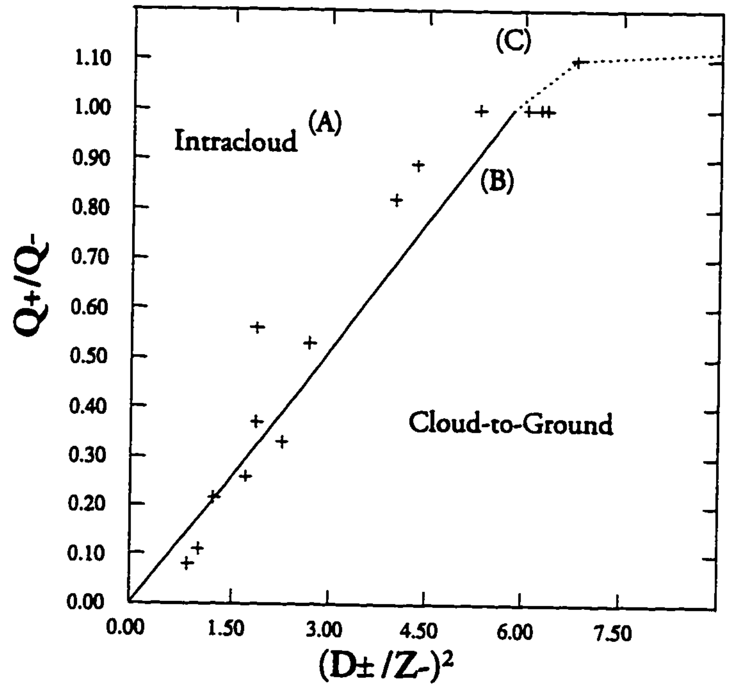


**Figure 2.6. Intracloud vs cloud-to-ground channels as functions of in-cloud charge and locations of symmetric charge centers (see text). Points A, B and C are discussed in the text.**

The '+' marks in Figure 2.6 show the point where OPAL predicts a switch in lightning initiation between the upper and lower charge region to initiation below the lower charge region. (Note that the model discretization causes a small amount of uncertainty in the actual location of the points.) For decreasing Q+/Q-, cloud-to-ground lightning channels are easier to initiate for larger Z- or smaller D±. The best fit to these points is shown by the solid line and is given by

$$\left(\frac{Q+}{Q-}\right)\left(\frac{Z-}{D\pm}\right)^2 \cong 0.2 \text{ for } \left(\frac{Q+}{Q-}\right) \leq 1.0 \qquad \text{(EQ 2.37)}$$

OPAL's cloud-to-ground flashes initiate in clouds with charge profile characteristics that fall to the right of this line.

As Q+(total)/Q-(total) decreases, cloud-to-ground lightning flashes are initiated at smaller values of D± /Z-. This is simply because the field between the lower charge region and the ground dominates over a larger range of Z-. The effect of the ground quickly becomes unimportant except when the lower charge region is very close to the ground.

**Sensitivity to shape of the charge regions**

Up to this point, we have assumed that the shapes of the two charge regions are the same and that the distribution of charge in each is symmetric about its center. This is not consistent with the general features of observed charge structures within thunderstorms. Typically, the lower negative charge is contained roughly in a region of space between the -10 and -20° C isotherms, while the positive charge is more diffusely distributed in the upper regions of the cloud (eg Krehbiel, 1986). In keeping with these observations, the shape of the lower charge region is altered while keeping the shape of the upper charge region more symmetric and diffuse.

We define W to be the ratio of the upper and lower widths of the lower charge region,

$$W \equiv \frac{\Gamma\text{-}_a}{\Gamma\text{-}_b} \qquad \text{(EQ 2.38)}$$

and alter the shape of the lower charge region by varying this ratio. The total amount of charge was chosen to give the same peak magnitude of the electric field. As W increases, the peak magnitude in the electric field moves below the maximum in charge, thus moving the initiation point of a lightning channel.

If W is large (the lower charge distribution falls off more rapidly below the maximum than above) the channel initiates below the negative charge center and the flash is cloud-to-ground. For $W < 1.5$ the channel is intracloud and for $W > 4.0$ the channel is intracloud. Between these two values the type of channel is not strictly determined by this ratio. Note that for these simple charge profiles, all flashes originating above the lower charge center are intracloud, while all those originating below the lower charge center are cloud-to-ground.

### 2.3.4 Evaluation of the lightning parameterization

In the next section we use the results obtained by the lightning parameterization to evaluate its usefulness in predicting observed trends in determining the type of flash and R.

#### Evolution of lightning behavior

We can attempt to follow the evolution of a "typical" storm by tracing a path through the space defined in Figure 2.6. Initially, in our conceptual model of cloud development, the two charge regions are relatively close together ($D\pm$ is small) and the cloud is neutral, which places the storm in a region that is favorable for intracloud channels (near point 'A' shown in Figure 2.6). As the storm matures, the distance between the charge regions increases (increasing $D\pm/Z-$), placing the storm in a regime that may be favorable for cloud-to-ground channels (near point 'B'). As the cloud produces cloud-to-ground channels, a charge imbalance will develop within the cloud (more positive charge than negative if we assume the majority of cloud-to-ground channels lower negative charge) which strongly favors more intracloud channels (point 'C'). Thus, there may be some oscillation between these two regimes. As the storm dies down, Z- decreases and, if an anvil forms, Q+(total) effective decreases. Both favor more cloud-to-ground channels.

### 2.3.5 Comparison of results with those of previous models

In their parameterization, Ziegler and MacGorman (1994) mimic the effects of lightning by reducing the space charge density in regions where it exceeds some threshold amount. This process is accomplished in such a way that there is no net charge gained by the cloud. Our results are similar to theirs for intracloud channels; most of the charge is induced on the channel in regions of the cloud where the space charge density is largest. However, we find some charge reduction in regions outside those of high space charge density and the deposition of charge in regions which previously held no charge. For cloud-to-ground channels OPAL allows for a net charge gain by the cloud, which Ziegler and MacGorman do not appear to allow.

Baker *et al* (1995) determined the type of flash (intracloud or cloud-to-ground) by assuming the channel proceeds from the initiation point only in that direction in which the magnitude of the local electric field gradient is smallest. In their model, the initiation point is always very near the top of the negative charge center, which is always very sharply peaked. In OPAL the channel proceeds in both directions in accordance with the ideas of Mazur (1989) and Mazur and Ruhnke (1993) and we find that the type of flash is determined only by the location of the initiation point relative to that of the maximum negative charge. In practise these two criteria are almost always the same for the simple charge profiles used in this chapter. If the initiation point is below the lower charge maximum, the gradient of the electric field has the largest magnitude above the initiation point so the flash is cloud-to-ground. Analogous reasoning makes the field gradient smaller above the initiation point if the latter is above the negative charge maximum. In Chapter III we use the lightning parameterization in the cloud model, where the charge profile may be much more complex and the model then differs from Ziegler and MacGorman (1994) and Baker *et al* (1995).

In the lightning parameterization used by Helsdon *et al* (1992), the final channel length is determined only by the ambient electric field within the cloud. Because of this there is no possibility of a cloud-to-ground channel unless very high fields extend all the way to the ground. We look at the electric field derived from the ambient charges in the cloud plus that due to the induced charges on the channel. These charges can be quite large and generate the required electric fields at the tip of the channel to allow for propagation beyond the low electric field regions within or below the cloud. The final channel length we predict is generally longer than that predicted using the criterion of Helsdon *et al.*

### 2.3.6 Summary of the lightning parameterization

We have examined the character of lightning flashes predicted by a one dimensional lightning parameterization for a range of highly idealized charge profiles. The lightning parameterization only requires the electric potential, which is known from the charge density, to calculate (1) where lightning initiates (if the proper threshold is met) and (2) the amount of charge induced by the electric field and, in the case of cloud-to-ground lightning, the amount of charge required to "ground" the lightning channel. We assume that lightning channels are vertically oriented and that only electrostatic mechanisms are responsible for generating charge along the lightning channel. In this parameterization the type of flash (intracloud or cloud-to-ground) is determined by the point where the lightning channel initiates relative to the maximum charge in the lower charge region. All channels that initiate above the lower charge center turn out to be intracloud, and all those initiating below are cloud-to-ground. The location of the initiation point can be roughly inferred from the ratios (D± /Z-), $\Gamma\text{-}_a/\Gamma\text{-}_b$ and Q+(total)/Q-(total). We have assumed the initiation position is the point at which the vertical electric field is maximum. If in fact the initiation point depends on hydrometeor type as well as mean electric field, the flash type may depend on the distributions of hydrometeors.

We feel confident that the lightning parameterization does a satisfactory job in evaluating the lightning characteristics observed within thunderstorms in a non-dynamic context. In the next section we outline the inclusion of the parameterization into FILIGREE to allow for the simulation of lightning in a dynamic framework in order to study the relationship between in-cloud processes and lightning flash rate and type.

## 2.4 The Thunderstorm Model

In the previous two sections we described a numerical cloud model with non-inductive collisional charge generation and a simple lightning parameterization. In this section we outline use of the lightning parameterization within the context of the numerical cloud model for the study of thunderstorm electrification. Hereafter we refer to the thunderstorm model as ONYX.

### 2.4.1 Initiation of lightning channels in the thunderstorm model

Initiation of lightning is quite similar to that described in the previous section except that the charge profile is generated by charges separated through non-inductive ice-graupel collisions and not the idealized profiles discussed in the previous section. Recent observations (eg

Marshall *et al*, 1995a,b) suggest that the initiation threshold electric field is a function of air density,

$$E_{init}(z)\left[\mathrm{kV\ m^{-1}}\right] = \pm E^0_{init}\,\rho(z)\ /\rho_0 \qquad \text{(EQ 2.39)}$$

where $\rho(z)$ is the air density [kg m$^{-3}$], $\rho_0$ the air density at sea level and $E^0_{init}$ is the initiation field at sea level, $E^0_{init}$ = 200 kV m$^{-1}$. In order to examine the effects of a density dependent initiation threshold. we use either a constant value for $E_{init}$ or allow the initiation threshold to vary with height according to equation 2.39.

If the vertical electric field at some point exceeds the initiation threshold for lightning, $E_{init}(z)$, a lightning channel is initiated. At the completion of the parameterized channel, the charge induced on the channel diffuses into the cloud, attaches to hydrometeors and modifies the in-cloud charge profile and electric field. (This process is explained more fully later in this chapter). ONYX then continues until the vertical electric field once again exceeds $E_{init}(z)$ at some point.

### 2.4.2 Final length of the lightning channel

Initial model runs with ONYX and the lightning parameterization suggested that the original propagation criterion (electric field at 25 m from the tip of the channel greater than 300 kV m$^{-1}$) was too strict. The charge profile provided by ONYX was much more structured than the simple charge profile used to test the sensitivity of the parameterization, and as a result in the thunderstorm model, a large number of lightning channels were not able to extend past their initial length for regions in the cloud where the charge profile varied considerably with altitude.

For the purposes of combining FILIGREE and OPAL, we have therefore adopted a different propagation criterion based on results of experiments of streamer propagation in gaps (Gallimberti, 1979). In these experiments, it is found that a streamer continues to propagate as long as the quantity of charge in the head of the streamer exceeds a critical value. Physically, this reflects the fact that, if the electron avalanche process necessary for leader propagation is to continue, the electric field due to the streamer charge must be high enough to continually accelerate electrons near the tip, despite dissipative processes such as ionization and attachment. Parameterization of these microscopic processes gave rise to the energy criteria used in earlier studies of lightning propagation (e.g., Griffiths and Phelps, 1976; Dawson and Winn, 1965). This is a microscopic variant of the energy criterion used in earlier studies of lightning propagation. In ONYX, we assume the lightning channel extends as long as the charge at the head of the channel does not change sign or go to zero. If the channel propagates into a region where the charge induced at the tip goes to zero or switches sign, propagation in that direction is halted.

### 2.4.3 Induced charge

Initial model runs also showed that the calculated charge induced on a lightning channel was often insufficient to reduce the electric field in the cloud to below $E_{init}$ at the initiation point. Instead, a number of consecutive lightning channels had to be initiated in order to reduce the electric field at the initiation point to below $E_{init}$.

To remedy this problem we have added a very crude correction to the induced charge calculation. The induced charge (equation 2.33) is simply multiplied everywhere by an integer factor that forces the electric field at the initiation point to fall below $E_{init}$. Using the same initial charge profile, Figure 2.7. shows the results of multiplying $\sigma_{ind}$ by 2. The effect of

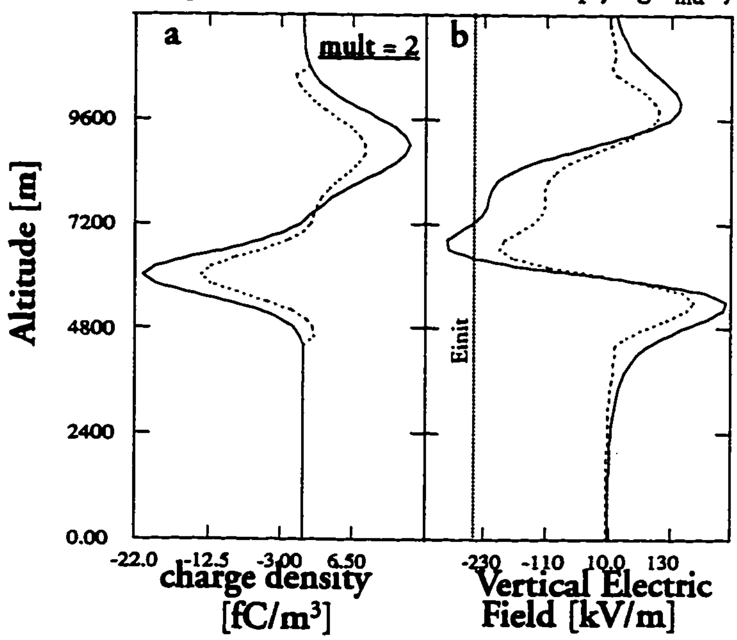


**Figure 2.7. (a) Vertical charge density profile before (solid line) and after (dotted line) modelled lightning flash, (b) vertical electric field before (solid line) and after (dotted line) lightning flash. Lightning induced charge includes a contribution from a "branching" parameter.**

this multiplicative factor is to increase the induced charge on the channel everywhere along the channel length thus crudely mimicking the effect of multiple channels and/or horizontal branching. Most of the increase in the charge induced on the channel is in those regions where $\bar{\sigma}_{ind}$ is maximum (and therefore $E_{radial} = \sigma_{ind}/\varepsilon_o$ is greatest). These are the regions in which cloud charge density is greatest, and thus the region in-cloud where one would expect some additional lightning development through horizontal branching.

### 2.4.4 Successive lightning channels

With the addition of the "branching parameterization," the electric field at the initiation point always falls below $E_{init}(z)$ upon completion of the lightning channel. However, the charge deposited by the lightning may cause the electric field elsewhere to be above $E_{init}(z)$. If this is the case, another lightning channel is initiated immediately after the previous channel. Once the vertical electric field is below the initiation threshold everywhere along the axis, ONYX resumes.

### 2.4.5 Charge screening current

When the charge screening current encounters the cloud boundary, charge is assumed to be collected by cloud particles and distributed horizontally throughout the outer region of the cloud at the side and vertically through a layer of depth dz at cloud top. Figure 2.8 gives an

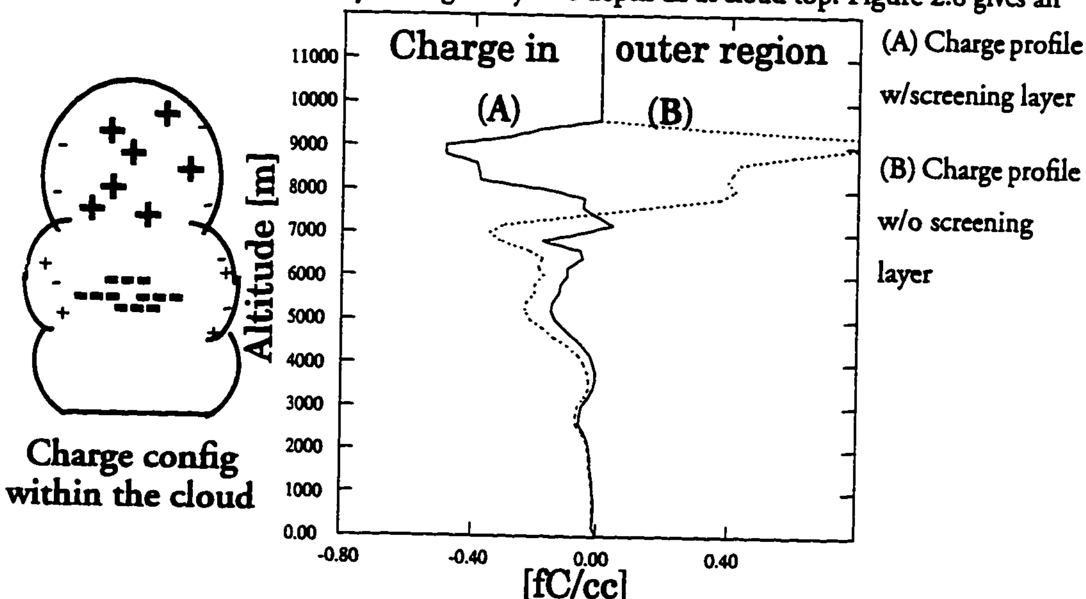


Figure 2.8. Charge profile in the outer cloudy region of ONYX with (A) and without (B) a contribution to charging from a screening current at the cloud boundary.

example of the differences in the charge profile in the outer region of ONYX with and without the screening current at the cloud boundary.

### 2.4.6 Distribution of induced or screening charge onto hydrometeors

The charge carriers within ONYX are hydrometeors. On the other hand, the charges induced on the lightning channel and carried by the charge screening current are ions and free electrons. The ions and electrons contained on the lightning channel are "liberated" by the collapse of the lightning channel. We assume the quantity of charge deposited on a hydrometeor is proportional to its cross sectional area.

For charge liberated from the lightning channel, the charge, $\delta q_i$ [C], added to each hydrometeor of radius $r_i$ in a layer with thickness $\delta z$ centered at z, is then

$$\delta q_i(z) = \left[\frac{q_{ind}(\eta_1, \eta_2)}{\pi R_a^2 \delta z} r_i^2\right] \Big/ \left[\sum r_i^2 n(r_i, z)\right] \qquad \text{(EQ 2.40)}$$

where $q_{ind}(\eta_1,\eta_2)$ is the induced charge on the lightning channel (from equation 2.33), $R_a$ is the radius of the inner cloud cylinder and $n(r_i)$ is the number concentration of hydrometeors with radius $r_i$. This charge is spread evenly throughout the layer. The redistribution is assumed to happen during a model time step, $\delta t$, which would require an effective mixing velocity of $l/\delta t$, where $l$ is the mixing length. Laroche (personal communications, 1995) reports observations of an aircraft flying through the remnants of a lightning channel some tens of seconds after the collapse of the channel. Conductivity of the air was seen to greatly increase for a few tens of meters, suggesting that the lightning charge was travelling at 1 to no more than 10 m/s. The excessively fast redistribution of the lightning charge in ONYX, is probably not important for subsequent development since the vertical electric field along the axis would not be different had we employed other means of mixing. The evolution of the radial field may be modified but that is rather unimportant for the model at the moment.

A similar procedure is followed for redistribution of charge from the charge screening current. Charge from the screening current (equation 2.20) is distributed throughout the outer cylinder and cloud top.

This charge redistribution results in the deposition of charge onto particles that were previously uncharged and/or the addition of charge of the opposite sign to already charged particles. In regions where the lightning channel propagates below cloud base, the induced charge is lost. This has a minimal effect on the reduction of the electric field; however, its importance in the initiation/propagation of future cloud-to-ground channels is unknown.

### 2.4.7 Summary of the thunderstorm model

Figure 2.9 is a black box diagram of the various communicating sections within ONYX. The main inputs to ONYX include the environmental sounding (temperature, pressure and dew-

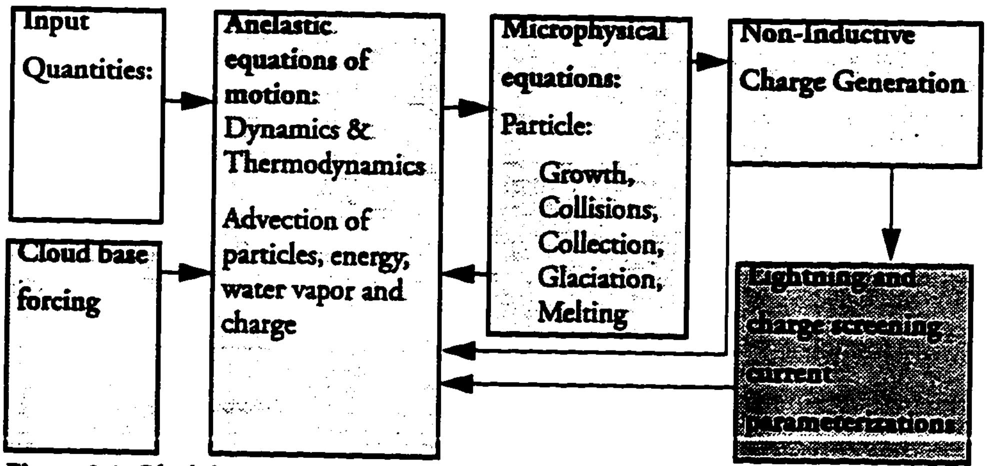


**Figure 2.9. Black box schematic illustrating the thunderstorm model (ONYX) flow. The light grey boxes designate those sections of the model referred to as FILIGREE where as the dark grey designates those sections referred to as OPAL.**

point temperature), various parameter values (eg, $E_{init}$, Fletcher or Meyers *et al* parameterization, etc) and the imposed cloud-base forcing. These are used to initialize all the various routines and kick off the dynamics. The dynamic routines are responsible for advection of energy, water vapor and all water and ice particles which are returned from the microphysical routines along with the latent heat release. The explicit microphysical routines are responsible for calculating the growth, collection, glaciation and melting of water and ice particles, 80 mass categories of both ice and water. The microphysical routines are also responsible for determining the number of ice-graupel collisions which is used by the Saunders *et al* (1991) parameterization of the non-inductive ice-graupel charge generation mechanism. This charge, carried by hydrometeors and treated as a passive tracer by the advection routines, is used to calculated the vertical electric field for use by the lightning parameterization and the radial electric field to determine the amount of charge arriving at the cloud boundaries from charge screening currents. The model output includes various microphysical quantities (eg, ice and water particle concentrations), cloud reflectivity, air velocity, cloud temperature, precipitation rate, charge separated per collision, charge density, electric field, screening current (all as functions of height and time) and the charge on each lightning channel.

Figure 2.10 presents a schematic of the charge sources and sinks within ONYX. Charge sources are non-inductive ice-ice collisions, charge screening currents and lightning. Intracloud

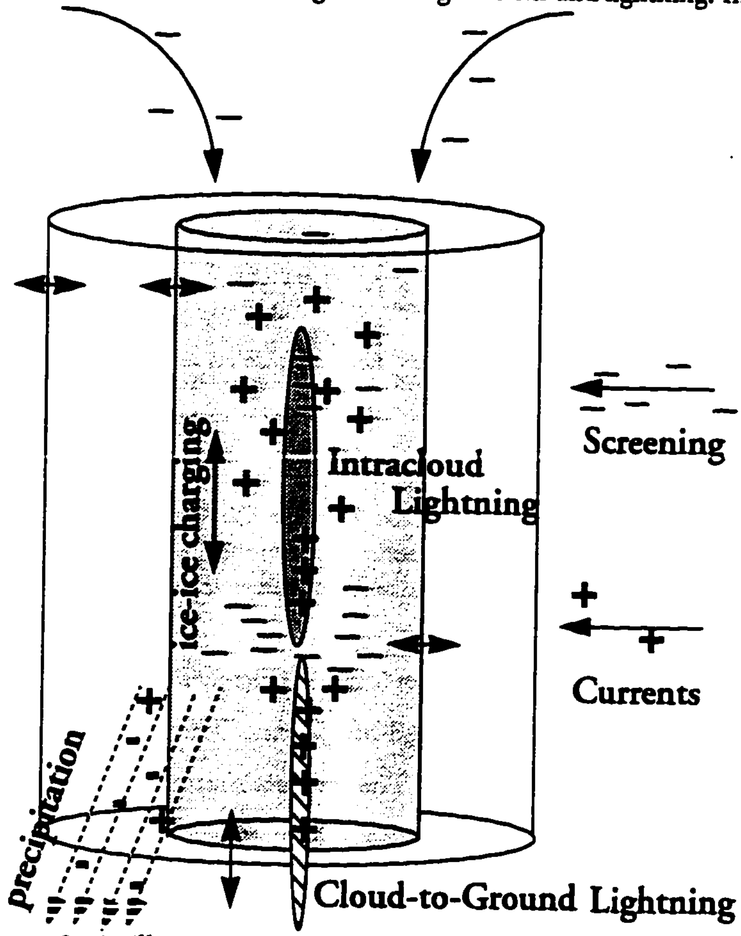


Figure 2.10. Illustration of charge sources and sinks within ONYX.

lightning introduces no net charge gain, whereas cloud-to-ground lightning does. Charge is lost through the removal of charged precipitation and advection of charged cloud particles into the environment. With the addition of the lightning parameterization to the cloud model, we are able to simulate the electrical aspects of thunderstorms throughout the entire life time of a cloud. In the next chapter we present various observations of clouds which we will simulate.

# III. Case Studies: Observations and Model Simulations

Thunderstorms develop in a wide variety of locations and environments. To study the trends and relationships between thunderstorm electrification and the physical processes within cloud in as general a context possible, we have used observations from a number of field projects conducted in mid-latitude continental, semi-tropical continental and tropical maritime environments.

We examine two groups of storms: clouds with cloudbase temperatures above and below/near 0°C. In the latter, exemplified by continental summer storms forming in the New Mexico mountains ($T_{cb} \sim 5°C$) warm cloud microphysical processes are relatively unimportant. The other group consists of tropical maritime and semi-tropical continental storms which have significantly warmer cloud bases ($T_{cb} \sim 20°C$), in which there is considerable warm cloud development.

Each section of this chapter is dedicated to storms forming in a unique environment. The first subsection of each briefly outlines the field project at which the observations where taken. (We direct the reader to Appendix B for a brief discussion on some of the instrumentation used to obtain electric field, lightning flash rate and charge per particle measurements at these field projects.) Then we summarize the overall features, electrical and non-electrical, of observations of these two groups of storms. These observations do not, in either case, include measurements of the cloud base forcing parameters. We show that by choosing reasonable values for the forcing parameters, ONYX can satisfactorily simulate the relevant features of these storms. We then vary the forcing to examine the dynamical, microphysical and electrical responses of the clouds to this unknown set of parameters.

Strong charging takes place only at in-cloud temperatures colder than approximately -5 to -10°C. Thus little, if any, charge generation occurs for clouds starting with small initial forcings, kinetic or thermal, simply because cloudtop never reaches a point where appreciable amounts of ice form. The necessary conditions for charging are not maintained for high values of forcing (either kinetic or thermal); graupel does not remain within the charging zone long enough to separate substantial amounts of charge. Larger forcing places the region of maximum charge separation higher in the cloud, less charge is generated due to the lower amount of liquid water available.

The duration of the imposed cloud base forcing can influence cloud development. If the duration is less than a few hundred seconds, the simulated cloud will decay as soon as the forcing is removed. Once the cloud has been established, with a vigorous updraft and actively growing particles, the simulated cloud is somewhat insensitive to cloud base forcing. The in-cloud updraft and increased buoyance from the release of latent heat are now responsible for the growth of the cloud. However, continuing to maintain the forcing for long times can extend the life of the simulated cloud beyond the duration of observed clouds.

## 3.1 Mid-Latitude Continental Storms

### 3.1.1 Mid-latitude continental storms: New Mexico

During the summer of 1984, a field project was conducted in the Magdalena Mountains in central New Mexico in which aircraft, radar and surface observations were used to study the relationships between precipitation and the onset of electrification in thunderstorms that formed over or near the mountains. Typically, these storms form in the late morning to early afternoon as solar heating results in upslope flow, which lifts moist air to its condensation level. The resulting storms are small and usually last no more than an hour and a half and exhibit a wide range of electrical activity (Raymond *et al,* 1991).

Aircraft observations consist of microphysical and electrical measurements taken by the National Center for Atmospheric Research (NCAR) Sailplane and the special purpose test vehicle for atmospheric research (SPTVAR) aircraft. Radar measurement were taken from two NCAR 3 cm-wavelength radars and two 3 cm-wavelength National Oceanographic and Atmospheric Administration (NOAA) radars. Additional electric field measurements were obtained from a network of five field mills maintained on the ground along the mountain ridge.

The SPTVAR typically made repeated penetrations in the clouds of interest at an altitude of 4 to 5 km and near 7 km (-20°C). It was equipped to measure the electric field and liquid water content. The NCAR sailplane entered the cloud near cloud base and ascended through the cloud while the aircraft remained within updraft regions of the cloud, reaching altitudes of

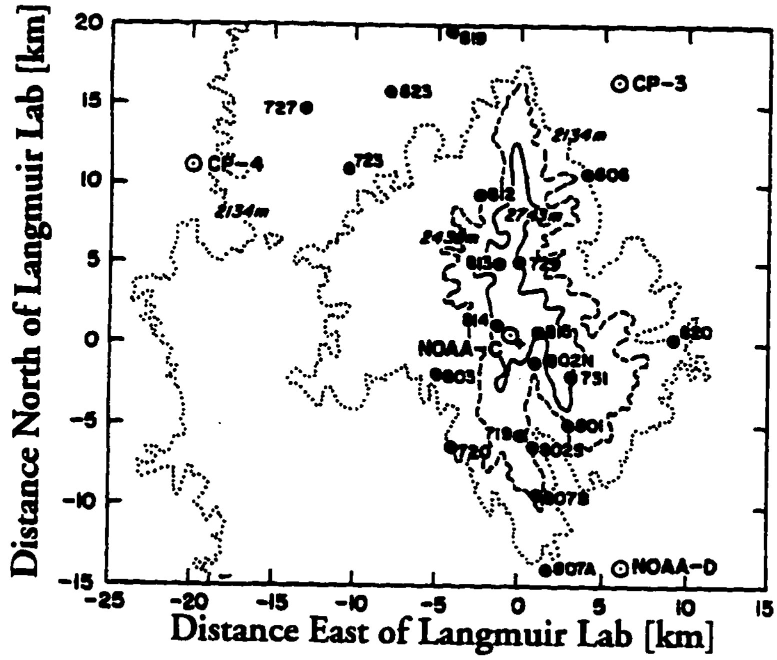


Figure 3.1. Locations of radars, o, and the cores of storms, •, labelled by month and day, at the time of initial electrification. From the field project in Socorro, New Mexico 1994. Contours of constant altitude of 2134, 2438 and 2743 m are indicated (Figure 1 from Dye et al, 1989).

approximately 7 km or occasionally higher. The sailplane was equipped to measure microphysical and electrical characteristics within the storms.

Rawinsondes were released daily at 730 MST from the Socorro airport (27 km east of the mountain ridge) and frequently from Langmuir Laboratory as well. Additional rawinsondes were often deployed at times when early storm formation seemed to be occurring. For details on data processing see Dye *et al* (1989) and Raymond *et al*, (1991).

### 3.1.2 Observations of Socorro, New Mexico storms

We confine our attention to a set of twelve thunderstorms that occurred over a three week period in July and August of 1984 over the Magdalena Mountains in New Mexico. Some of the storms discussed here have been discussed in detail in the literature; see, for example, Breed and Dye 1989, Dye *et al* (1989), Raymond and Blyth (1989) and Blyth and Latham (1993). Because the circumstances surrounding cloud formation are fairly similar for all the storms in the study, we hope to learn which relatively small environmental changes play the biggest roles in determining the very large differences in observed electrical development.

Table 3.1 (Solomon and Baker, 1994) summarizes the observations of cloud structure and

**Table 3.1: Statistics on Storms and Soundings: Socorro New Mexico (1984)**

| date (1984) | cloud base pressure [mb] | CAPE [J kg$^{-1}$] | $\theta_w$ [K] | *Li* [C] | $Z_{ct,max}$ [km] | lightning events & avg. flash rate (# min$^{-1}$) | comments |
|---|---|---|---|---|---|---|---|
| 23 July | 655 | 234 | 294.5 | 0.0 | ~9 | none | very weak electrification |
| 27 July | 644 | 43 | 294.3 | -1.2 | ~10.5 | > 3 | |
| 29 July | 660(?) | 208 | 294.8 | -1.6 | 9 | none | very weak electrification |
| 31 July | 655 | 924 | 294.2 | -1.6 | 14 | > 100 (~1.6) | |
| 1 Aug | 638 | 854 | 294.5 | -3.0 | 9.5 | none | storm did electrify |
| 2 Aug | 631 | 441 | 294.7 | -5.8 | 13.5 | > 10 (~0.4) | |
| 3 Aug | 614 | 412 | 294.9 | -3.8 | 12 | 6 (~0.4) | |
| 6 Aug | 660(?) | 322 | 295.2 | -2.7 | ~8 | none | |
| 13 Aug | 693 | 321 | 294.8 | -2.0 | 12 | 18 | |
| 14 Aug | 676 | 935 | 295.8 | -2.3 | 9.5 | none | moderate(?) electrification observed |
| 15 Aug | 693 | 2038 | 295.3 | -1.1 | 11 | 6 (~0.2) | inverted dipole (initially) |

lightning development in the 1984 storms. Values for the predictors discussed in Chapter I are listed in all cases for which there were sufficient data.

Figure 3.2 shows total lightning number and the average total lightning flash rate during the electrically active life of the storms for the New Mexico storms outlined in the table. Figure 3.3 shows the maximum observed cloud height, $Z_{ct,max}$, versus total lightning number and average total lightning flash rate. For those storms that do produce lightning, CAPE does reasonably well at predicting the trend in total lightning number and average flash rate.

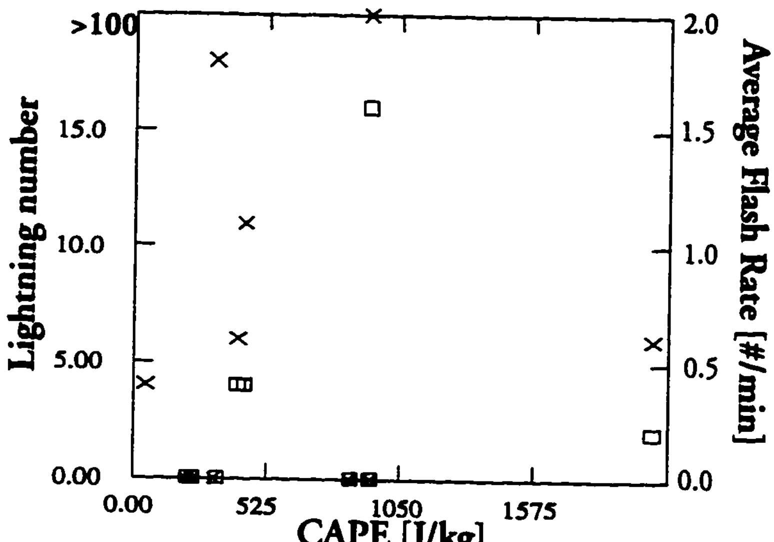


Figure 3.2. Observed number of lightning events, X, and average flash rate, [], versus CAPE [J $kg^{-1}$] of New Mexico storms.

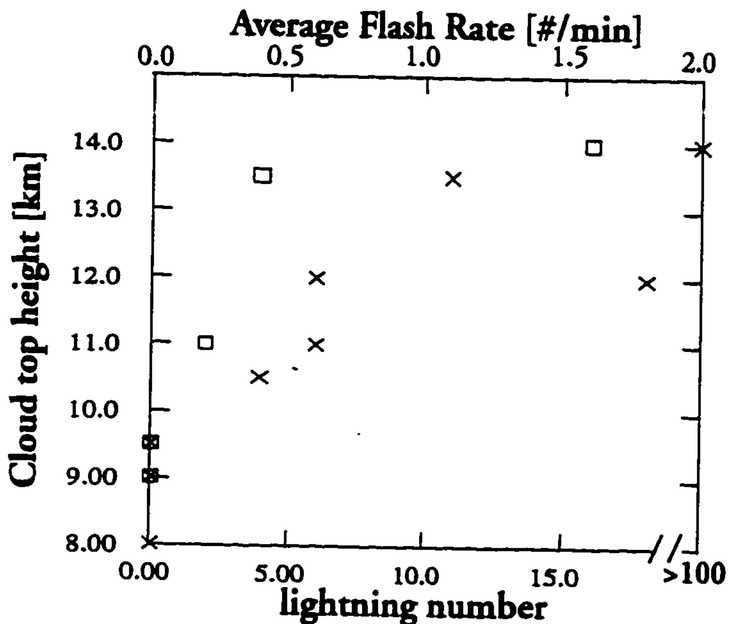


Figure 3.3. Maximum cloud height versus number of lightning events, X, and average lightning flash rate, [], for various New Mexico storms from 1984.

However, CAPE was also high in some clouds that did not become electrified. $Z_{ct,max}$ is also reasonably well correlated with lightning and flash rate, which occurred in all of the New Mexico clouds whose tops rose above approximately 9.5 km and in no smaller clouds.

We use the storm that formed on 2 August 1984 as representative of this set of thunderstorms. The 2 August 1984 Socorro sounding is given in Figure 3.4. The sounding

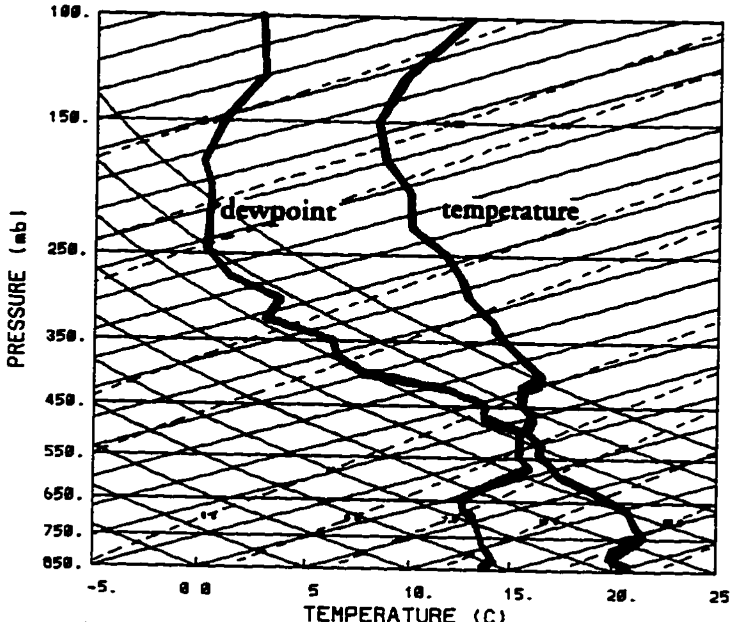


**Figure 3.4. Sounding taken from Socorro on 2 August 1984. Temperature and dewpoint shown on a skew-T plot.**

had an inversion near 400 mb and was relatively dry with a moist layer between 650 and 450 mb. The CAPE of a parcel of air starting near cloudbase, 625 mb, is 441 J $kg^{-1}$. This storm produced more than 10 lightning events with an average flash rate of 0.4 $min^{-1}$. The maximum altitude of the 0 dBZ reflectivity echo was ~13 km with a peak in radar reflectivity of 50 dBZ and 30 dBZ echoes extending as high as 12 km. The regions of highest reflectivity tended to correspond with the region of highest updraft velocity, at least 12 m/s in the upper regions of the cloud (Raymond and Blyth, 1989)

In the next section we initialize ONYX with the 2 August 1984 sounding (Figure 3.4) and compare the model results with observations.

### 3.1.3 Model studies

We ran ONYX for a range of values of $F_{th}$ and $F_{kin}$ (see section 2.1.1), leaving all other input quantities unchanged, to determine the effects of cloudbase forcing on subsequent electrification. New Mexico mountain storms typically form from a combination of thermal and kinetic forcing as solar heating creates upslope flow. The 2 August 1984 Socorro sounding (Figure 3.4) was used for all model runs. We integrated ONYX forward 1900 seconds (by which time the cloud had either passed through a maximum in cloud top height or reached a quasi-steady state); the imposed cloudbase forcing was maintained for 1500 seconds.In tests of the effects of kinetic forcing, $F_{kin}$, we varied the values of cloudbase velocity from 0 to 3.0 m $s^{-1}$. For model tests of thermal forcing, $F_{th}$, the cloudbase temperature was increased by 0 to 3.0°C and the cloudbase velocity was set to zero.

Although we have no *in situ* measurements of cloud microphysics from the 1984 field experiments, we use studies from other New Mexico storms (for example, Blyth and Latham, 1993) that show that at temperatures around -10°C to -15°C the liquid water content was 1.75 g $m^{-3}$ in updraft regions and approximately 0.75 g $m^{-3}$, with ice, in downdraft regions. Ice particles were first detected when the cloudtop temperature fell below approximately -10°C; small ice particles were observed in the updrafts with sizes indicating origins from about the -12°C level, and ice particles were observed in clouds whose tops never became colder than approximately -12°C.

Model simulations give a maximum cloud top height of ~12 km with a peak updraft velocity near 15 m/s. ONYX results are consistent with these observations as well as with observed radar reflectivities, cloud top heights and updraft velocities. Solomon and Baker (1994) give more details

**3.1.4 Effects of forcing on cloud dynamics, microphysics and electrification**

Near the inversion at about 400 mb, the buoyancy goes through a minimum for that forcing which just pushes cloudtop through the inversion, but the buoyancy then rises to near neutral or positive with increased forcing. This increase is due to the fact that the inversion is near the level where glaciation becomes significant; the temperatures in-cloud just above the inversion range from -10 to -15°C. Thus for these New Mexico soundings the inversion plays an important role not only dynamically but electrically.

The modelled New Mexico storms reach breakdown electric field values (~250 kV/m) for $F_{kin}$ ~ 1.0 m $s^{-1}$ or $F_{th}$ ~ 1.0 °C. For those model runs in which electric field magnitudes were sufficient to cause electrical breakdown within cloud, the first appearance of graupel occurred at ~450 s after initialization of ONYX and the breakdown electric field ~450 s after the appearance of graupel.

## 3.2 Semi-Tropical Continental Storms

### 3.2.1 Semi-tropical continental storms: Florida

Central Florida has the highest annual number of days with thunderstorms and the highest density of cloud-to-ground lightning in the United States (Orville, 1994). With a large probability of potential thunderstorm days and the availability of facilities near Cape Kennedy Space Flight Center, Florida has continually been used as a site to study thunderstorm electrification and lightning (Kosah and Krider, 1989; Dye *et al*, 1992; Breed, 1993; etc).

The Convective and Precipitation/Electrification Experiment (CAPE) was conducted in the summer of 1991 near Kennedy Space Center, Florida. (See Figure 3.5 for layout of the project

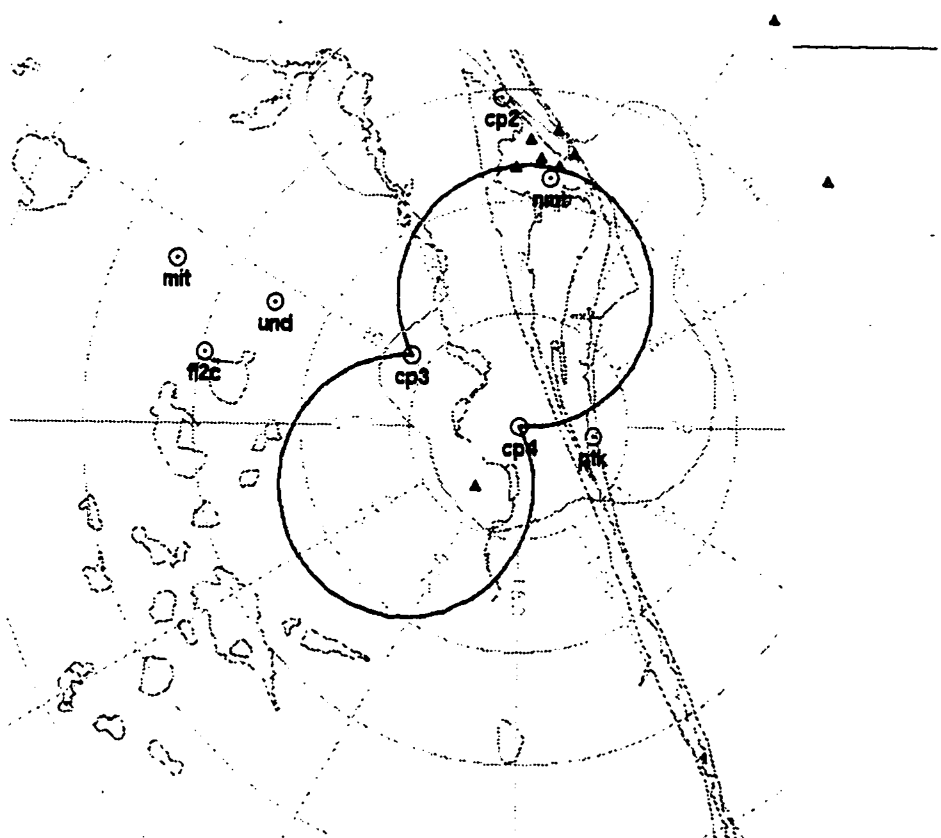


**Figure 3.5. Location of the various radars, o, and Cape Canaveral lightning detection units, Δ. during the CAPE field project in Florida, 1991.**

along the Florida coast.) Included among the goals of this project were (1) identification of the relationships among the co-evolving wind, water and electric fields within convective clouds; (2) determination of the meteorological and electrical conditions in which natural and triggered lightning can (and cannot) occur and (3) understanding the initiation and propagation of lightning.

During the CAPE project, six Doppler radars were available, as well as ground based temperature, wind, humidity, electric field, cloud-to-ground lightning sensors. There were numerous atmospheric soundings throughout each day, and microphysical and electrical measurements taken by numerous aircraft such as the NCAR Sailplane, two King Air aircraft and the South Dakota T-28.

The two King Air aircraft were equipped with instruments to measure the thermodynamic, kinematic and microphysical characteristics of the clouds. The King Air aircraft flew a series of vertically stacked and/or horizontally adjacent flight paths below cloud base or repeated penetrations at a constant altitude. The NCAR King Air was equipped with six electric field mills. Both King Air aircraft confined their observations to the initial development of the storms. Once the electric field exceeded approximately 10 kV $m^{-1}$, the aircraft left for "safer" clouds.

The NCAR Sailplane was deployed in a fashion similar to that in the Socorro study. In addition to the instrumentation on the sailplane during the Socorro study, two charge induction rings and PMS probe were attached to the aircraft. This allowed the resolution of cloud particle type and any charge on the particles. Typically, the sailplane remained on tow until a suitable cloud was reached. The sailplane would attempt to penetrate the cloud near, or just above, cloud base and ascend through the cloud as long as the aircraft could remain within the cloud updraft. Unlike the King Air aircraft, the Sailplane remained in-cloud during the most electrically active periods of the storm if the updrafts permitted.

### 3.2.2 Observations of Florida storms

We concentrate on a storm that formed at 1400 EDT on 29 July 1991 on the east coast of Florida during the CAPE field project. (Observations from this storm will be shown in the next section along with model results to facilitate comparison.) Figure 3.6 is a sounding from 29

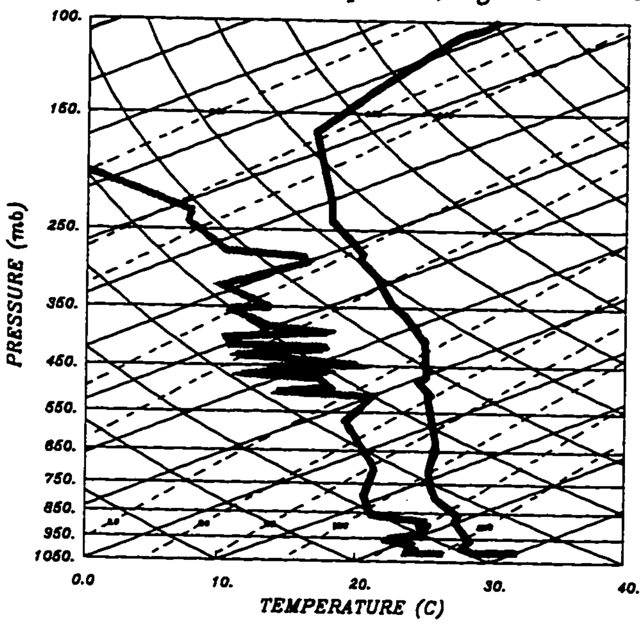


**Figure 3.6. Sounding take from the CAPE project at 22Z from Cape Canaveral on 29 July 1991 at 22Z**

July 1991 at 22Z with CAPE exceeding 1850 J kg$^{-1}$. For the first 25 minutes the cloud tops remained below ~8 km (-20°C). During this time, the King Air observed slightly elevated electric fields of 2 kV/m. Ice first appeared around 1414. The first lightning flash occurred just after 1425 and further growth of the cloud continued. By 1435 the maximum cloud top height was reached with radar reflectivity > 0 dBZ extending to ~11.5 km. Large amounts of ice were detected by the King Air and the electric field was greater than 10 kV/m. The vertical electric field measured by the sailplane is consistent with negative charge above the sailplane.

### 3.2.3 Model studies

We initialized ONYX with the 29 July 1991, 22Z sounding from the CAPE project (Figure 3.6) and used a similar range of values for forcing as described with the New Mexico storms. Again, cloud forcing in CAPE storms can arise from both kinetic forcing (convergence of land and sea breezes or other synoptic sources) and thermal forcing (solar heating of the land). Ice nucleus concentrations were taken from equations 2.12 and 2.13 and the production of secondary ice particles was included (equation 2.14).

Figure 3.7 shows the observed radar cross section of this storm with the flight path of the sailplane superimposed, lightning flash rate as determined by the sailplane field mills (note:

that the data are quite 'noisy' so the lightning flash rate is probably overestimated since some spikes in the electric field are not due to lightning), updraft velocity and electric field measurements from the sailplane.

Figure 3.8 gives an example of the modelled reflectivity from a model run initialized with the 29 July 1991 CaPE sounding and $F_{kin} = 3$ m s$^{-1}$. This example compares quite favorable with observations (see Figure 3.7). Both the observed and simulated cloud exhibit similar cloud top heights and the magnitude and location of regions of high reflectivity are consistent with each other as is the updraft velocity. The observed electric field shows more structure than the modelled cloud, but his is to be expected since the model has homogeneous charge layers and the electric field is not influenced by nearby cloud, remnants of previous clouds or small localized charge regions that may be present in the observed cloud. Note, as with most days, ONYX is initialized with a range of forcings. Clouds initialized with other values of $F_{kin}$ and/or $F_{th}$ do not compare as well, though they are representative of many clouds that formed on 29 July 1991 and never became electrified as well as numerous other storms that became electrified but did not have the same electrical structure and history as the 22Z cloud.

In section 4.2.1 we also present observations of cloud-to-ground lightning and radar reflectivity from the 15 August 1991 CaPE storm. (See Figure 4.8.) Storms forming on this day were very active with peak reflectivities around 55-60 dBZ and radar velocities of 20 m s$^{-1}$.

### 3.2.4 Effects of forcing on cloud dynamics, microphysics and electrification

With little forcing, $F_{kin} < 1.5$ m s$^{-1}$, there is no mixed phase development within the charging zone (most precipitation was generated through warm rain process) and no lightning. With moderately strong forcing, $F_{kin} = 2.0$ m s$^{-1}$, ONYX produces two intracloud lightning flashes, moderate amounts of graupel form and charging begins approximately 800 sec after forcing is initiated and first lightning occurs at 1123 sec. The development of the charging zone occurs ~800 sec after model initialization and corresponds to the beginning of charge generation. As the storm ages, the updrafts within the charging zone subside and the liquid water is gradually removed. By 1400 sec, the cloud has become completely glaciated for $T < -5°C$ and no further charge is generated.

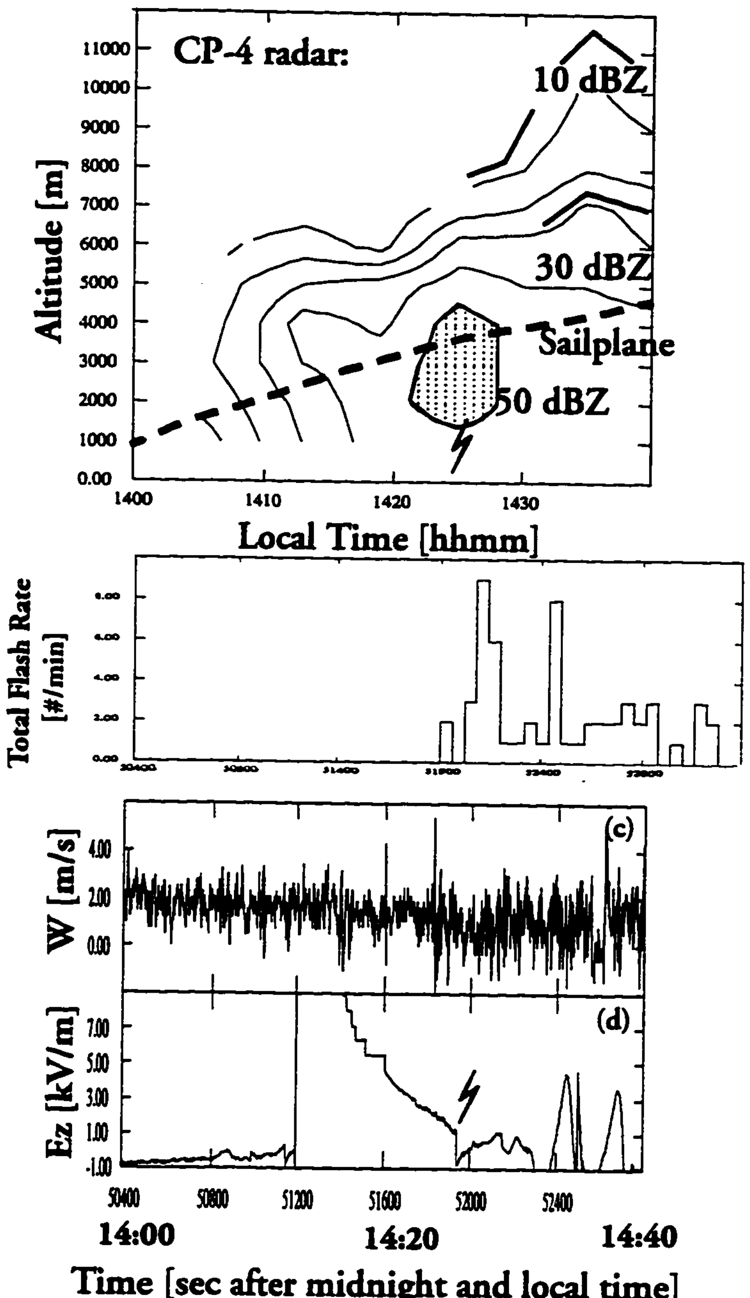


Figure 3.7. (a)Vertical profile of the 29 July 1991 CaPE storm with radar reflectivity as measured by the CP-4 radar (adapted from Dye *et al*, 1992) with the flight path of the NCAR Sailplane superimposed on the figure. (b) total lightning flash rate estimated from the Sailplane field mills (c) vertical velocity [m/s] and (d) vertical electric field [kV/m].

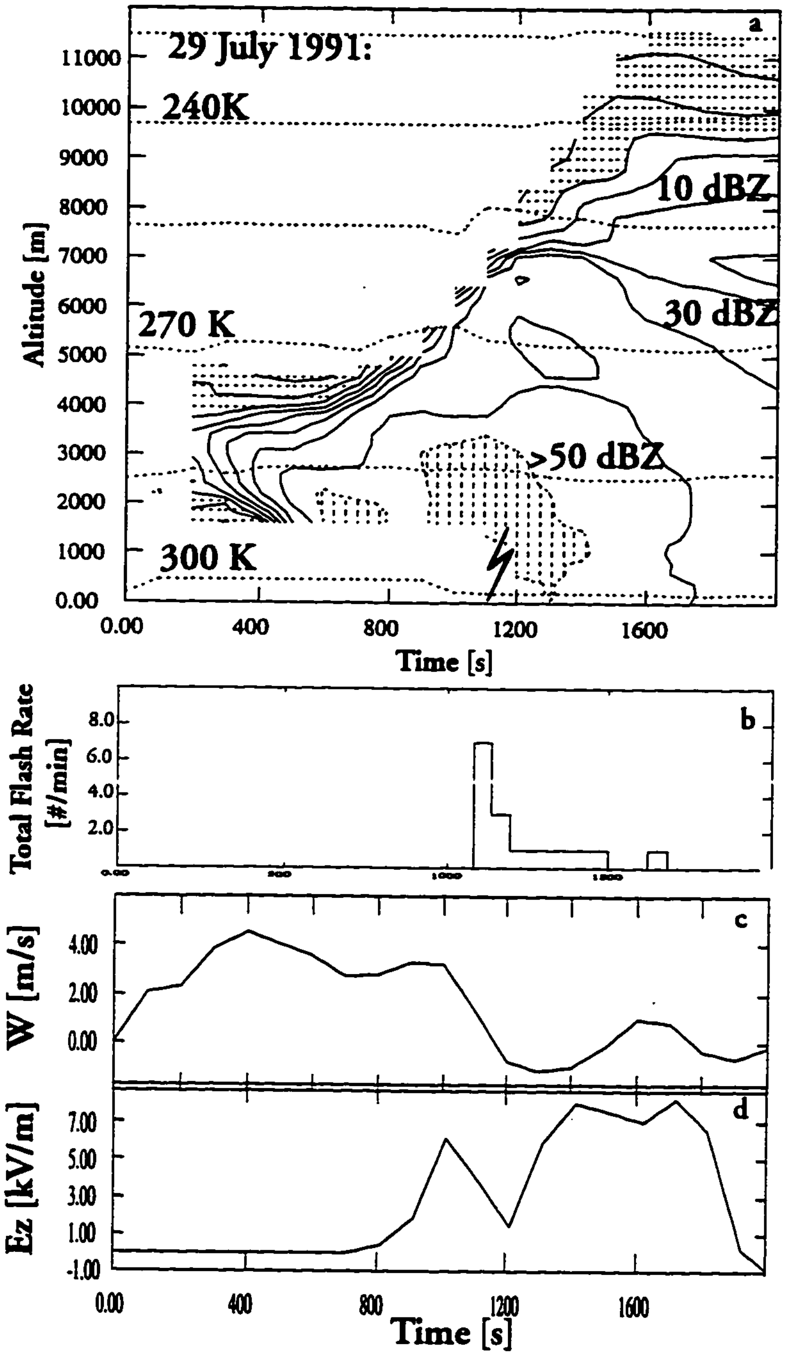


**Figure 3.8.** (a) Modelled cloud reflectivity and temperature contours for the 29 July 1991 CAPE storm. Time of first intracloud lightning is indicated. (b) Modelled lightning flash rate (c) vertical velocity in the outer region of the model and (d) vertical electric field in the outer region of the model. (c) and (d) are taken at altitudes corresponding to the sailplane altitude in Figure 3.7a.

## 3.3 Tropical Maritime Storms

### 3.3.1 Tropical maritime storms: South Pacific Ocean

The Tropical Ocean-Global Atmosphere Coupled Ocean-Atmosphere Response Experiment (TOGA-COARE) field project was conducted from 1 November 1992 through 28 February 1993 in the western equatorial Pacific Ocean warm pool region (Figure 3.9).

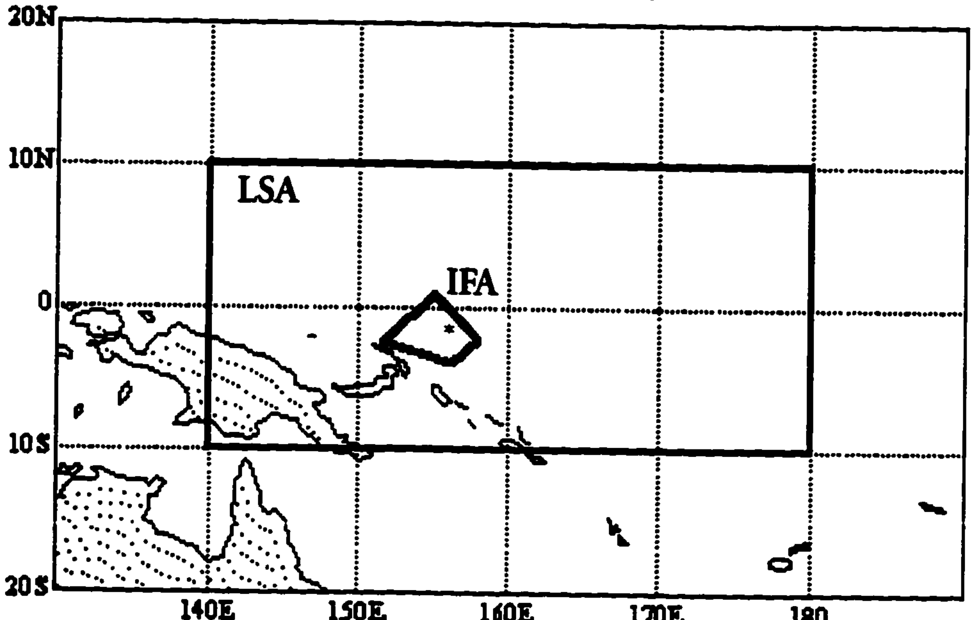


**Figure 3.9. Map of the TOGA-COARE Large Scale Array and Intensive Flux Array areas. Location of the R/V Vickers research vessel is marked *.**

Although the scientific goals of TOGA-COARE did not specifically include the investigation of thunderstorms and lightning, the project itself provides a large array of observations that can be used to characterize the electrical activity of storms forming in the Tropical Pacific Ocean.

During the intensive observational periods of the experiment, the MIT Doppler radar and an electric field mill were maintained on the research vessel R/V Vickers which was fixed at 2.04°S 156.1°E. Optical lightning detectors were used onboard to record intracloud and cloud-to-ground lightning.

A number of these storms have been examined in detail in the literature (e.g., Petersen *et al*, 1993; Petersen *et al*, 1995). We will make use of these observations to make comparisons with the thunderstorm model.

### 3.3.2 Observations of South Pacific storms

We rely on the data analysis by Petersen *et al* (1993), who examined two storm systems forming on 31 January 1993. The earlier, 6 Z storm developed small electric fields but with no observed lightning. Peak reflectivity was 45 dBZ (with most regions of high reflectivity confined to altitudes less than 5 km); the altitude of 0 dBZ contours was near 10-11 km. As the storm developed and moved over the R/V Vickers, surface electric fields on the order of 200 V $m^{-1}$ were observed (negative charge above). Higher fields were observed later but appeared to be from the region of stratiform precipitation forming behind the system. The observed CAPE for a sounding taken near this time was ~200 J $kg^{-1}$.

A second storm forming around 2200 Z was much more active electrically; flash rates were up to 4-5 $min^{-1}$ (2305 Z) and peak reflectivity was 50 dBZ, with regions of 25 dBZ extending up to approximately 8-9 km. Cloud tops were similar to those in the earlier storm. None of the convection was closer than 10 km from the R/V Vickers, but peak electric fields measured at the ship were near 4 kV $m^{-1}$. The observed CAPE exceeded 1200 J $kg^{-1}$ prior to this period of time. Figure 3.10 shows two soundings from 31 January 1993 taken at 6Z and 12 Z.

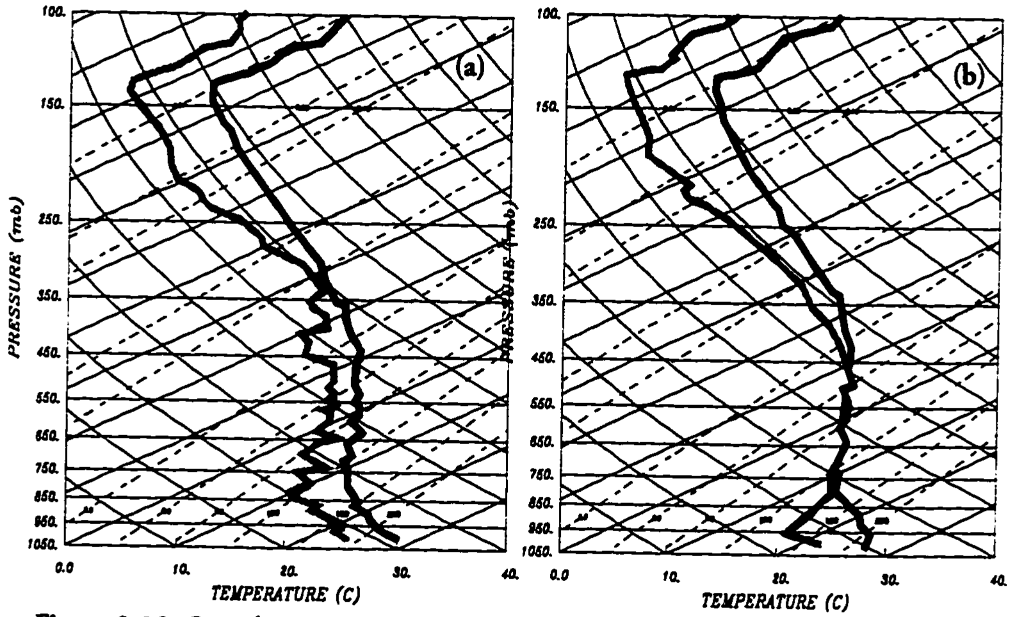


**Figure 3.10. Soundings taken from the R/C Vickers research vessel on 31 January 1993 at (a) 6Z and (b) 12Z.**

Observations from both storms will be presented in the next section along with model results.

### 3.3.3 Model studies

For modelled clouds, the cloudbase forcing was varied from 0.5 m $s^{-1}$ < $F_{kin}$ < 3.0 m $s^{-1}$ and 0.5°C < $F_{th}$ < 3.0°C and maintained for 1000 sec. The Pacific Ocean warm pool may be a source of thermal forcing for storms in this environment as well as some source of surface convergence. The ice nucleus concentrations are computed from equations 2.12 and 2.13 and secondary ice production (equation 2.14) is included for these model studies.

We initialized the thunderstorm model with the 6Z 31 January 1993 TOGA-COARE sounding (Figure 3.10a), CAPE = 298 J/kg. For $F_{th}$ = 1.1°C, the model shows weak electrification (no lightning) with a peak model vertical electric field of -80 kV $m^{-1}$ and a maximum vertical velocity of 11 m $s^{-1}$. In general, the simulated clouds could not sustain updrafts greater than 5 m/s within the charging zone and cloud top height did not exceed 11-12 km for any value of forcings used. Figure 3.11 shows the radar reflectivity as measured by the MIT radar on board the R/V Vickers for the 651Z, 31 January 1993 and the reflectivity with time from the simulation when initiated with the 6Z sounding (Figure 3.10a).

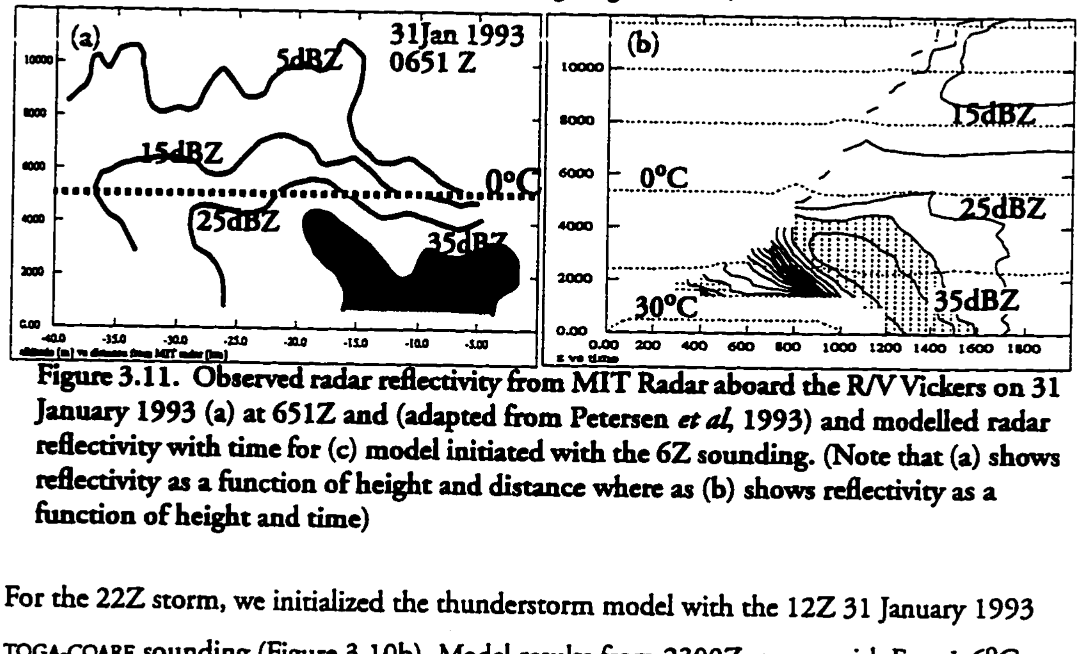


**Figure 3.11. Observed radar reflectivity from MIT Radar aboard the R/V Vickers on 31 January 1993 (a) at 651Z and (adapted from Petersen *et al*, 1993) and modelled radar reflectivity with time for (c) model initiated with the 6Z sounding. (Note that (a) shows reflectivity as a function of height and distance where as (b) shows reflectivity as a function of height and time)**

For the 22Z storm, we initialized the thunderstorm model with the 12Z 31 January 1993 TOGA-COARE sounding (Figure 3.10b). Model results from 2300Z storm, with $F_{th}$ =1.6°C, showed very strong electrification, a peak cloud-to- ground flash rate of 3 $min^{-1}$ and a peak total flash rate of 23 $min^{-1}$. Maximum model vertical velocity was 25 m $s^{-1}$. The modelled values are consistent with the observations of Petersen *et al* (1993). Figure 3.12 shows the radar reflectivity as measured by the MIT radar on board the R/V Vickers for the 22Z, 31 January 1993 and the reflectivity with time from the simulation.

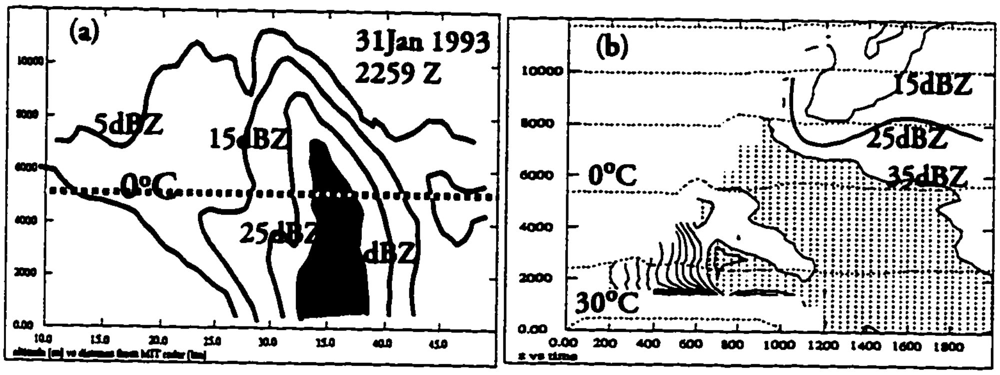


**Figure 3.12. As in Figure 3.11 except for the 22Z storm and its simulation initiated with the 12Z sounding.**

Both the observations and simulation of the earlier storm show no region of reflectivity greater than 25 dBZ extending above 0°C, whereas in both the observations and simulation of the later storm, regions of 25 dBZ extend well up to 9000 m, ~ -20°C.

### 3.3.4 Effects of forcing on cloud dynamics, microphysics and electrification

Simulations initialized with the 12Z sounding ranged from electrically inactive, electrically active with no lightning to strongly electrified with lightning as forcing was varied. With low forcing the average updraft velocity within the charging zone, $\overline{w}_{cz}$ (averages within the charging zone are denoted by an overbar) was less than 7.5 m/s for the entire duration of the cloud. The depth of the charging zone, $Z_{cz}$ [m], is only a few hundred meters. Graupel within the charging zone is short lived and falls out before any charge separation can occur. The resulting cloud never becomes electrified.

With higher forcing $\overline{w}_{cz}$ peaks near 12 m/s with sustained updrafts greater than 6 m/s. $Z_{cz}$ is much larger than the previous case, peaking at 3000 m, near the maximum size of the charging zone. Graupel first appears at 500 s into the model run with active charging and first lightning at 741 s. Charging ceases around 1400 s when there is no more liquid water present in the charging zone.

When the model was initialized with the 6 Z sounding, ONYX produced no clouds that became electrified for the same range of forcing described for the 12 Z storm. In general, simulated clouds could not sustain updrafts greater than 5 m/s within the charging zone, and cloud top height did not exceed 12-13 km.

# IV. Thunderstorm Electrification and Lightning Flash Rate†

We use ONYX to examine the sensitivity of the electrical behavior of storms to a range of dynamical and microphysical factors. We focus on initial electrification (the period required for the magnitude of the electric field to become large enough to initiate lightning at some point within the cloud, $E(z) > E_{init}$) and the flash rate in storms that actively produce lightning. The model results in this chapter are obtained from the simulated storms discussed in the previous chapter, where we utilized a set of soundings with a range of forcings to simulate the variety of storms that can form in each environment. In addition to these, we used one modelled storm from each region to examine the sensitivity of electrification and lightning flash rate to the following microphysical parameters: CCN concentration, primary ice nucleation and secondary ice generation efficiencies. For each of the latter model studies, the parameter in question was varied while all other inputs remained unchanged. Initially, we will show some general characteristics of thunderstorms from observations and simulations.

Figure 4.1 shows the observed locations of radio noise received by SAFIR during the electrically active period of a Florida thunderstorm on 18 August 1992. If the distance between consecutive points is less than $\delta t\, c/3$, where $\delta t$ is the time between consecutive signals and c is the speed of light, the two points are considered to constitute part of the same lightning channel and are shown connected in the figure.

Intracloud channels (eg lightning channels (A) and (B) shown in Figure 4.1) typically precede cloud-to-ground channels (eg lightning channels (C) and (D) in Figure 4.1) by several minutes (Krehbiel, 1981) and appear to develop vertically except near the lower end of the channel, and to a lesser extent near cloud top. Most intracloud channels, (A) and (B), are initiated at an altitude of 6 km or 12 km. Cloud-to-ground channels are initiated at an altitude of 5-6 km and appear to be vertically inclined throughout most of their length except at the upper end of the channel where an overhead projection shows some horizontal development for a number of these channels (see lightning channel (D) for example). Other orientations of lightning channels seem to arise later in the life of the cloud as previous lightning channels and air motions with the cloud redistribute and rearrange charge within

---

†. Large portions of this chapter are reproduced from Solomon and Baker, 1994 & 1997.

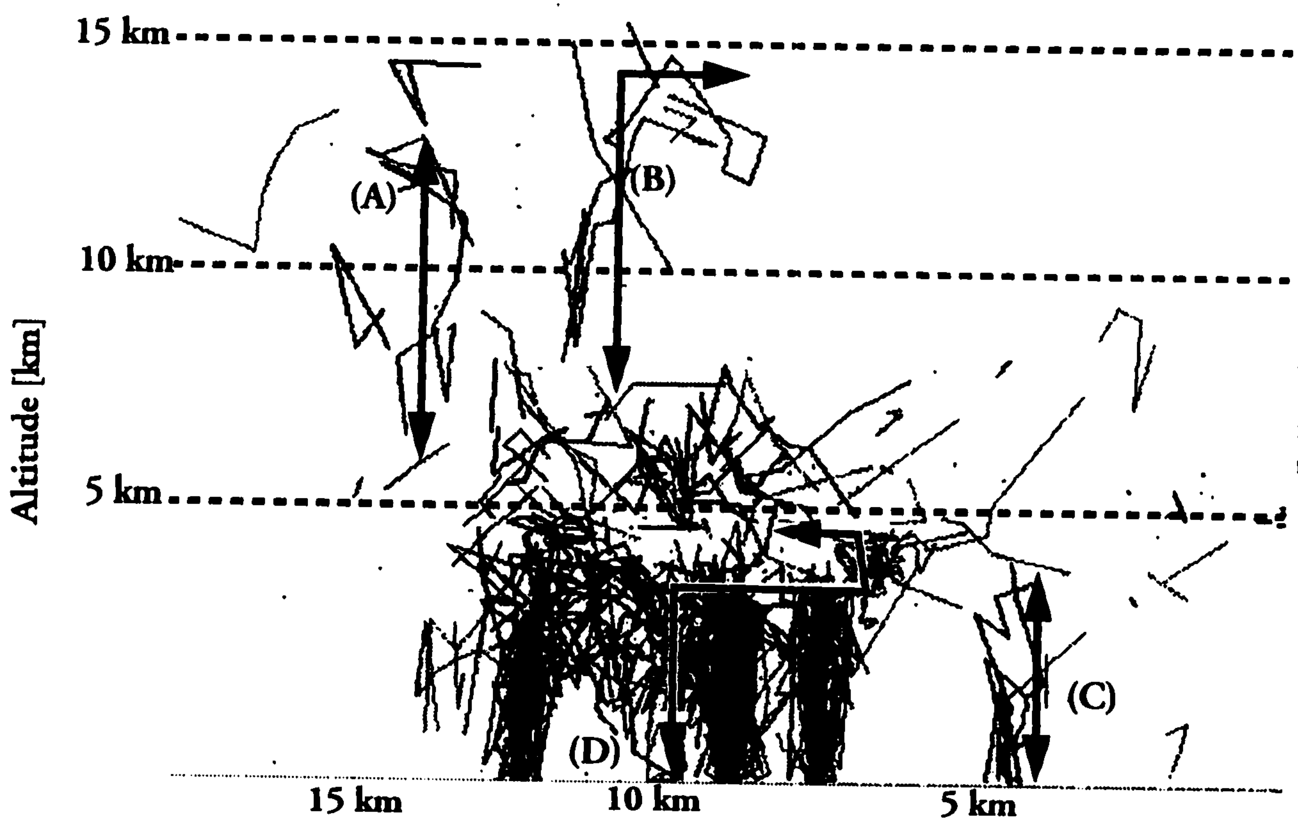


Figure 4.1. Horizontal projection of radio noise sources recorded by SAFIR from a thunderstorm occurring on 18 August 1992. Each color represents all signals during a 2.5 minute interval (see key) for a total duration of 15 minutes (see text for more details).

the cloud (Liu and Krehbiel, 1985). It is also interesting to note that there are numerous sources of radio noise that do not seem to be a part of a given lightning channel. These 'sparks' may be due to lightning channels that failed to meet some requirement to propagate.

Figure 4.2 shows a typical model predicted time evolution of the positive and negative charge centers in the inner region of a modelled cloud as well as the lightning flash rate. In this case,

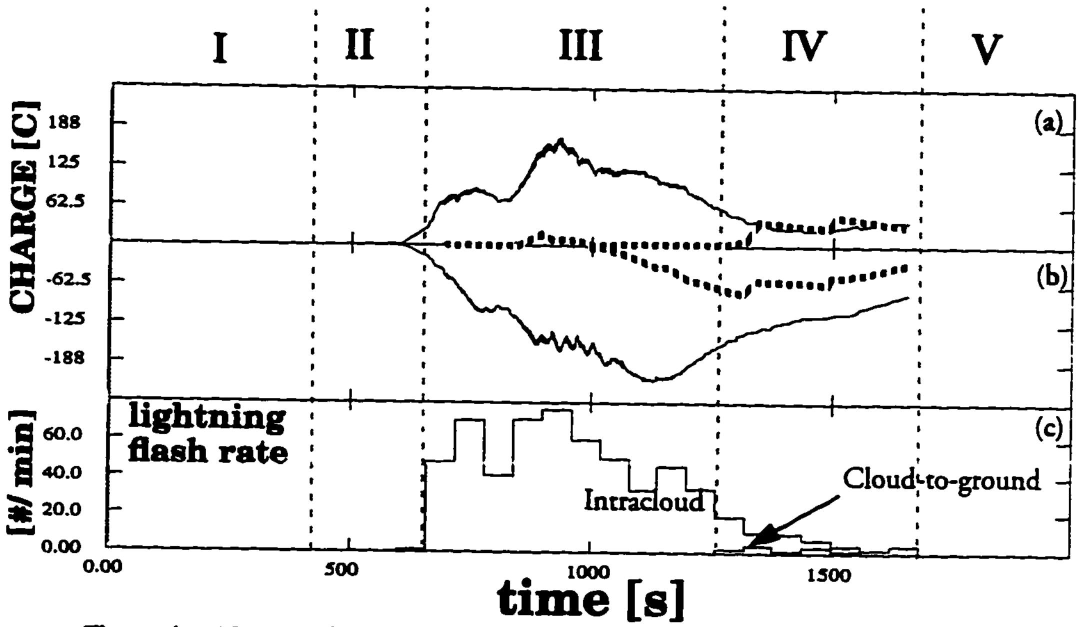


**Figure 4.2. Time evolution of charges in the inner region of a typical model generated thunderstorm (here the 29 July 1991 CAPE storm). (a) positive charge above (solid line) and below (dotted) 6 km (b) the negative charge above (solid) and below (dotted) 5 km and (c) number of lightning flashes per minute (intracloud and cloud-to-ground).**

ONYX was initiated with the 29 July 1991 CAPE sounding (Figure 3.4), and $F_{kin} = 3.0$. Note that the charge in the inner cloud region is not conserved because positive charge is advected horizontally, near the cloud top, and accumulates in the outer region

During early thunderstorm development, period I shown on Figure 4.2, the conditions for charge generation (coexistence of riming graupel, ice and supercooled liquid water) have not been established within the cloud. Approximately 400 sec into the model run, period II, the charging zone is established and charge generation and separation via ice-graupel collisions begins. This period lasts until the magnitude of the electric field between the charge centers is sufficient to initiate lightning. Period III of Figure 4.2 is characterized by continued charge generation and separation and the initiation of intracloud lightning channels between 6 km and 7 km. Intracloud lightning channels generally reduce the electric field by 10-15% while maintaining cloud neutrality. The charge structure at the beginning of period II is typically a very simple electrical dipole. Sometimes a small region of positive charge exists below the main region of negative charge and a small amount of negative charge accumulates at cloud top from the screening layer currents. The thunderstorm reaches its maximum cloud top height, peak reflectivity and the largest reservoirs of charge (in excess of 150 C as shown in this example) during this time. With time and the onset of intracloud lightning, the vertical charge profile quickly becomes much more structured. Intracloud lightning channels deposit positive charge in and around the lower negative charge region and negative charge in the upper regions of the cloud. This is especially true of long channels initiated after the time that cloudtop has reached its maximum height. Cloud-to-ground lightning channels, marking the beginning of period IV, are initiated when sufficient positive charge has been deposited below the lower negative charge region to raise the magnitude of the electric field to greater than $E_{init}$ below the lower negative charge region, typically between 5 and 6 km for the Florida thunderstorms. The main supplier of positive charge to this lower region is charge deposited from long intracloud channels. In addition, cloud-to-ground channels are also initiated as the main region of negative charge begins to descend as the updraft begins to subside, allowing the image charge to be more influential on the electric field between the cloud and ground. Both intracloud and cloud-to-ground lightning flashes continue until the charging rate no longer maintains a sufficient amount of charge to maintain high electric fields for initiating lightning, period V of Figure 4.2. This can be due to subsiding updrafts which prevent graupel from being processed in the charging zone and the removal of liquid water from the charging zone by glaciation.

With this general picture of the time course of a single storm in mind, we now use the ONYX results to examine the sensitivity of the electrical behavior of storms to a range of dynamical and microphysical factors, and thus to investigate the questions presented in the Introduction.

## 4.1 Initial Electrification

### 4.1.1 Sensitivity to updraft velocity and liquid water flux

We examined the modelled dependence of electrification on the liquid water flux entering the charging zone. Figure 4.3 shows the depth of the charging zone; i.e., the depth of the region

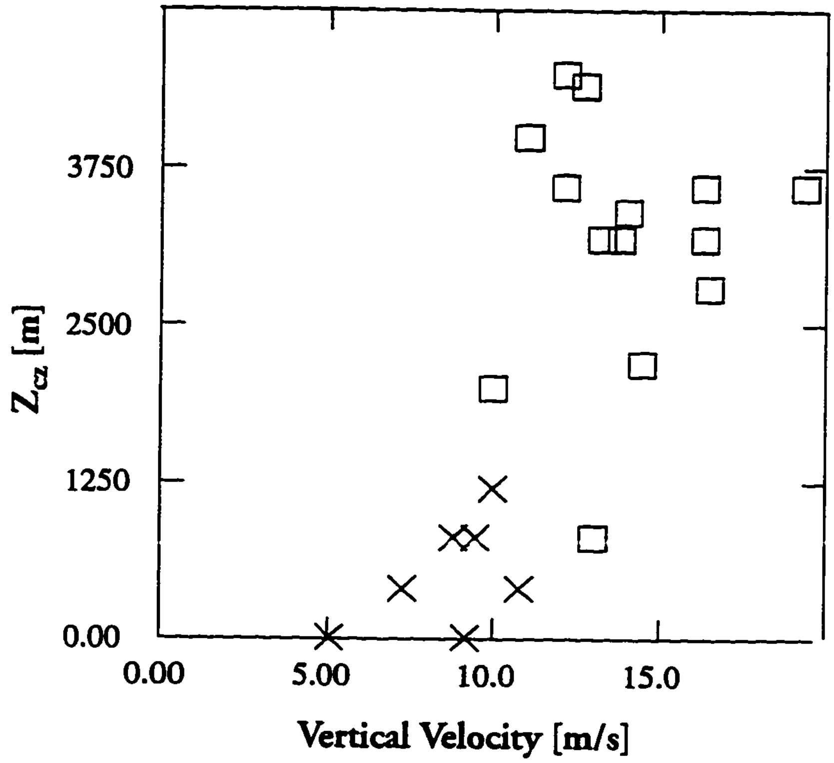


**Figure 4.3. Maximum depth of the charging zone as a function of the peak velocity just below the charging zone for electrified ([]) and non-electrified (x) storms.**

where ice, graupel and supercooled liquid water co-exist, as a function of the peak average vertical velocity in the charging zone, $\bar{w}_{cz}$. An increase in the depth of the charging zone results in more charge separating collisions, and thus a greater charging rate. Since $\delta q$ increases with the diameter of the ice particles (see equation 2.18), both the number of collisions and charge per collision increase as vertical velocity increases. If we consider the base of the charging zone to be located near 0 to -5°C, we can establish that cloudtop must be colder than approximately -10°C; otherwise, the depth of the charging zone will be too small and there will not be enough charge generation to result in a lightning producing storm.

Figure 4.4 shows the dependence of the electrical characteristics of the modelled storm on (a)

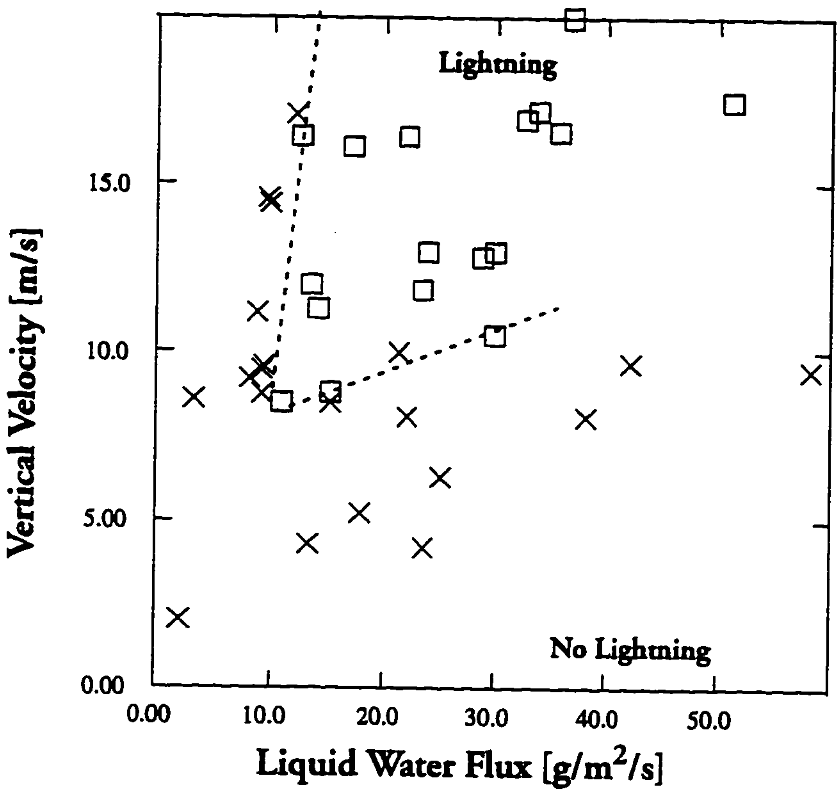


**Figure 4.4. Electrification as a function of peak updraft velocity just below the charging zone and vertical liquid water flux entering the charging zone, electrified ([]) and non-electrified (x) storms**

the peak updraft velocity just below the charging zone prior to the first lightning flash (for electrified storms) and (b) the peak vertical liquid water flux entering the charging zone, $LWF_{cz}$, which usually occurs at or near the same time as the peak updraft velocity. Those storms whose maximum updraft velocity falls below a threshold, $w_{thresh} \sim 7$ m/s, or whose maximum liquid water flux falls below a threshold, $LWF_{thresh} \sim 8$ g/m$^2$/s, never become electrified. In dry environments updrafts may exceed $w_{thresh}$, but there is not a sufficient amount of liquid water flux into the charging zone to provide the liquid water and produce the large riming graupel that are necessary for charge separation. In moist environments sufficient liquid may enter the charging zone but weak updrafts are unable to suspend large particles or keep large riming particles in the charging zone for any length of time. Therefore lightning generation is a very strong function of the updraft velocity within the charging zone as implied by observations (e.g., Zipser, 1994).

There is also a time constraint on how long updrafts and LWF must remain near $w_{thresh}$ and $LWF_{thresh}$. in order to produce lightning. If the updraft velocities do not remain large enough for a long enough period of time, graupel and large drops precipitate from the cloud and charging is too low to raise the electric field magnitude to greater than $E_{init}$. The updraft velocity $w_{cz}$ must exceed $w_{thresh}$ at least until $E(z) > E_{init}$ at some point within the cloud. For simulated clouds, the time needed to produce the necessary electric field magnitude was at least 150 s. This condition on $\overline{w}_{cz}$ must be maintained longer if lightning flashes are to continue. Finally, if the LWF does not remain above $LWF_{thresh}$ for at least the same amount of time, there is insufficient liquid water for efficient charge generation.

### 4.1.2 Sensitivity to cloud condensation nucleus concentration

We examine sensitivity of electrification to variations in the CCN concentration by varying the number of CCN between 100 to 600 $cm^{-3}$, while keeping all other parameters constant. For otherwise identical model runs, changes in the CCN concentration never changed a non-electrified cloud to an electrified cloud, or vice versa. In this series of tests, these changes in CCN concentration did change the concentration of large droplets and number of ice crystals found within the charging zone. Figure 4.5 illustrates the variations in the time to first lightning after charging has begun for a number of modelled storms from Florida and the tropics. The tropical maritime storm requires more time to generate lightning than the continental storm for identical CCN concentrations because the maritime storm has lower updrafts within the charging zone, reflecting a lower charging rate. The simulations run with low CCN concentrations generally take longer to produce lightning because the clouds tended to precipitate sooner than in those simulations with large CCN concentrations. There were also fewer particles within the charging zone and hence fewer charge separating collisions.

### 4.1.3 Sensitivity to cold microphysical processes

Observations of clouds often show that the concentration of ice particles can be much greater than that predicted by primary ice nucleus mechanisms (eg, Rangno and Hobbs, 1991, 1994; Blyth and Latham, 1993). The mechanisms responsible for these elevated concentrations of ice particles is not know. Unfortunately, *in situ* observations of glaciation within clouds are limited. We use ONYX simply to estimate the sensitivity of electrification to variations in some of the most uncertain ice phase processes. For this series of tests we use model results from simulations of New Mexico storms.

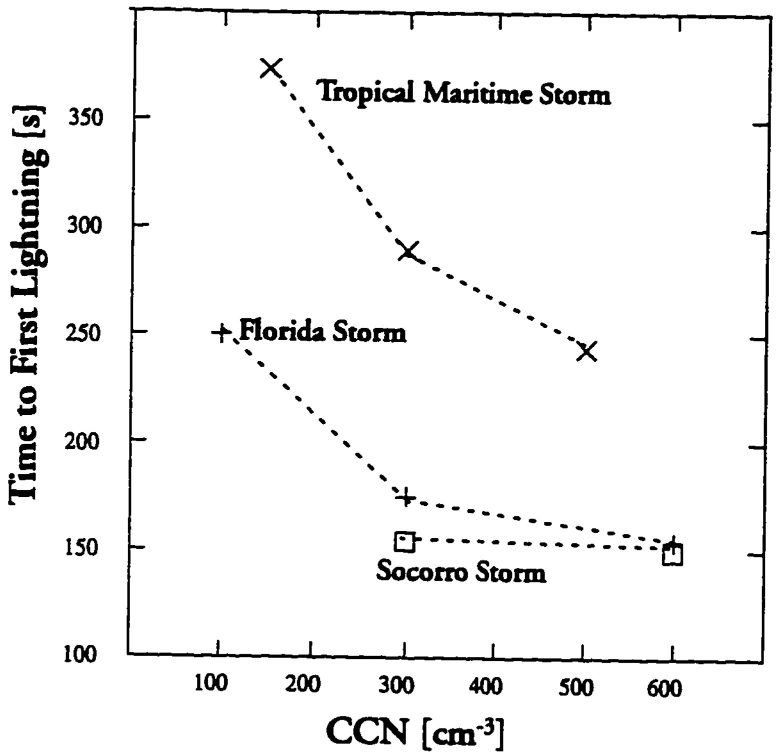


Figure 4.5. Time to first lightning after the onset of charging for a range of cloud condensation nucleus concentrations.

We first examine the sensitivity of predicted charge characteristics to ice nucleus concentration profiles. The ice particle concentrations in the charging zone determine both (a) the magnitude of the charging rate and (b) the sign of the charge delivered to each of the colliding particles. We discuss these each in turn.

If the ice nucleus concentrations are very large, rapid glaciation of the cloud removes liquid water in the charging zone and charging stops at relatively warm temperatures, decreasing the total charge separated. Lowering the ice nucleus concentration slows glaciation, permitting liquid water to exist for longer periods of time and to reach colder temperatures. However, if the ice nucleus concentration in the charging zone is too low, charging rate again drops off, so that the total charge separated is maximum for intermediate ice particle concentrations in the charging zone.

Figure 4.6 is a qualitative illustration of the impact of these changes in ice nucleus

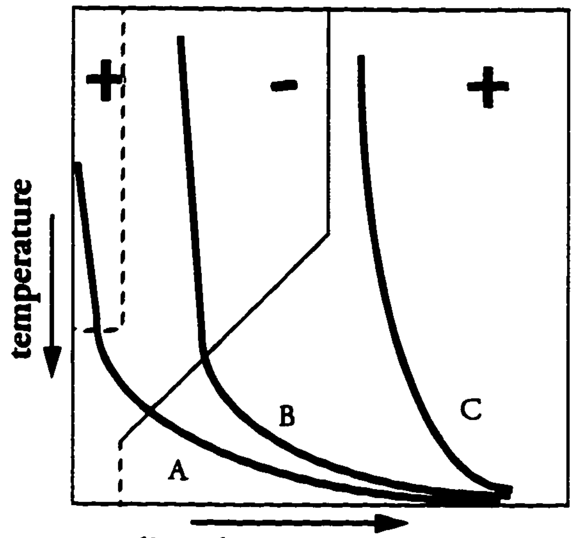


**Figure 4.6. Schematic representation of sign of the charge received by hail during collisions within the charging zone as a function of temperature and liquid water content for a range of ice nucleus concentration: (A) high ice nucleus concentration, (B) intermediate values and (C) low ice nucleus concentrations. (See text.)**

concentrations on the predicted sign of charge transferred to graupel particles during collisions with ice particles within the charging zone. The curves represent the liquid water content as a function of temperature (or height) for (A) high ice nucleus concentrations, (B) intermediate values and (C) low concentrations. Superimposed on these curves is the sign of the charge received by graupel during collisions within the charging zone (Saunders *et al*, 1991) (See equation 1.4.). It is important to note that for the extremes represented by curves A and C, hail receives positive charge while inside the charging zone. This would lead to an 'inverted' dipole structure with positively charged hail residing below negatively charged ice crystals. However, it is also important to note that there is some controversy among laboratory scientists surrounding the existence of positive charging at low liquid water contents at the present time. Therefore, results based on this feature should be treated with particular caution.

We examined the effect of modifications in primary glaciation profiles on electrification in the model, using the parameterizations of ice nucleus concentrations of Fletcher (1962) and Meyers *et al* (1992), (hereafter referred to as 'F' and 'M') to provide reasonable variations in the profiles. Ice crystal concentrations are higher at lower altitudes and lower at higher altitudes in model runs 'M' than in 'F'. As the number of ice crystals increases at lower altitudes, charge separation within the cloud begins lower and sooner. As can be seen in Figure 4.6, an increase in the number of ice nuclei at low levels leads to an inversion in the sign of charge transferred and therefore the possibility of negative dipole storms (negative over positive charge). With 'M', the cloud initially develops an inverted dipole with a small amount of negative charge above positive charge because the warm temperatures and high liquid water contents in the lower portion of the charging zone favor positive charging of graupel during collisions. However, usually no more than 1 C of charge is generated during this time, never producing strongly electrified clouds with inverted dipoles. These conditions only exist for a short period of time before some liquid water is removed by riming and glaciation and the graupel balance levels move to colder temperatures. The graupel now charges negatively, although the initial lower positive charge can persist for some time. This process is potentially one source of the observed lower positive charge center. Conditions along curve 'A' were never observed during the initial electrification of modelled storms but were observed toward the end of the electrically active life of some clouds. Any charge separation that occurred during this time was confined to a relatively short period of time, less than one or two minutes, and resulted in minimal charge separation and most of the this charge only served to reduce the charge on already charged particles.

Inclusion of a parameterization of the Hallet-Mossop secondary ice production mechanism can influence the number and location of ice crystals within modelled clouds. Typically, the modelled warm cloud base storms have large riming particles in the -3 to -8°C region, as required for significant ice production by the Hallet-Mossop mechanism. The general effect of including secondary ice particle production in the modelled clouds was to initiate lightning 25 to 50 s earlier than in clouds modelled without it. The appearance of secondary ice particles increases the number of small ice crystals produced in the lower region of the charging zone. Graupel particles experience more collisions throughout the charging zone and carry larger amounts of charge along with a greater number of positively charged ice crystals. Secondary ice production never determined whether a modelled cloud became electrified or not.

From these simulations, we conclude that (1) the temperature at cloud top must be below -10°C, (2) the liquid water flux entering cloud base must exceed ~ 8 g $m^{-2}$ $s^{-1}$ for approximately 100-150 sec and (3) the updraft velocity must exceed ~ 7 m $s^{-1}$. If these criterion are not meet, the cloud will not produce lightning. If these criterion are meet, the ice nuclei concentration can have dramatic effects on the development of the charge within the cloud by changing the altitude at charging takes place. Though changing the glaciation mechanism in these simulations did not affect the eventual production of lightning, it did change the amount of time to first lightning.

## 4.2 Lightning Flash Rate

In the previous section we studied the conditions required for the electrification of a convective cloud. In this section we examine electrified clouds only, in order to identify the sensitivity of to the time between lightning flashes and the duration of lightning to variations in cloud characteristics. We use ONYX to simulate the lightning flash rate for variations in CCN, glaciation and secondary ice production while maintaining all other inputs fixed, using the environments discussed in the previous chapter.

### 4.2.1 Sensitivity to updraft velocity and liquid water flux

Figure 4.7 shows the average updraft in the charging zone and the total lightning flash rate for the subsequent minute from each of the storms simulated from TOGA-COARE, CAPE and Socorro.

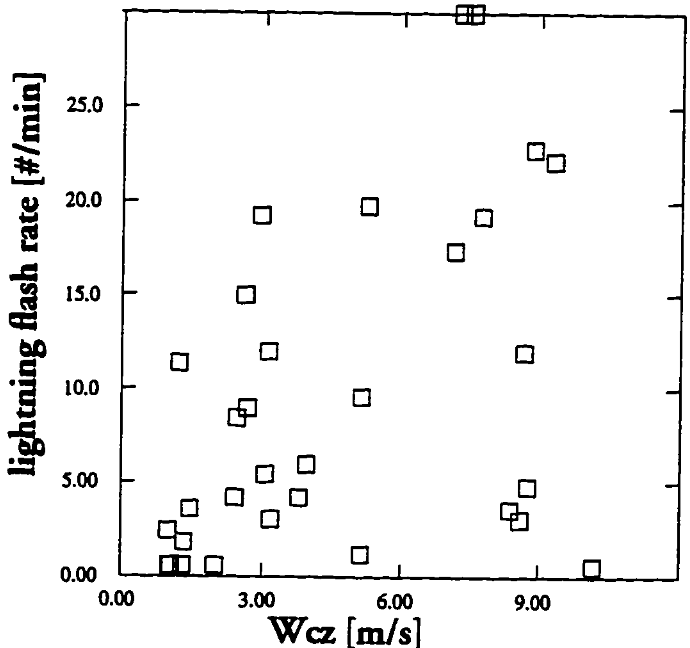


**Figure 4.7. Total lightning flash rate versus average updraft velocity in the charging zone from simulated TOGA-COARE, CAPE and Socorro storms.**

Though there is a definite trend for higher lightning flash rates to be associated with higher updraft velocities in the charging zone, there is a substantial amount of scatter. Figure 4.7 contains the entire history of the updraft velocity and lightning flash rate. Relatively high average updraft velocities and low lightning flash rate, generally reflect the early electrification period within the storms. The storm is very active but the updrafts have not been sufficiently high for a long enough period of time to generate large amounts of charge. Alternatively, low average updraft velocities and high lightning flash rates, generally reflect the later period of electrical activity when the updrafts are subsiding but there is still a substantial amount of charge in the cloud.

Figure 4.8 shows the observed peak vertical velocity at -10°C and the cloud-to-ground

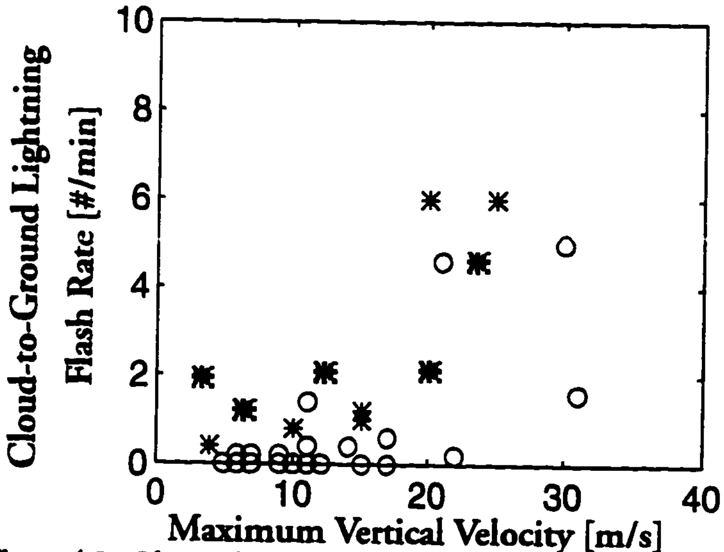


**Figure 4.8. Observed, O, and modelled, *, instantaneous peak cloud-to-ground lightning flash rates [#/min] versus vertical velocity [m/s] (from Solomon *et al*, 1996)**

lightning flash rate for the 5 minutes after the peak updraft velocity from the 15 August 1991 CaPE storm as well as modelled values of the same parameter from the 31 January 1993 TOGA-COARE and 29 July 1991 CaPE storms. The model results show the same trend as the observations. The increase in flash rate with increasing updraft velocity can be attributed to the increase in number and size of particles being suspended in the updrafts, as discussed section 4.1.1.

Baker *et al* (1995) concluded through dimensional analysis that the lightning flash rate is proportional to $w^6$. As Figure 4.8 and Figure 4.7 suggest, we do not see such a strong relationship. The model suggests that total lightning flash rate is strongly correlated with $\overline{w}_{cz}$, but there is large variability from storm to storm and throughout the lifetime of an individual storm as well.

Next, we examine the relationship between lightning and liquid water flux into the charging zone. For all simulations, the peak in lightning flash rate comes approximately 2-4 minutes after the peak in liquid water flux into the charging zone.

Figure 4.9 shows the relationship between the modelled vertical liquid water mass that has been lofted into the charging zone (defined as the vertical flux passing through the 0°C

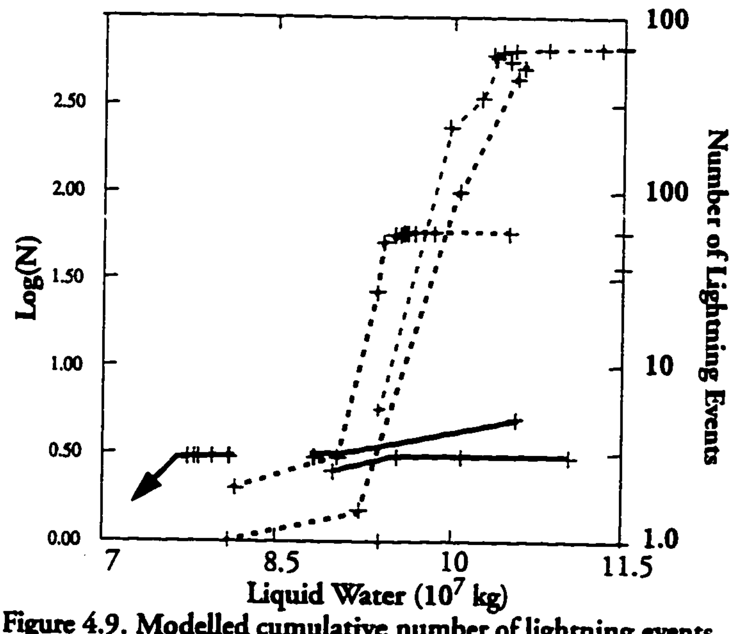


**Figure 4.9. Modelled cumulative number of lightning events versus the liquid water mass that has been lofted into the charging zone for CAPE (dotted lines) and TOGA-COARE (solid lines) storms.**

isotherm) and the total number of lightning events prior to this. There is a very strong sensitivity between the mass of water in the charging zone and the number of lightning events for continental storms. Once a sufficient amount of material has been lofted into the charging zone lightning begins. With continued liquid water flux into the charging zone, there is an increase in the total number of lightning events until the cloud glaciates or development stops. The relationship is not clear for the modelled maritime storms.

### 4.2.2 Sensitivity to cloud condensation nucleus concentrations

We examine sensitivity of lightning flash rate to variations in CCN concentration, using the tests as described in section 4.1.2. In general, the model results show that the time to first lightning decreases by up to a few minutes when the concentration of CCN is increased from 100 cm$^{-3}$ to 600 cm$^{-3}$. Once lightning begins, the lightning flash rate and the total lightning flash number increase for an increase in the CCN concentration. Figure 4.10 shows the

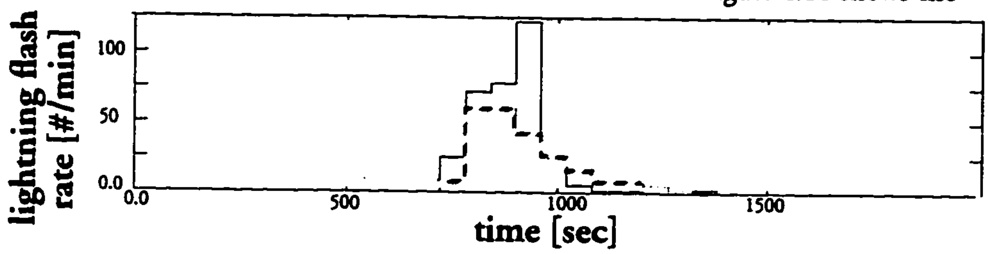


**Figure 4.10. Time dependence of modelled lightning flash rate [#/min] for a cloud with an initial CCN concentration of 600 cm$^{-3}$ (solid line) and a cloud with an initial CCN concentration of 300 cm$^{-3}$ (dashed line).**

modelled lightning flash rate for two storms initialized with a sounding from the CaPE field project (Figure 3.6) having identical input parameters except CCN concentration was 300 cm$^{-3}$ for one simulation and 600 cm$^{-3}$ for the other. In the higher CCN simulation more droplets were activated, entered the charging zone and froze. The larger number of collisions between graupel and small ice particles provided a larger charging rate and allowed for the magnitude of the electric field to reach the breakdown threshold more rapidly between lightning flashes for the storm with higher CCN concentrations.

### 4.2.3 Sensitivity to glaciation mechanism

Variations in the primary glaciation mechanism give rise to large differences in the modelled lightning flash rate. We initialized ONYX with a sounding from Socorro, 2 August 1984 (Figure 3.4) using the ice nucleus concentrations predicted by the Fletcher (1962) parameterization and then with the Meyers *et al* (1992) parameterization. For a cloudbase forcing of $w_{cb}$ = 1.5 m s$^{-1}$, the simulated storm initialized with the Fletcher parameterization produced several hundred lightning flashes with a peak flash rate of 39 min$^{-1}$, whereas the storm initialed with the Meyers *et al* parameterization produced one lightning flash. Again, as in the results presented previously for initial electrification (section 4.1.3), the large difference is due predominantly to the larger number of ice crystal nuclei predicted by the Fletcher parameterization, especially in the colder regions of the charging zone. Fletcher and Meyers *et al* represent the same (primary nucleation) process; the importance of improved knowledge of the parameters of that process is dramatically demonstrated by the difference in predicted electrical behavior the two parameterizations produce.

Figure 4.11 shows the strong dependence of the peak modelled lightning flash rate on the

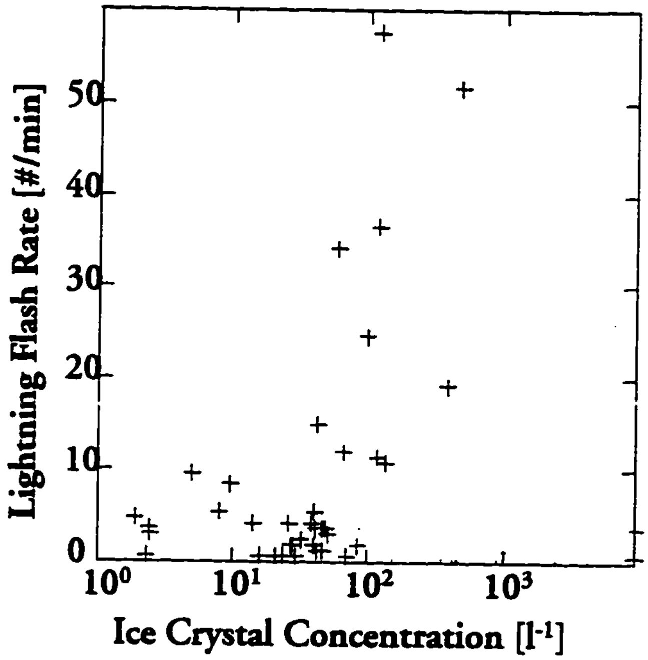


**Figure 4.11. Modelled peak lightning flash rate and peak ice crystal concentration averaged throughout the depth of the charging zone.**

peak concentration of ice crystals for lightning producing storms. Figure 4.11 combines the results from modelled storms that use Fletcher, Meyers *et al* parameterizations as well as secondary ice generation via the Hallet-Mossop mechanism. Ice crystal concentration is most clearly correlated to peak lightning flash rate in these modelled storms. It is important to note that the presence of large concentrations of ice crystals does not imply an electrified cloud. Maritime clouds may have large concentrations of ice crystals (Hobbs and Rangno, 1991) but do not produce lightning because the updraft velocity is insufficient to suspend graupel within the charging zone.

### 4.2.4 Sensitivity to secondary ice production

Inclusion of the Hallet-Mossop secondary ice production mechanism generally increases the total number of lightning flashes by approximately 10-20% in storms where conditions are favorable for the formation of secondary ice particles by this mechanism. This increase is due to the increase in the number of small ice particles in the charging zone and therefore the charging rate. The increase was particularly marked in those clouds that had large riming particles in the charging zone; e.g. maritime clouds that had sufficient updrafts to keep particles aloft in the charging zone for a substantial amount of time. Figure 4.12 illustrates the

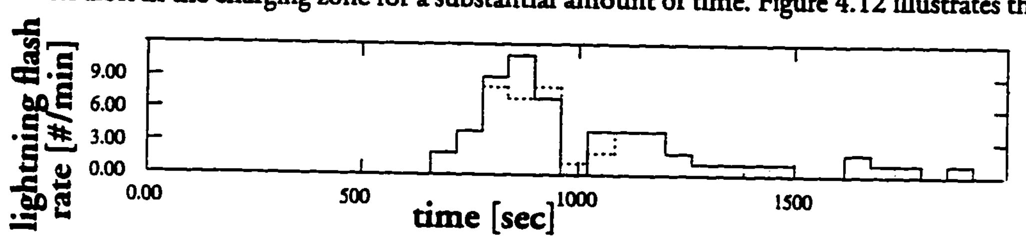


**Figure 4.12. Modelled lightning flash rate [#/min] for a cloud with secondary ice production (solid line) and a cloud with no secondary ice production (dashed line).**

change in the lightning flash rate for a simulated thunderstorm initialized with a sounding from the TOGA-COARE project (Figure 3.10) in which one model run included secondary ice production and the other did not.

The duration of lightning within the model is somewhat sensitive to the duration of the imposed forcing. Maintaining the forcing for longer times can artificially keep the liquid water flux and updraft velocity above the required thresholds for maintaining charge generation and separation. In most simulations that we examine, once the forcing is removed, the modelled cloud sits in a quasi-steady state for up 100-300 s and then begins to decay fairly rapidly and lightning soon ceases.

The lightning flash rate appears to be the most sensitive to ice crystal concentrations and their distribution with altitude. Charging is most efficient when a moderately large concentration of ice crystals exists at an altitude where the temperature is -10 to -15°C. Very large numbers of ice crystals can deplete the liquid water, stopping charge separation. Finally, if ice crystals are only present at very cold temperatures, > -25°C, charge generation and separation is very inefficient because there is very little mixed phase development in the charging zone.

### 4.3 Cloud-to-Ground /Intracloud Lightning Ratio

We now investigate the mechanisms that are responsible for the observed patterns in ratio of cloud-to-ground/intracloud lightning, R. The intracloud lightning channels initiated in ONYX during the developing stage of the cloud are relatively unimportant in depositing positive charge in lower region of the cloud because they tend to be relatively short and have little charge induced on their surfaces. The longer channels that are initiated around the time that cloud has reached its full depth are more efficient at "eating" away at the lower negative region and depositing significant amounts of positive charge below or within the lower part of the negative charge region. Thus, within ONYX, cloud-to-ground lightning usually initiates only after long intracloud channels deposit positive charge below the main body of negative charge. This happens after the cloud has reached full development.

Figure 4.13 shows vertical profiles of the charge density and vertical electric field taken at various times from a simulated thunderstorm. Initially, the charge profile is relatively simple, showing a lower negative charge region with a very small amount of positive charge (not discernible in this picture) below and positive charge above. A small amount of negative charge can be seen above the main positive charge region. This charge is created by the screening charge currents at cloud top. As the thunderstorm ages, more positive charge accumulates below the main negative charge region and more negative charge at high altitudes. Most, if not all, of the lower positive charge is deposited by lightning channels. The upper negative charge results from charge deposited by lightning channels and the charge brought by screening currents at cloud top. After some time, the amount of positive charge deposited below the main negative charge region is large enough that the electric field exceeds $E_{init}$ below the main negative charge region, resulting in the initiation of cloud-to-ground lightning channels.

Occasionally lightning channels initiate below the lower charge region but are unable to extend toward the ground. This appears to be an artifact of the geometry constraint for the lightning channel. The upper region of the channel only extends a few hundred meters above the initiation point before halting. Very little positive or negative charge is induced as the lightning channel extends downward and the charge at the lower tip quickly falls off and halts propagation before the channel reaches ground. Within actual clouds, the upper portion of

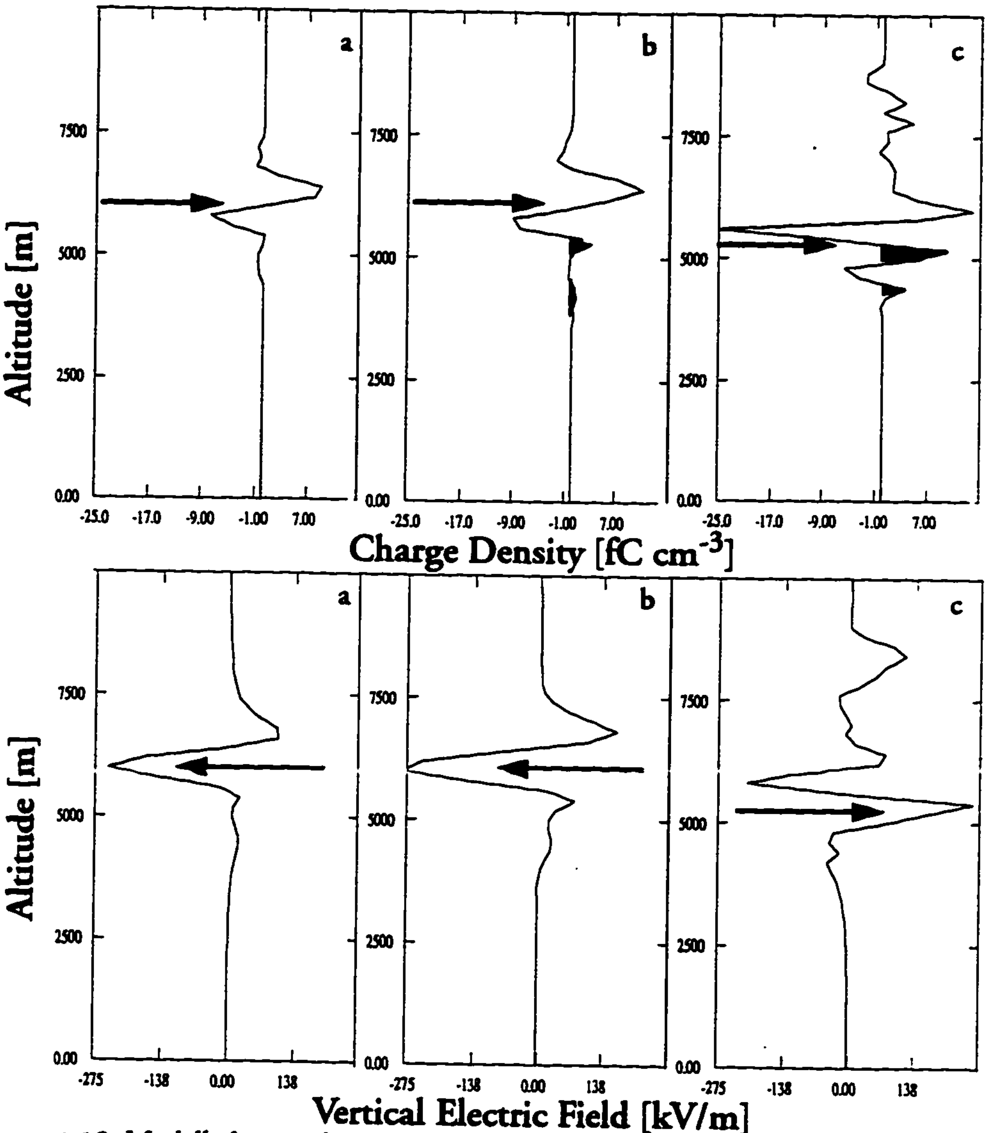


**Figure 4.13. Modelled vertical profiles of the charge density vertical electric field taken at (a) the time of the first lightning flash, (b) at approximately the time that cloud maximum height was reached and (c) just before initiation of the first cloud-to-ground channel. The arrows point to the approximate point where the subsequent lightning channel was initiated within ONYX.**

the lightning channel branches and propagates horizontally, allowing for continued development of the lightning channel (Mazur and Ruhnke, 1993).

### 4.3.1 Sensitivity of lightning flash rate and R to $E_{init}$

In light of the recent observations given by Marshall *et al* (1995a) showing that the maximum electric fields observed within cloud decrease with altitude, we used the pressure dependent form of the initiation electric field (see Figure 2.39) in a number of simulations. However, instead of using $E^0_{init}$ = 200 kV m$^{-1}$ as suggested by Marshall *et al*, we chose $E^0_{init}$ such that the initiation electric field at 6 km (the approximate altitude at which a large number of the lightning channels were initiated within ONYX) matched the constant value used in all other simulations. The main effect was to decrease the number of cloud-to-ground channels and to initiate more channels at higher altitudes in the cloud (11-12 km). The overall lightning flash rate was only negligibly changed. Since the majority of cloud-to-ground lightning channels initiate at lower altitudes than intracloud channels, the magnitude of the electric field required to initiate cloud-to-ground channels increases, making it more difficult to initiate cloud-to-ground channels. The time to the first cloud-to-ground channel is greater than in simulations using the constant value of $E_{init}$. Subsequent cloud-to-ground channels are also more difficult to initiation using the pressure dependant form $E_{init}$, reducing R.

If we were to include the pressure dependent form of $E_{init}$ with $E^0_{init}$ = 200 kV m$^{-1}$, as suggested by Marshall *et al* (1995a), we would expect (1) an increase in the total lightning flash rate due to the decreased electric field required to initiate lightning and hence the smaller amount of charge induced on each channel and (2) fewer cloud-to-ground lightning channels, because the initiation field is higher for these strokes, which are initiated lower in the cloud than intracloud strokes.

### 4.3.2 Lightning flash rate and precipitation

With the advent of satellite borne lightning sensors, it is of interest to ascertain the relationships between satellite measurements of lightning flash rate and parameters of climatological interest, particularly those that are difficult to measure *in situ*. Precipitation and the redistribution of water high in the atmosphere are two such parameters. We use ONYX to examine the usefulness of lightning flash rate as a surrogate for precipitation, using the same simulations as discussed above and in the previous chapter.

Figure 4.14 shows the modelled rain rate versus total lightning flash rate for all the TOGA-COARE and CAPE simulations. The modelled rain rate and the modelled flash rate are taken at the same instant. It becomes quite apparent that it is difficult to find a "universal" relationship between instantaneous lightning flash rate and rain rate. The peak lightning flash rate and peak rain rate show variability from storm to storm. These studies show that the absence of lightning can not be taken as an absence of precipitation, and thus the use of lightning flash rate as a surrogate for precipitation rate on a storm-by-storm basis requires care. Rather, as Figure 4.9

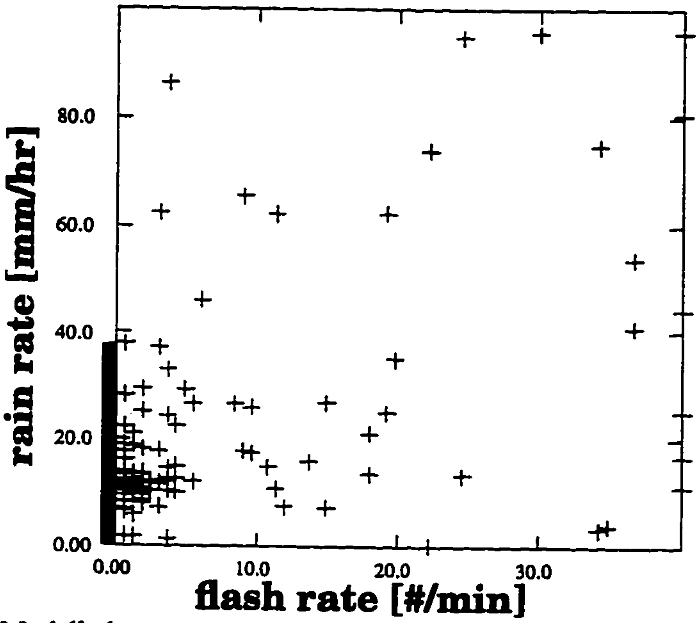


**Figure 4.14. Modelled rain rate versus total lightning flash rate using the results of all TOGA-COARE and CAPE simulations. The shaded side bar give the range of observed rain rates for an observed and modelled non-lightning producing TOGA-COARE storm.**

suggests, total lightning number is better correlated to the amount of water mass that has entered the charging zone.

## 4.4 Predicting Cloud Electrical Properties

Now we examine the possibility that the a cloud's electrical properties can be predicted from soundings alone. We consider the predictors in Table 3.1 for both New Mexico and tropical storms. A cursory look at Table 3.1 suggests that a CAPE threshold might be a good lightning predictor for the New Mexico storms. Measuring CAPE accurately is problematic and often the soundings from which CAPE is calculated do not represent the environment at the time and location where storms form, due to spatial and temporal variations in temperature and water vapor. With this problem in mind, we look at the trends in observed CAPE and the future electrical development of storms. In Table 4.1 We attempt to predict the occurrence of

**Table 4.1: CAPE threshold predictions for New Mexico Storms**

| date (1984) | CAPE [J kg$^{-1}$] | is CAPE over threshold value? (400 J/kg) | correct guess |
|---|---|---|---|
| 23 July | 234 | no | yes |
| 27 July | 43 | no | no |
| 29 July | 208 | no | yes |
| 31 July | 924 | yes | yes |
| 1 Aug | 854 | yes | yes(?) |
| 2 Aug | 471 | yes | yes |
| 3 Aug | 412 | yes | yes |
| 6 Aug | 322 | no | yes |
| 7 Aug | 1463 | yes | yes |
| 13 Aug | 321 | no | no |
| 14 Aug | 935 | yes | no(?) |
| 15 Aug | 2038 | yes | yes |

lightning by assuming it is triggered in those storms forming in environments with CAPE > 400 J kg$^{-1}$. This CAPE threshold is quite successful as a predictor, although there were a few days when it failed. (The 27 July and 13 August predicted CAPE fell below the threshold though those days produced electrified storms and the 14 August CAPE was above the threshold but did not produce lightning though moderate electrification was noted.) It may be that stronger forcing caused the 27 July and 13 August storms to produce lightning. In fact, Sabreliner measurements on 13 August 1984 show air at cloudbase was warmer than in the environment by at least 1°C. On the other hand, there may have been insufficient forcing on 14 August.

The CAPE threshold predicting the onset of lightning determined above for New Mexico storms is not very useful for tropical storms. There are numerous maritime storms with CAPE above the New Mexico threshold of 400 J/kg which never become electrified. For the tropical storms, a threshold around 700 J/kg is suggested from examination of soundings from environments that are representative of monsoon and continental environments.

Table 4.2 follows the same format as Table 4.1 and evaluates the effectiveness of CAPE as a

**Table 4.2: CAPE threshold predictions for tropical storms**

| Location | date | CAPE [J kg$^{-1}$] | lightning? | is CAPE over threshold value? (700 J/kg) | correct guess? |
|---|---|---|---|---|---|
| Florida | 19 July 1991 | 1786 | yes | yes | yes |
| | 29 July 1991 | 1850 | yes | yes | yes |
| | 9 August 1991 | 788 | yes | yes | yes |
| South Pacific | 31 Jan 1993 6 Z | 200 | no | no | yes |
| | 31 Jan 1993 12 Z | 1222 | yes | yes | yes |
| | 15 Feb 1993 | 771 | yes | yes | yes |
| | 12 Jan 1990 | 196 | no | no | yes |
| | 19 Jan 1990 | 1357 | yes | yes | yes |

predictor of electrification within tropical storms. Increased CAPE does seem to "predict" an increased probability in storm electrification.

The attempt to predict the future electrical status of a storm from one environmental quantity seems quite optimistic, given the large amount of potential variability within Nature. However, the combination of observed cloud behavior and modelled results suggest that CAPE is a good lightning predictor for the New Mexico and tropical storms.

In order to understand the success of the CAPE threshold and cloudtop height as lightning predictors, we performed a series of model tests in which the 2 August 84 sounding was modified in order to increase the CAPE of a parcel starting from cloudbase. This was done in three ways: 1) by decreasing the temperature in the 600 to 500 mb region, 2) by decreasing the temperature in the 450 to 350 mb region (and thereby decreasing the strength of the inversion) and 3) by a combination of the two above. For all of these, the cloudbase temperature was unchanged.

The modifications to the sounding increased CAPE by as much as 200 J kg$^{-1}$. ONYX was run with a forcing that produced some charge separation, but not enough to produce fields above the breakdown threshold when initialized with the unmodified sounding. Figure 4.15 shows that in each case an increase in CAPE increased the total charge separated and pushed the electric field to a value that would cause breakdown. In cases in which the inversion strength

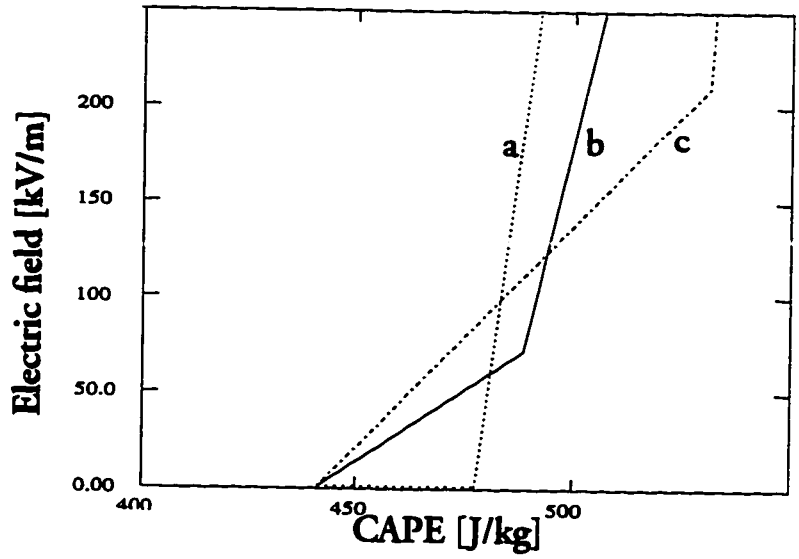


**Figure 4.15. Model predicted maximum electric field [kV m$^{-1}$] as a function of CAPE for the modified soundings (a) modified in the 600-500 mb region, (b) 450-350 region and (c) modified in both regions (see text).**

was reduced water was transported above -10°C more easily and more charge was separated than for the unmodified sounding. When the temperature in the lower portion of the cloud was decreased (increasing CAPE) the amount of charge separated was also increased, though not as much as the previous case.

The use of $Z_{ct,max}$ as a predictor requires that it be estimated in advance of cloud development. $Z_{ct,ad}$, the cloudtop estimated on the assumption of moist adiabatic ascent from cloudbase, is approximately as effective a predictor as CAPE. For the New Mexico storms, neither $\theta_w$ nor $L_i$ were useful lightning predictors (see Figure 4.16).

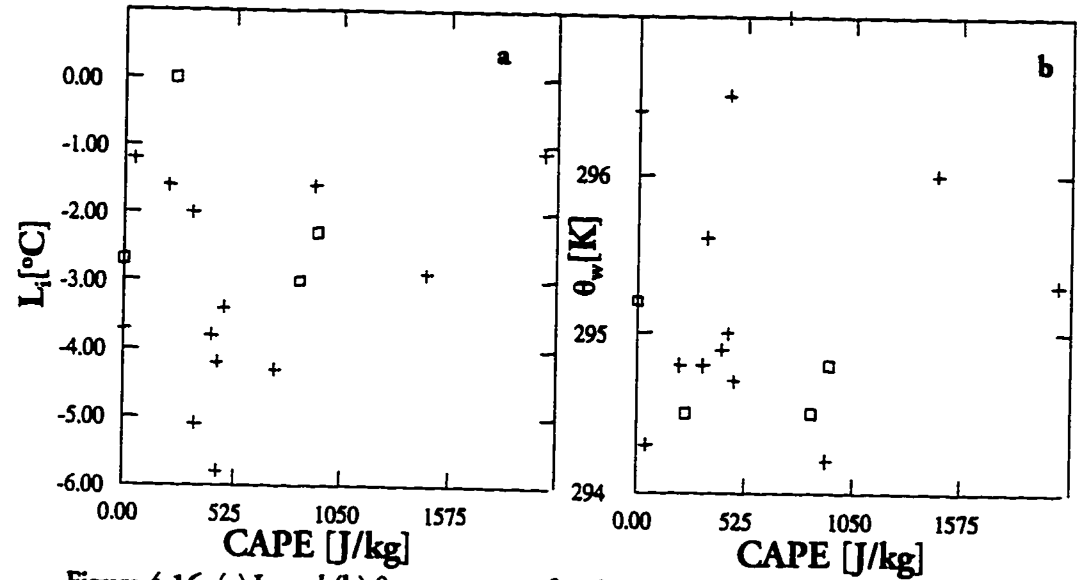


**Figure 4.16.** (a) $L_i$ and (b) $\theta_w$ versus CAPE for the New Mexico storms for electrified, '+' and non-electrified '[]' storms.

As mentioned in the introduction, there are numerous climatological studies that indicate that cloud top height is correlated with lightning flash rate. Figure 4.17 gives the modelled

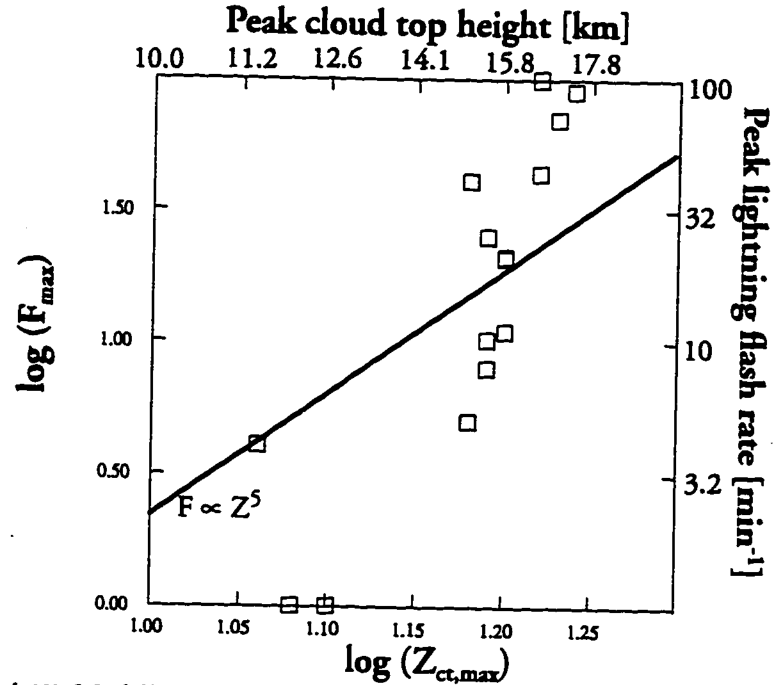


**Figure 4.17.** Modelled peak cloud top height versus peak lightning flash rate for simulated TOGA-COARE and CAPE storms. The line is from Price and Rind (1992).

peak cloud top height (defined as the altitude where the total water mixing ratio falls below 0.1 g m$^{-3}$) versus the peak flash rate for simulated TOGA-COARE and CAPE storms that became electrified. Generally for those storms that become electrified, an increase in the maximum cloudtop height reflects a deeper charging zone and a larger overall charging rate within the cloud. However, a number of the simulated 31 January 1993, 6Z TOGA-COARE storms reached 12-15 km but never became electrified (see Figure 3.11) suggesting that cloudtop height alone is not sufficient to predict peak lightning flash rate.

Price and Rind (1992) find $F \sim Z_{ct}^5$ (equation 1.3) for observed thunderstorms in Florida, New Mexico and New England whereas we see a greater sensitivity from the modelled thunderstorms. For very active storms, ONYX may have to initiate several consecutive channels during a single time step to reduce the magnitude of the electric field to below $E_{init}$, so the greater sensitivity may be an artifact of lightning parameterization.

# V. Summary and Conclusions

## 5.1 Summary of Results

In the next section we briefly summarize the results to the questions outlined in Chapter I and we present the processes that have the greatest influence on initial electrification, lightning flash rate and type.

### 5.1.1 What factors determine which storms produce lightning?

Our results suggest that variations in cloud forcing may be responsible for the wide variations in observed electrical behavior in regions, such as Socorro, NM where atmospheric soundings are relatively uniform. High cloud forcing may also account for the pockets of increased lightning observed from space (Christian, 1996). Electrification appears to be relatively insensitive to CCN concentrations but highly sensitive to ice particle concentrations. We find that in order for a convective storm to produce lightning, (1) $w_{cz}$ (vertical velocity within the charging zone) > ~7 m $s^{-1}$ and (2) $LWF_{cz}$ (vertical liquid water flux into the charging zone) > ~ 8 g $m^{-2}s^{-1}$ for 100 to 150 sec or more and (3) the temperature at cloud top must be below -10°C. This implies that in situations where coalescence can remove much of the liquid water before it reaches the freezing level, or where the updraft in the charging zone is insufficient to keep graupel in the charging zone for at least 100 to 150 sec, lightning production is diminished or never realized. These requirements reflect the necessity for sufficient development of the charging zone and ice content to generate charge and for the particles responsible for separating the charge to remain in the charging zone for a long enough period for the electric field to reach the magnitude to initiate lightning, $E_{init}$. If any of these criteria are not met, small amounts of charge may be generated, but it will be insufficient to generate the required breakdown electric fields during the normal lifetime of a thunderstorm. The oft-observed correlation between CAPE and propensity for lightning is due to the trend for higher CAPE environments to result in storms with larger updrafts in the charging zone, $\overline{w}_{cz}$. However, forcing may be sufficient to produce an electrified cloud in low CAPE environments.

### 5.1.2 Why is there more lightning over continents than oceans?

We do not find a strong dependence of lightning production on CCN concentrations. Instead, the results suggest that the low values of $\overline{w}_{cz}$ and, for some storms, $LWF_{cz}$, are responsible for the low lightning production over the oceans. In storms forming in low CAPE maritime environments, large cloudbase forcing can generate the required updrafts and liquid water flux in the charging zone to allow for graupel, ice and supercooled liquid water to co-exist within the charging zone; however, without this forcing, the conditions outlined in section 5.1.1 are never met and the particles precipitate out of the warm sector of the cloud before participating in charge separating collisions.

An increase in cloud forcing may explain the relatively high amounts of lightning in storms forming over the Gulf Stream (Biswas and Hobbs, 1990) or along the Inter Tropical Convergence Zone (ITCZ) and the near absence of lightning in storms forming away from the influence of the Gulf Stream in the North Atlantic.

### 5.1.3 What factors determine lightning flash rates in thunderstorms?

We find some dependence of lightning flash rate on CCN concentrations, but lightning flash rate is more sensitive to ice formation processes. The lightning flash rate is high in those cases where glaciation is effective at relatively warm temperatures (approximately -10°C) either because of primary nucleation or secondary ice production. However, very rapid glaciation at warm temperatures results in either very little charging due to the loss of liquid water or positively charged graupel and an inverted dipole (see curve 'A' in Figure 4.6). $LWF_{cz}$ is crucial in maintaining lightning within thunderstorms. If too little liquid water enters the charging zone, charging stops. It is important to note that the magnitude of $LWF_{cz}$ for maintaining favorable conditions in the charging zone is less than the threshold for initial electrification. For those storms that produce lightning, the lightning flash rate and amount are strongly correlated with $\overline{w}_{cz}$ and the total amount of liquid water that has been lofted into the charging zone.

### 5.1.4 What factors determine the intracloud/cloud-to-ground lightning ratio?

Within the simplified context of an axially symmetric numerical model, we find that the presence of a lower positive charge center greatly increases the likelihood of cloud-to-ground channels, although on occasion these develop in its absence. Cloud-to-ground channels in general begin only after (a) intracloud lightning flashes have deposited sufficient positive charge at low levels and/or (b) the negative charge center has lowered. Since intracloud flashes appear to be more successfully represented by our parameterization than do cloud-to-ground flashes, it appears that horizontal development of the lightning channel is more important for the latter than for the former to drive the channel toward the ground.

### 5.1.5 What is the relation between lightning flash rate and precipitation?

It appears from our studies on individual convective storms that lightning flash rate is correlated to precipitation rate when there is lightning, but that nonelectrified storms, particularly marine storms, can produce the same amount of precipitation as lightning producers. The use of lightning flash rate as a surrogate for precipitation rate on a storm-by-storm basis appears problematic. Instead, the total number of lightning events is more strongly correlated with the mass of liquid water entering the charging zone for continental storms. This correlation may be useful in establishing the redistribution of water through the atmosphere for mesoscale/global water budget studies and global circulation models.

## 5.2 Limitations of the Thunderstorm Model

The basic limitations of the thunderstorm model's lightning parameterization lie in its neglect of all but electrostatic effects in determining lightning initiation and charge redistribution due to lightning. The fact that the parameterization seems to give reasonable trends and reasonable magnitudes of charge transfer per flash appears to vindicate its use in numerical studies of electrified clouds. However, there are further limitations of ONYX which could be overcome by relatively minor changes, and we now discuss these.

A one-dimensional cloud and lightning model cannot capture the effects of horizontal development of charge centers, which may be of particular importance in the development of cloud-to-ground channels. While the thunderstorm model could accommodate non-vertically propagating channels, the lightning parameterization could not in its present, analytic form, be used for complicated trajectories. Extension of the shape of the conductor is in principle possible but would entail numerical computation of the charges induced on it.

We have assumed that lightning is initiated at points where the vertical electric field is a maximum and greater than $E_{init}$, which we took to be a constant. If in fact $E_{init}$ depends on hydrometeor type as well as mean electric field, the channel type may depend on the distributions of hydrometeors.

It is clear that the results presented here are suggestive only in part because we look at a small handful of observations and because the cloud model geometry limits the ability to investigate any but the simplest unsheared air mass thunderstorms. The cloudbase forcing is imposed and the cloud environment does not change as the storm evolves. We have included only the simplest electrostatic parameterization of an unbranched lightning channel. However, in view of the uncertainties surrounding the electrical processes in cloud, it is perhaps not worthwhile to attempt more detailed quantitative modelling studies, but rather to examine the implications of simpler studies in the light of better and more extensive field and laboratory data.

## 5.3 Future Work

Given the simplicity of the thunderstorm model, its use in conducting a large number of sensitivity tests and predicting trends in a variety of environments is of great value. This study as well as more sensitivity tests in different environments would prove useful in helping to establish the relationships between satellite observations (such as lightning flash rate and cloudtop height) and the microphysical processes throughout the depth of lightning producing clouds. Although the instantaneous correlations between lightning flash rate, precipitation rate and updraft velocity within the charging zone were somewhat scrambled due to the variations with storm age, further studies utilizing other information, such as cloud top height as an indicator of cloud age, may give a clearer relationship between lightning flash rate and climatologically import parameters. Correlating the lightning flash rate with precipitation at some point in the future, rather than the instantaneous value, may also prove useful in understanding the relationship between lightning flash rate and precipitation and/or updraft velocity within the charging zone.

Since lightning flash rate is very sensitive to ice crystal concentrations within the charging zone, clouds that develop near the debris of previous clouds may be more likely to produce large amounts of lightning. The model can be modified to accept an initial ice crystal concentration or to allow for a series of "thermals" that progressively modify the ice crystal concentrations within the cloud to examine the sensitivity of modelled electrification and lightning flash rate to ice enhancement and successive thermals.

Further work is needed to quantify the mechanisms responsible and the conditions required for initiating lightning and the condition(s) that determine whether a lightning channel propagates to ground or remains within the cloud. Lightning mapping has proved useful in providing the location of lightning initiation and the vertical/ horizontal extent of the lightning channel. Interferometer measurements provide this information and subsequent points along the lightning's path of travel. The in-cloud microphysical, dynamic and thermodynamic properties, however, are not so easily measured. The thunderstorm model can be used to simulate a number of electrified storms for which interferometer data exist and examination of the simulated cloud at the point where lightning is initiated could help to establish the microphysical characteristics associated with lightning initiation.

There is anecdotal evidence of electrified clouds that cease producing lightning when they move over lakes or from continental areas to the ocean. The model can be used to study this transition between "continental" to "maritime" regimes and establish the reasons and time required to go from an electrically active to non-lightning producing state.

## Bibliography


Asai, T and A Kasahara, 1967: A Theoretical Study of the Compensating Downward Motions Associated with Cumulus Clouds., *J Atmos Sci*, **24**, 487-96

Baker, B, M B Baker, E Jayaratne, J Latham and C Saunders, 1987: The Influence of Diffusional Growth Rates on the Charge Transfer Accompanying Rebounding Collisions Between Ice Crystals and Hailstones. *QJ R Met Soc*, **113**, 1193-1215.

Baker, M B and J G Dash, 1989: Charge Transfer in Thunderstorms and the Surface Melting of Ice., *J Crystal Growth*, **97**, 770-6.

Baker, M B, H Christian and J Latham, 1995: A One-Dimensional Model of Lightning from Convective Clouds., *Quart J Roy Met Soc.*, **121**, 1525-1548.

Berry, E X, 1967: Cloud Droplet Growth by Collection., *J Atmos Sci*, **24**, 688-701.

Berry, E X and M R Pranger, 1974: Equations for Calculating the Terminal Velocities of Water Drops., *J Appl Meteor*, **13**, 108-113.

Biswas, Kumud R and Peter V Hobbs, 1990: Lightning Over the Gulf Stream., *Geophys Res Let*, **7**, 941-3.

Blyth, Alan M and John Latham, 1993: Development of Ice and Precipitation in New Mexican Summertime Cumulus Clouds. *QJ R Met Soc*, **119**, 91-120.

Bondiou, A, I Taudière, P Richard and F Helloco, 1990: Analyse Spatio-temporelle du Rayonnement VHF-UHF Associé àl'Éclair, *Revue Phys Appl*, **25**, 147-157.

Breed, Daniel W and James E Dye, 1989: The Electrification of New Mexico Thunderstorms, 2. Electric Field Growth During Initial Electrification., *J Geophys Res*, **94**, 14841-14854.

Breed, Daniel W, 1993: Electric Field Development and Multi-Parameter Radar Measurements in a Florida Storm., proceedings to the 17th Conference on Atmospheric Electricity, 4-8 October 1993, St Louis., J16-J19.

Brook, Marx, R W Henderson and Richard B Pyle, 1989: Positive Lightning to Ground., *J Geophys Res*, **94**, 13,295-303.

Buechler, D E, P D Wright and S J Goodman, 1990: Lightning/Rainfall Relationships During COHMEX., Part II: An Ice Phase Parameterization., *J Rech Atmos*, **16**, 295-320.

Cherna, E V and E J Stansbury, 1986: Sferics Rate in Relation to Thunderstorm Dimensions., *J Geophys Res*, **91**, 701-7.

Christian, H J, K T Driscoll, S J Goodman, R J Blakeslee, D A Mach and D E Buechler, 1996: "The Optical Transient Detector (OTD)" 10th International Conference on Atmospheric Electricity, Osaka, Japan, 368-371.

Cotton, W R, M A Stephens, T Nehrkorn and G J Tripoli, 1982: The Colorado State University Three-Dimensional Cloud/Mesoscale Model - 1982, Part II: An Ice Phase Parameterization., *J Rech Atmos*, **16**, 295-320.

Dawson, G A and W P Winn, 1965: A Model for Steamer Propagation., *Z Physik*, **183**, 159-71.

Driscoll, Kevin T, Richard J Blakeslee and Michael E Baginski, 1992: A Modeling Study of the Time-Averaged Electric Currents in the Vicinity of Isolated Thunderstorms., *J Geophys Res*, **97**, 11,535-51.

Dye, J E, J J JOnes, W P Winn, T A Cerni, B Gardiner, D Lamb, R L Pitter, J Hallett and C P R Saunders, 1986: Early Electrification and Precipitation Development in a Small, Isolated Montana Cumulonimbus., *J Geophys Res*, **91** 1231-47.

Dye, J E, W P Winn, J J Jones, and D W Breed, 1989: The Electrification of New Mexico Thunderstorms, 1. The Relationship between Precipitation Development and the Onset of Electrification. *J Geophys Res*, **94**, 8643-8656

Dye, J E, D W Breed, G M Barnes, J J Jones and R Solomon, 1992: The Co-evolution of Precipitation and Electric Fields in Florida Cumuli during CaPE., 9th International Conference on Atmospheric Electricity, St Petersburg, Russia.

Fletcher, N M, 1962: *The Physics of Rainclouds*, Cambridge Univ Press, 386.

Gallimberti, I, 1979: The Mechanism of the Long Spark Formation., *J de Physique*, **40**, C7-193 - C7-250.

Gardiner, B, D Lamb, R Pitter, J Hallett and C Saunders, 1985: Measurements of Initial Potential Gradients and Particle Charges in a Montana Summer Thunderstorm. *J Geophys Res*, **90**, 6079-6086.

Gillespie, D T, 1975: Three Models for the Coalescence Growth of Drops., *J Atmos Sci*, **32**, 600-607.

Goodman, S J, D E Buechler, P D Wright, W D Rust, 1988: Lightning and Precipitation History of a Microburst-producing Storm., *Geophys Res Let*, **15**, 1185-1188.

Goodman, Steven J, Predicting Thunderstorm Evolution using Ground-Based Lightning Detection Networks. NASA Technical Memorandum-103521, November 1990.

Griffiths, R F and C T Phelps, 1976: A Model for Lightning Initiation Arising From Positive Corona Streamer Development. *J Geophys Res*, **81**, 3671-3676.

Gurevich, A V, G M Milikh and R Roussel-Dupre, 1992: Runaway Electron Mechanism of Air Breakdown and Preconditioning During a Thunderstorm., *Phys Let A*, **165**, 463-468.

Hall, W D, 1980: A Detailed Microphysical Model Within a Two-Dimensional Dynamical Framework: Model Description and Preliminary Results., *J Atmos Sci*, **37**, 2486-2507.

Hallett, J and S C Mossop, 1974: Production of Secondary Ice Particles During the Riming Process., Nature, **249**, 26-28.

Harris-Hobbs, R L and W A Cooper, 1987: Field Evidence Supporting Quantitative Predictions of Secondary Ice Production Rates., *J Atmos Sci*, **44**, 1071-1081.

Helsdon, J H and R D Farley, 1987: A Numerical Modeling Study of a Montana Thunderstorm: 2. Model Results Versus Observations Involving Electrical Aspects. *J Geophys Res*, **92**, 5661-5675.

Helsdon, John H, Jr, Gang Wu and Richard D Farley, 1992: An Intracloud Lightning Parameterization Scheme for a Storm Electrification Model., *J Geophys Res*, **97**, 5865-5884.

Heymsfield, A J, 1978: The Characteristics of Graupel Particles in Northeastern Colorado Cumulus Congestus Clouds., *J Atmos Sci*, **35**, 284-295.

Heymsfield, A J and J C Pflaum, 1985: A Quantitative Assessment of the Accuracy of Techniques for Calculating Graupel Growth., *J Atmos Sci*, **42**, 2264-74

Huzita, A and T Ogawa, 1976: Charge Distribution in the Average Thunderstorm Cloud., *J Meteorol Soc Japan*, **54**, 284-288.

Jayaratne, E R, C P R Saunders and J Hallett, 1983: Laboratory Studies of the Charging of Soft-Hail During Ice Crystal Interactions., *Q J R Met Soc*, **109**, 609-630.

Kasemir, H W, 1960: A Contribution to the Electrostatic Theory of a Lightning Discharge, *J Geophys Res*, **65**, 1873-1878.

Keith, W D and C P R Saunders, 1989: Charge Transfer During Multiple Large Ice-Crystal Interactions with a Riming Target., *J Geophys Res*, **94**, 13,103-13,106.

Kombayasi, M, T Gonda and K Isono, 1964: Lifetime of Water Drops Before Breaking and Size Distribution of Fragment Droplets., *J Met Soc Japan*, **42**, 330-340.

Koshak, W J and E P Krider, 1989: Analysis of lightning field changes during active Florida thunderstorms., *Geophys Res*, **94**, 1165-86.

Krehbiel, R P, M Brook, R L Lhermitte and C L Lennon, 1980: Lightning Charge Structure in Thunderstorms., 6th International Conference on Atmospheric Electricity, Manchester.

Krehbiel, Paul, 1981: An Analysis of the Electric Field Change Produced by Lightning., Ph.D. dissertation, Univ of Manchester Institute of Science and Technology, 400pp.

Krehbiel, Paul, 1986: *The Earth's Electrical Environment*, National Academy Press, (The Electrical Structure of Thunderstorms) 90-113.

Krider, E P, R C Noggle and M A Uman, 1976: A Gated, Wideband Magnetic Direction Finder for Lightning Return Strokes., *J Appl Meteor*, **15**, 301-6.

Latham, J and B J Mason, 1962: Electrical Charging of Hail Pellets in a Polarizing Field., *Proc Roy Soc London*, **266A**, 387-401.

Latham, J, 1981: The Electrification of Thunderstorms., *Q J R Met Soc*, **107**, 277-295.

Liu, X and P R Krehbiel, 1985: The Initial Streamer of Intracloud Lightning Flashes., *J Geophys Res*, **90**, 6211-6218.

Macklin, W C, 1962: The Density and Structure of Ice Formed by Accretion. *Quart J R Met Soc*, **88**, 30-55.

MacGorman, D R and W D Rust, 1989: An Evaluation of the LLP and LPATS Lightning Ground Strike Mapping Systems, 5th Int'l Conf on Interactive Information and Processing Systems, Amer Meteor Soc, 249-254.

MacGorman, D R, K E Nielsen, 1991: Cloud-to-Ground Lightning in a Tornadic Storm on 8 May 1986., *Mon Wea Rev*, **119**, 1557-74.

Malan, D J, 1963: *The Physics of Lightning.*, English Univ Press, London.

Marshall, Thomas C, Michael P McCarthy and W David Rust, 1995a: Electric Field Magnitudes and Lightning Initiation in Thunderstorms., *J Geophys Res*, **100**, 7097-103.

Marshall, Thomas C, W Rison, W D Rust, M Stolzenburg, J C Willet and W P Winn, 1995b: Rocket and Balloon Observations of Electric Field in Two Thunderstorms., *J Geophys Res*, **100**, 20,815-28.

Mazur, V, 1989: Triggered Lightning Strikes to Aircraft and Natural Intracloud Discharges., *J Geophys Res*, **94**, 3311-3325.

Mazur, V and L H Ruhnke, 1993: Common Physical Processes in Natural and Artificially Triggered Lightning., *J Geophys Res*, **98**, 12,913-12,930.

McKenzie, A M, 1991: *Plucking Feathers from a Bald Frog*, Psychick Release Production Cerebrum & Press, Stockholm.

McTaggart-Cowan, J D and R List, 1975: Collision and Breakup of Water Drops at Terminal Velocity., *J Atmos Sci*, **32**, 1401.

Meyers, M P, P J DeMott and W R Cotton, 1992: New Primary Ice-Nucleation Parameterizations in an Explicit Cloud Model., *J Appl Meteor*, **31**, 708-721.

Molinie, J, C Asselin de Beauville and C A Pontikis: Influence of the ITCZ Position on the Development of Thunderstorms on the French Guyana Coast., proceedings to the Conference on Atmospheric Electricity, St Louis, 1993.

Morse, Philip and Herman Feshbach, 1953: *Methods of Theoretical Physics*, McGraw-Hill, New York, Vol. 2, 1284-6.

Mossop, S C, 1976: Production of Secondary Ice Particles During the Growth of Graupel by Riming. *Q J R Met Soc*, **51**, 474-478.

Mossop, S C, 1978: The Influence of Drop Size Distribution on the Production of Secondary Ice Particles During Graupel Growth., *Q J R Met Soc*, **104**,323-330.

Mossop, S C and E R Wishart, 1978: The Mechanism of Splintering During Rime Growth., *Geophys Res Let*, **5**, 1083-5.

Muhler-Hillebrand, D, 1954: Charge Generation in Thunderclouds by Collision of Ice Crystals with Graupel Falling Through a Vertical Electric Field., *Tellus*, **6**, 367-81.

Murphy, M, P Krider and Michael W Maier, 1996: Lightning Charge Analyses in Small Convection and Precipitation Electrification (CaPE) Experiment Storms., *J Geophys Res*, **101**, 29,615-26.

Neumann, C J, 1971: The Thunderstorm Forecasting System at the Kennedy Space Center., *J Appl Meteor*, **10**, 921-36.

Norville, K, M Baker and J Latham, 1991: A Numerical Study of Thunderstorm Electrification: Model Development and Case Study. *J Geophys Res*, **96**, 7463-7481.

Orville, Richarge E, 1986: *The Earth's Electrical Environment*, National Academy Press, (Lightning Phenomenology) 23-29.

Orville, Richard E and Ronald W Henderson, 1986: Global Distribution of Midnight Lightning: September 1977 to August 1978. *Mon Wea Rev*, **114**, 2640-2653.

Petersen, W A, S A Rutledge, D J Boccippio and E R Williams, 1993: The Electrification of Tropical Oceanic Convective Clouds Observed During TOGA-COARE., proceedings to the 17th Conference on Atmospheric Electricity, 4-8 October 1993, St Louis. 796-802

Petersen, W A, R Cifelli, S A Rutledge, and B F Smull, 1995: Cloud-to-Ground Lightning and the Related Kinematic Structures of Two Tropical Oceanic MSC's: Contrasting Cases., Conf on Cloud Phys, 75th AMS annual Meeting, 15-20 January 1995, Dallas, Texas.

Pielke, R, 1974: A Three-Dimensional Numerical Model of the Sea Breezes Over South Florida., *Mon Wea Rev*, **102**, 115-39.

Pierce, E T, 1970: Latitudinal Variation of Lightning Parameters., *J Appl Meteor*, **9**, 194-5.

Prentice, S A and D Mackerras, 1977: The Ratio of Cloud to Cloud-Ground lightning flashes in Thunderstorms., *J Appl Met*, **16**, 545-550.

Price, Colin and David Rind, 1992: A Simple Lightning Parameterization for Calculating Global Lightning Distributions. *J Geophys Res*, **97**, 9919-9933.

Price, Colin and David Rind, 1993: What Determines the Cloud-to-Ground Lightning Flash Rate in Thunderstorms., *Geophys Res Let*, **20**, 463-6.

Pruppacher, H R and J D Klett, *Microphysics of Clouds.*, D Reidel. Hingham, Massachusetts, 1978.

Randell, Scot C, Steven A Rutledge, Richard D Farley and John H Helsdon, Jr, 1994: A Modeling Study on the Early Electrical Development of Tropical Convection: Continental and Oceanic (Monsoon) Storms. *Mon Wea Rev.* **122**, 1852-1877.

Rangno, A L and P V Hobbs, 1991: Ice Particle Concentrations and Precipitation Development in Small Polar Maritime Cumuliform Clouds., *Q J R Met Soc*, **117**, 207-41.

Rangno, A L and P V Hobbs, 1994: Ice Particle Concentrations and Precipitation Development in Small Continental Cumuliform Clouds., *Q J R Met Soc*, **120**, 573-601.

Raymond, D J and A M Blyth, 1989: Precipitation Development in a New Mexico Thunderstorm. *Q J R Met Soc*, **115**, 1397-1424.

Raymond, D J, R Solomon and A M Blyth, 1991: Mass Fluxes in New Mexico Mountain Thunderstorms from Radar and Aircraft Measurements. *Q J R Met Soc*, **117**, 587-622.

Richard, P, P Laroche and A Soulage, 1989: Lightning monitoring and warning: the SAFIR system. *Revue Generale de l'Electricite*, **3**, 39-46.

Roble, Raymond G and Israel Tzur, 1986: *The Earth's Electrical Environment*, National Academy Press, (The Global Atmospheric-Electrical Circuit) 206-231.

Rogers, R R and M K Yau, 1989: *A Short Course in Cloud Physics.*, Pergamon Press, U.K., p23.

Rutledge, Steve A, Chungu Lu, Donald R MacGorman, 1990: Positive Cloud-to-Ground Lightning in Mesoscale Convective Systems., *J Atmos Sci*, **47**, 2085-2100.

Rutledge, S A, E R Williams and T D Keenan, 1992: The Down Under Doppler and Electricity Experiment (DUNDEE): Overview and preliminary results. *Bull Amer Meteor Soc*, **73**, 3-16.

Saunders, C, W Keith and R Mitzeva, 1991: The Effect of Liquid Water on Thunderstorm Charging. *J Geophys Res*, **96**, 11,007-11,017.

Saunders, C, 1993: A Review of Thunderstorm Electrification Processes., *J Appl Meteor*, **32**, 642-55.

Saunders, C, 1994: Thunderstorm Electrification Laboratory Experiments and Charging Mechanisms., *J Geophys Res*, **99**, 10,773-9.

Smolarkiewicz, P K, 1984: A Simple Positive Definite Advection Scheme with Small Implicit Diffusion., *Mon Wea Rev*, **111**, 479-86.

Solomon, Robert and Marcia Baker, 1994: Electrification of New Mexico Thunderstorms., *Mon Wea Rev*, **122**, 1878-1886.

Solomon, Robert and Marcia Baker, 1996: A One-Dimensional Lightning Parameterization., *J Geophys Res*, **101**, 14,983-90.

Solomon, R, Vicki Hoffman and Marcia Baker, 1996: Lightning Frequency and Type in Tropical Storms: Model and Observations. 10th International Conference on Atmospheric Electricity, Osaka, Japan.

Solomon, R and Marcia Baker, 1997: Lightning Flash Rate and Type in Convective Storms., submitted to *J Geophys Res*.

Squires, P, 1958: The Microstructure and Colloidal Stability of Warm Clouds., *Tellus*, **10**, 256-71.

Srivastava, R C, 1971: Size Distribution of Raindrops Generated by Breakup and Coalescence., *J Atmos Sci*, **28**, 410-415.

Takahashi T, 1978: Riming Electrification as a Charge Generation Mechanism in Thunderstorms. *J Atmos Sci*, **35**, 1536-1548.

Taylor, G R, 1989: Sulfate Production and Deposition in Mid-latitude Continental Cumulus Clouds, Part I: Cloud Model Formulation and Base Run Analysis., *J Atmos Sci*, **46**, 1971-1990.

Twomey, S and T A Wojciechowski, 1969: Observations of the Geographical Variation of Cloud Nuclei., *J Atmos Sci*, **26**, 684-688.

Uman, M A, 1987: *The Lightning Discharge*, Academic Press, Inc. Vol 39 in the International Geophysics Series.

Vonnegut, B, 1953: Possible Mechanism for the Formation of Thunderstorm Electricity. *Bull Amer Meteor Soc*, **34**, 378.

Weinheimer, A J, J E Dye, D W Breed, M P Spowart, J L Parrish, T L Hoglin, T C Marshall, 1991: Simultaneous Measurements of the Charge, Size and Shape of Hydrometeors in an Electrified Cloud., *J Geophys Res*, **96**, 20809-29.

Williams, E R, 1989: The Tripole Structure of Thunderstorms., *J Geophys Res*, **94**, 13151- 67.

Williams, E R, and N Renno, 1991: Conditional Instability, Tropical Lightning, Ionospheric Potential, and Global Change., 19th Conference on Hurricanes and Tropical Meteorology, Miami, Florida: 8-10 May.

Williams, E R., S A Rutledge, S G Geotis, N Renno, E Rasmussen and T Rickenbach, 1992: A Radar and Electrical Study of Tropical 'Hot Towers.' *J Atmos Sci*, **40**, 1386-1395.

Williams, E R, and S J Heckman, 1993: The Local Diurnal Variation of Cloud Electrification and the Global Diurnal Variation of Negative Charge on the Earth., *J Geophys Res*, **98**, 5221- 34.

Winn, W P, 1993: Aircraft Measurement of Electric Field: Self-Calibration., *J Geophys Res*, **98**, 7351-65

Yau, M, 1980: A Two-cylinder Model of Cumulus Cells and its Application in Computing Cumulus Transports., *J Atmos Sci*, **37**, 2470-85.

Ziegler, C, D MacGorman, J Dye and P Ray, 1991: A Model Evaluation of Noninductive Graupel-Ice Charging in the Early Electrification of a Mountain Thunderstorm. *J Geophys Res*, **96**, 12,833-12,855.

Ziegler, C L, D R MacGorman, 1994: Observed Lightning Morphology Relative to Modeled Space Charge and Electric Field Distributions in a Tornadic Storm., *J Atmos Sci*, **51**, 833-851.

Zipser, Edward J 1994: Deep Cumulonimbus Cloud Systems in the Tropics with and without Lightning., *Mon Wea Rev,* **122**, 1837-1851.

Zipser, Edward J and Kurt R Lutz, 1994: The Vertical Profile of Radar Reflectivity of Convective Cells: A Strong Indicator of Storm Intensity and Lightning Probability?, *Mon Wea Rev,* **122**, 1751-9.

# Appendix A: List of Symbols

| Symbol | brief definition† | page‡ |
|---|---|---|
| $\Gamma^{+}_{a(b)}$ | standard deviation of Gaussian positive charge distribution [m] | 32 |
| $\Gamma^{-}_{a(b)}$ | standard deviation of Gaussian negative charge distribution [m] | 32 |
| $\delta Q(d,D)$ | non-inductive charge separated during a collision between graupel and snow [fC] | 25 |
| $\delta q_{ctg}$ | charge transferred by clout-to-ground lightning channel[C] | 32 |
| $\delta v$ | difference in fall velocities between two particles [m/s] | 21 |
| $\delta z$ | vertical resolution of the lightning channel [m] | 29 |
| $\delta Z_{cz}$ | difference between $Z_{bal}$ and $Z_{rev}$ | 12 |
| $\varepsilon_0$ | dielectric permittivity of free space [$C^2/Nm^2$] | 29 |
| $\eta$ | prolate spheroidal coordinate | 27 |
| $\theta_w$ | potential wet bulb temperature [K] | 10 |
| $\xi$ | prolate spheroidal coordinate | 27 |
| $\xi_0$ | initial surface of lightning channel | 28 |
| $\rho_s$ | effective charge density from screening currents [$fC/m^3$] | 25 |
| $\sigma$ | surface charge density on lightning channel [$C/m^2$] | 29 |
| $\sigma_a$ | conductivity of air [$\Omega^{-1}\ m^{-1}$] | 25 |
| $\varphi$ | prolate spheroidal coordinate | 27 |
| $\psi$ | total electric potential [kV] | 29 |
| $\psi_{conductor}$ | electric potential of the lightning channel [kV] | 29 |
| $\psi_{ext}$ | ambient electric potential [kV] | 29 |
| a | distance between the foci of prolate spheroid [m] | 27 |
| CAPE | convectively available potential energy [J/kg] | 10 |
| CCN | cloud condensation nuclei [$\#/cm^3$] | 11 |
| d | diameter of snow or droplet [$\mu m$] | 21 |
| D | diameter of graupel or rain [$\mu m$] | 21 |
| D± | distance between positive and negative charge regions [m] | 32 |
| dt | time step [sec] | 21 |

†. Units given are the default unless otherwise stated in within the text, please refer to the paragraph referred to for more information.

‡. Page number referes to paragraph where the symbol is introduced.

| | | |
|---|---|---|
| $E_{breakdown}$ | electric field magnitude required to breakdown clear air [kV/m] | 3 |
| $E_{conductor}$ | electric field of the lightning channel [kV/m] | 31 |
| $E_{diss}$ | dissipation electric field [kV/m] | 30 |
| $E$, $E_{ext}$ | electric field [kV/m] | 25 |
| $E^0_{init}$ | initiation electric field at ground [kV/m] | 40 |
| $E_{init}$ | magnitude of the electric field to initiate lightning [kV/m] | 27 |
| $E_{si}$ | sticking efficiencies | 21 |
| $E_{tip}$ | electric field near tip of the lightning channel [kV/m] | 30 |
| $F$ | lightning flash rate [#/min] | 13 |
| $F_{kin}$ | cloud base kinetic forcing [m/s] | 18 |
| $F_{th}$ | cloud base thermal forcing [°C] | 18 |
| IN | ice nuclei concentration via Fletcher parameterization [#/m$^3$] | 22 |
| $K_{cc}(d,D)$ | collection kernel [m$^3$/s] | 21 |
| $l$ | depth of the screening layer [m] | 25 |
| $L$ | length of lightning channel [m] | 27 |
| $L_0$ | initial length of lightning channel [m] | 28 |
| $L_i$ | lifted index [°C] | 13 |
| $L_{final}$ | final length of the lightning channel [m] | 30 |
| LWF | liquid water flux [g/m$^2$/s] | 69 |
| $LWF_{cz}$ | liquid water flux into charging zone [g/m$^2$/s] | 69 |
| $LWF_{thresh}$ | liquid water flux threshold required for electrification [g/m$^2$/s] | 69 |
| $N_{collisions}$ | number of collisions | 21 |
| $N_{CTG}$ | number of cloud-to-ground lightning channels | 9 |
| $N_{IC}$ | number of intracloud lightning channels | 9 |
| $N_{id}$ | deposition ice nuclei concentration via Meyers *et al* [l$^{-1}$] | 22 |
| $N_{ic}$ | contact ice nuclei concentration via Meyers *et al* [l$^{-1}$] | 22 |
| $n_{small}$ | number of small (ice crystals or droplets) particles [#/m$^3$] | 21 |
| $P_n$ | Legendre polynomial of order n | 29 |
| $Q_n$ | Legendre polynomial of the second kind of order n | 29 |
| Q+max | maximum positive charge [C] | 32 |
| Q-max | maximum negative charge [C] | 32 |
| Q+(total) | total positive charge [C] | 32 |
| Q-(total) | total negative charge [C] | 32 |

| | | |
|---|---|---|
| $R$ | ratio of $N_{IC}$ to $N_{CTG}$ | 9 |
| $R_a$ | radius of inner cylinder [m] | 18 |
| $R_b$ | radius of outer cylinder [m] | 18 |
| $R_{cloud}$ | cloud radius [m] | 32 |
| $R_0$ | radius of lightning channel at center [m] | 28 |
| $T_{rev}$ | charge reversal temperature [°C] | 4 |
| $T_{v,ad}$ | virtual temperature along a reversible moist adiabat [K] | 12 |
| $T_{v,env}$ | virtual temperature of the environment [K] | 12 |
| $\delta T_v$ | cloud base temperature perturbation [°C] | 18 |
| $W$ | ratio of Gaussian standard deviations | 37 |
| $w_{cb}$ | cloud base vertical velocity [m/s] | 18 |
| $w_{cz}$ | charging zone updraft velocity (overbar denotes average) [m/s] | 63 |
| $w_{thresh}$ | updraft velocity required for electrification [m/s] | 69 |
| $Z_{cb}$ | cloud base altitude [m] | 12 |
| $Z_{ct}$ | cloud top altitude [m] | 12 |
| $Z_{bal}$ | altitude where graupel fall speed equals updraft velocity [m] | 12 |
| $Z_{rev}$ | altitude of charge reversal temperature | 12 |
| $Z_{cz}$ | depth of the charging zone [m] | 63 |
| $Z_{ct,max}$ | maximum cloud top height [m] | 13 |
| $Z_{ct,ad}$ | adiabatic cloud top height | 86 |
| $Z+$ | height of the maximum positive charge center [m] | 32 |
| $Z-$ | height of the maximum negative charge center [m] | 32 |

# Appendix B: Instrumentation

## B.1 Lightning direction finder

A large scale lightning detection system is employed by the lightning location and protection (LLP) system (Krider *et al*, 1976). It is comprised of a large array of sensors spread throughout the United States. The sensors detect the signal generated by cloud-to-ground lightning, utilizing that part generated by return stroke near the ground at 100 kHz, where ground flashes radiate much more energy than cloud flashes. Errors are generally the result of terrain and man made structures. By using the signal from a number of sensors this system can detect the location, polarity and charge transferred during cloud-to-ground lightning. Two sensors are assumed to have observed the same lightning event if the signals from two or more stations are received within a certain time of each other (usually $< 0.02$ s). Several evaluations of the LLP system give a detection efficiency between 60-90% at ranges of a few hundred kilometers and errors of 0.5-1.0° in measured azimuths (MacGorman and Rust, 1989).

## B.2 Lightning mapping systems

Several methods have been developed to map the location and development of lightning by using the radio noise it generates. The Systeme de Surveillance et d'Alerte Foudre par Interferometrie Radioelectrique (SAFIR) is an interferometric technique that can be used to map the location of 300 MHz VHF-UHF radio noise from lightning with 10 μs resolution (Richard *et al*, 1989; Bondiou *et al*, 1990). Using the time of arrival of radio noise from several sensors, the location of consecutive noise events can be mapped in space and time. If the time between two events is less than some threshold related to the distance over which the events are located and an assumed speed for travelling that distance, the two points are considered to constitute part of a single lightning channel.

A puzzle arising from most mapping techniques and a subject of much controversy, is the fact that they do not detect positive streamers, one in which the net charge contained in the tip of the channel is positive. It is unclear whether simply do not exist within clouds, if their signal is too weak to be detected or they generate very specific radio frequencies that are not being monitored.

### B.3 Electric field measurements

In order to measure electric fields, two styles of sensors have been developed. One style of electric field sensor is the field mill. The field mills used in all of the field projects reported here use a rotating-shutter (Figure B.1). The King Air, Sailplane and Socorro field mills all

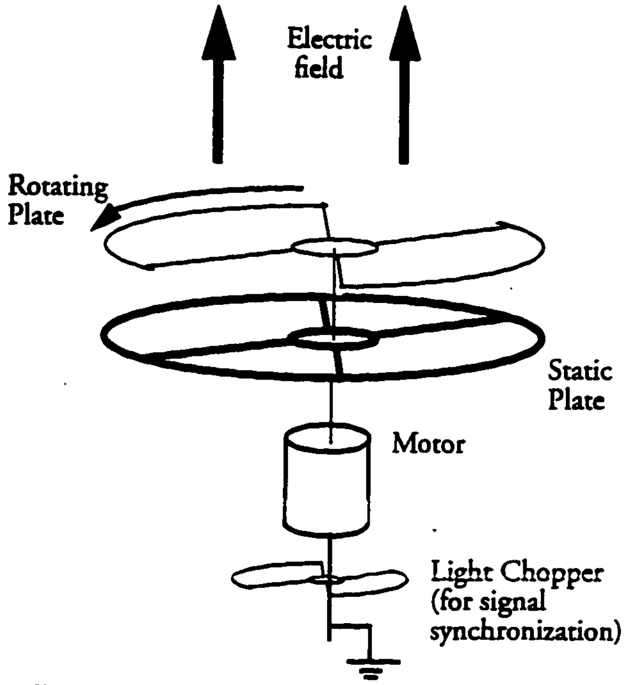


**Figure B.1. Illustration of basic field mill design (after Winn, 1993)**

follow a design used by New Mexico Institute of Mining and Technology (NMIMT) with a rotating metal shutter parallel and above a stationary plate identical in design. As the rotating shutter turns, it alternately exposes the lower plate to the external electric field and then hides the plate from the field. This induces a charge on the lower plate that is a function of the electric field and angular velocity of the rotating shutter. The current to the lower plate is measured and can be calibrated with a known electric field. There is a sensitive and insensitive setting for these field mills. The sensitive scale recorded fields from about ±50-1200 V $m^{-1}$ while the insensitive scale recorded fields from ±0.5 to 300 kV $m^{-1}$. The ground based NASA field mills used in the CaPE field project follow a similar design though their sensitivities differ slightly.

Figure B.2 gives a schematic diagram of a very simple plate antenna that is used to measure

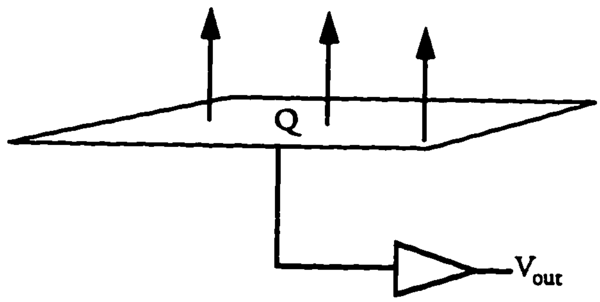


**Figure B.2. Schematic of a "plate antenna" used to measure rapid electric field changes usually associated with lightning.**

changes in the electric field, which can be used to identify lightning flashes. Changes in the electric field induced changes in the charge induced on the plate, Q. Using an amplifier or a current integrator, the changes in Q can then be related to the electric field. Both intra-cloud and cloud-to-ground channels can be detected. The minimum detectable charge is a function of the electronic noise. Within storms, lightning transients and corona can be the largest sources of noise. The minimum detectable charge can change with environments but can usually be estimated from data.

The rapid electric field changes due to lightning flashes recorded by field mills on aircraft or ground based platforms record both intracloud and cloud-to-ground lightning events though it is not always possible to determine if a given lightning flash was intracloud or cloud-to-ground.

## B.4 Microphysical instrumentation

The sailplane was equipped with a 2D particle probe with two charge induction rings (basically a coil of wire connected to an amplifier) for determination of charge on individual particles. Induced charge is measured in the first ring as a charged particle travels through it (see Figure B.3). A PMS probe then captures the 2D image of the particle and then the particle travels through the second charge ring producing the same induced charge signature slightly later in time. The same charge signature must be observed by both charge rings with the expected time delay in order to identify the particle.

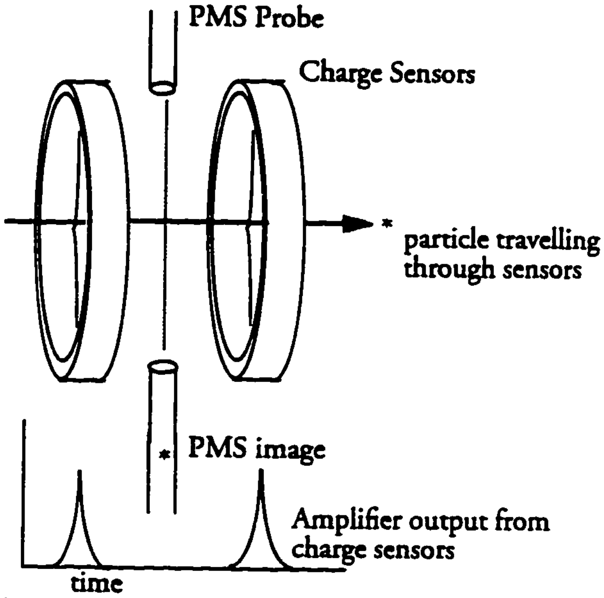


**Figure B.3. Illustration of the instrument used to measure charge per particle on board the NCAR Sailplane.**

Generally, the smallest charge measurable by this instrument is 1 - 3 pC (±20%). This range of charges were usually found on larger particles, primarily graupel. Particles between 50 μm and 8 mm were detected, though particles less than 200 μm and greater than 1 mm were difficult to resolve clearly (Weinheimer *et al*, 1991).

# Vita

robert calvin solomon, 'bubba s' to some, was born on 26 February 1968 in Sydney, Nebraska, though most of his early years were spent in Hardy, Arkansas. His favorite pastimes include the creation and active listening of less than conventual sounds and rereading Les Chants de Maldoror by Comte de Lautréamont and In Watermelon Sugar by Richard Brautigan. Max Ernst would probably be his favorite artist. Favorite musical artists are too numerous to list. However, of particular interest to the work contained herein, I recommend works by Disinformation (eg, Stargate and R&D) which contain field recordings of thunderstorms at a variety of frequencies.

**Education:**

1990 - 1997: University of Washington, Department of Atmospheric Sciences PhD in Atmospheric Sciences.

1986 - 1990: Undergraduate education obtained from New Mexico Institute of Mining and Technology (NMIMT). Received a B.S. with highest honors in Physics and Environmental Science in May of 1990.

**Publications:**

Solomon, Robert and Marcia Baker: Lightning Flash Rate and Type in Convective Storms., Submitted to *J Geophys Res* Oct 1997.

Solomon, Robert and Marcia Baker, 1996: A One-Dimensional Lightning Parameterization., *J Geophys Res*, **101**, 14,983-90.

Solomon, R and Marcia Baker, 1994: Electrification of New Mexico Thunderstorms., *Mon Wea Rev*, **122**, 1878-1886

Raymond, D R, R Solomon and A M Blyth, 1991: Mass Fluxes in New Mexico Mountain Thunderstorms from Radar and Aircraft Measurements., *Quart J R Met Soc*, **117**, 587-622.

**Conference proceedings:**

Solomon, R, Vicki Hoffman and Marcia Baker, 1996: Lightning Frequency and Type in Tropical Storms: Model and Observations. 10th International Conference on Atmospheric Electricity, Osaka, Japan.

Solomon, R and Marcia Baker, 1994: A One-Dimensional Lightning Parameterization, AGU winter conference, San Francisco.

Solomon, R and Marcia Baker, 1993: Electrified and Non-electrified Storms Forming from similar Environments. Conference on Atmospheric Electricity, St Louis.

Dye, J E, D W Breed, G M Barnes, J J Jones and R Solomon, 1992: The Co-evolution of Precipitation and Electric Fields in Florida Cumuli during CaPE., 9th International Conference on Atmospheric Electricity, St Petersburg, Russia.

Raymond, D J, R Solomon, A M Blyth, 1989: Mass Fluxes in New Mexico Mountain Thunderstorms., AGU winter conference, San Francisco.

Solomon, R, D J Raymond and A M Blyth, 1989: Inter-comparison of Mass Fluxes from Radar and Aircraft measurements., AGU winter conference, San Francisco.